

MASTER

Dynamic Surface Processes in Cobalt-Based Fischer-Tropsch Synthesis

Roefs, S.P.L.

Award date:
2020

[Link to publication](#)

Disclaimer

This document contains a student thesis (bachelor's or master's), as authored by a student at Eindhoven University of Technology. Student theses are made available in the TU/e repository upon obtaining the required degree. The grade received is not published on the document as presented in the repository. The required complexity or quality of research of student theses may vary by program, and the required minimum study period may vary in duration.

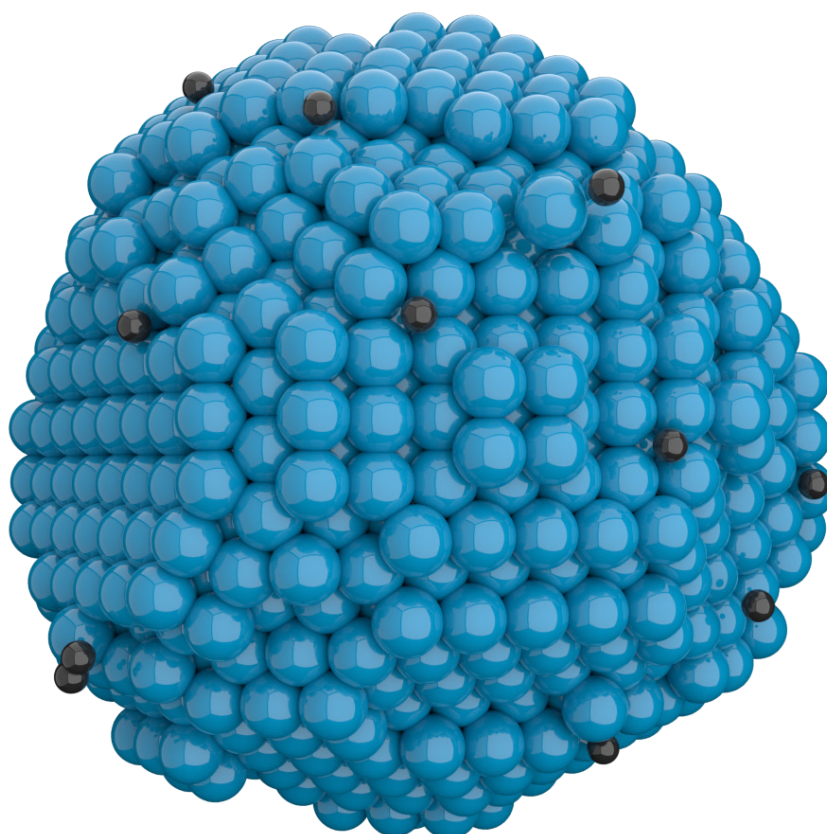
General rights

Copyright and moral rights for the publications made accessible in the public portal are retained by the authors and/or other copyright owners and it is a condition of accessing publications that users recognise and abide by the legal requirements associated with these rights.

- Users may download and print one copy of any publication from the public portal for the purpose of private study or research.
- You may not further distribute the material or use it for any profit-making activity or commercial gain

Dynamic Surface Processes in Cobalt-Based Fischer-Tropsch Synthesis

Sven P.L. Roefs



Master Thesis

June 27th, 2019

Graduation Committee:

Prof. dr. ir. E.J.M. Hensen

Dr. ir. I.A.W. Filot

Dr. ir. M.W. Baltussen

Ir. M.P.C. van Etten

ABSTRACT

In order to advance the rational design of the next-generation catalysts, dynamic surface processes occurring on the surface of cobalt-based Fischer-Tropsch catalysts are investigated. Through density functional theory and grand canonical Monte Carlo simulations on the basis of a ReaxFF reactive force field, surface reconstruction and lateral interactions on surface slabs are studied, as well as carbon deposition on a nanoparticle. The process is aided by in-house developed tools for force field training and structure site recognition. A thorough analysis of energies and geometries has been carried out. Calculated energies have resulted in the determination of relative stabilities of structures. By inspection of geometries, it was found that cobalt fcc(110) surfaces exhibit surface reconstruction behaviour. Cobalt fcc(111) and fcc(211) surfaces were found to allow for stabilizing lateral interactions. Furthermore, an existing cobalt force field was successfully extended with a carbon force field, for which a method was developed. Less successful were the extension towards cobalt carbide and surface-adsorbate interactions. Force field evaluation, as well as grand canonical Monte Carlo results, have shown that significant improvements and additions are required in order to study carbon deposition on cobalt nanoparticles with the desired accuracy. Finally, suggestions have been made for the approach of future research on the topic.

TABLE OF CONTENTS

1	Introduction	1
1.1	Societal Relevance	1
1.2	The Role of Catalysis	3
1.3	The Role of Fischer-Tropsch Synthesis	4
1.4	The Scope of This Thesis	6
2	Computational Methods	9
2.1	Density Functional Theory	9
2.2	ReaxFF Reactive Force Field	15
2.3	ReaxFF Fitter	16
2.4	Grand Canonical Monte Carlo	17
2.5	Site Recognition	19
3	Results & Discussion	23
3.1	Lateral Interactions and Surface Reconstruction	23
3.2	Evaluation and Comparison of a Created Force Field	35
3.3	Grand Canonical Monte Carlo Simulations	48
4	Conclusion	53
5	Outlook & Recommendation	55
6	Acknowledgements	57
7	Bibliography	59
8	Appendices	63
8.1	Appendix A – RF ₃ Settings File	63
8.2	Appendix B – Extension of a Force Field Using RF ₃	72
8.3	Appendix C – Geometry and Energy Results After DFT	77
8.4	Appendix D – Original Results of the Fitting Procedure	86
8.5	Appendix E – Parameter Sets of Used Force Fields	99

1 INTRODUCTION

1.1 SOCIETAL RELEVANCE

For the most part of history, humans have viewed the state of the climate as stable, only occasionally being interrupted by natural catastrophes such as earthquakes and volcanic eruptions.¹ Although mankind has been affected by the climate and its change for thousands of years,² the realisation that mankind in turn also affects the climate on a global scale only dawned upon humanity during the early 19th century.¹

One of the first examples of widespread climate change is illustrated in the book *Études sur les glaciers*, published in 1840.³ In this book, the geologist Jean Louis Rodolphe Agassiz provides a coherent Ice Age theory, herewith demonstrating that the Alpine climate had once been very different to its climate at the time. In an 1861 follow-up study on glaciers conducted by John Tyndall, experimental evidence was provided for what later came to be known as the ‘greenhouse effect’.⁴ However, it was not until 1896 that the contribution of carbon dioxide to the greenhouse effect was quantified by Svante August Arrhenius.⁵

In his later publication *Worlds in the Making; the Evolution of the Universe* Arrhenius argued that the increasing percentage of carbon dioxide in the atmosphere, due to the combustion of fossil fuels by mankind, would lead to a change in climate in the near future.⁶ Although this hypothesis was initially widely disputed or refused, stating gross oversimplification of the climate system as the reason, it increasingly received support during the latter half of the 20th century.⁷

Perhaps one of the most authoritative documents published on climate change is the *Scientific Assessment of Climate Change* report by the Intergovernmental Panel on Climate Change (IPCC), published in 1990.⁸ Not only does it list the greenhouse effect as one of the most important factors for climate change, it also finds that temperature on Earth has been increasing since the late 19th century, a finding which is strongly supported by the worldwide recession of mountain glaciers. In Figure 1.1, the correlation between local temperature and the greenhouse gas concentrations of methane and carbon dioxide is shown, as it was originally represented in the 1990 IPCC report.

The current-day importance of combatting further climate change is well reflected by the adoption of the Paris Agreement which “aims to strengthen the global response to the threat of climate change, in the context of sustainable development and efforts to eradicate poverty”.⁹ With 195 participating countries at the time of writing,¹⁰ it is safe to say that acting on climate change has become a global challenge. At the same time, however, the world is faced with rapid population growth and increasing energy consumption in developing countries. This situation, in which an increasing global demand for energy should be met in a non-polluting and sustainable way, is often coined as the ‘energy challenge’.

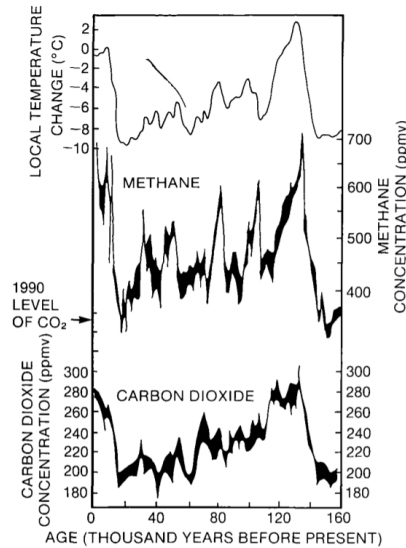


Figure 1.1: Analysis of air trapped in Antarctic ice cores shows that methane and carbon dioxide concentrations were closely correlated with the local temperature over the last 160,000 years. Concentrations of carbon dioxide at the time of the original publication (1990) are indicated. ⁸

As can be seen from Figure 1.2, fossil fuels dominate present-day energy consumption and are expected to continue in doing so for the next few decades, as there is currently no alternative in sight which can fully replace fossil fuels as an energy source.^{11,12} Besides being a major source of energy, fossil fuels are also the main source of organic chemical commodities.¹³ With fossil fuels being required on such an enormous scale, it is easy to see that even small alterations or improvements to fossil fuel technology can have a drastic impact on the world's energy challenge. The focus should, therefore, be on areas where these alterations and improvements can be made. It is here that catalysis and the Fischer-Tropsch synthesis come into play.

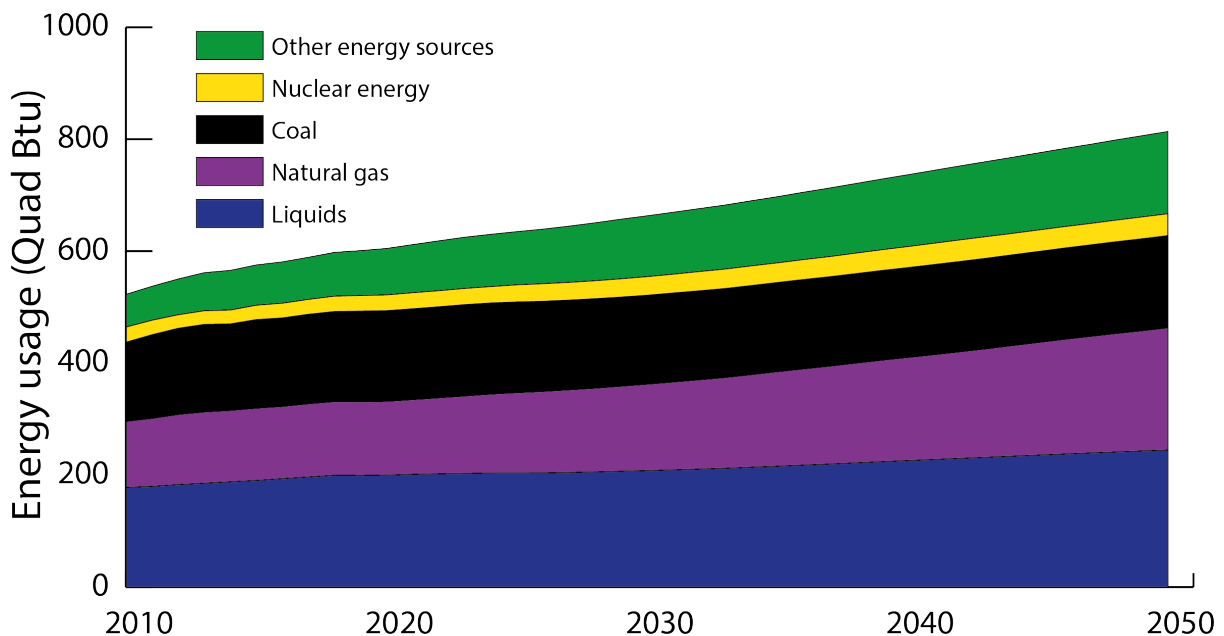


Figure 1.2: World total energy consumption, categorized by fuel. Data was obtained from the U.S. Energy Information Administration.¹²

1.2 THE ROLE OF CATALYSIS

According to the IUPAC Compendium of Chemical Terminology a catalyst is “a substance that increases the rate of a reaction without modifying the overall standard Gibbs energy change in the reaction”.¹⁴ It adds to this description that “the process is called catalysis” and that “the catalyst is both a reactant and product of the reaction”. In Figure 1.3, the effect of a catalyst on the reaction is exemplified. From this figure, it can be seen that the activation energy of the catalysed reaction is lowered, as energy barriers of dissociation and association steps are lowered, due to the formation of bonds between the catalyst and the reactants, intermediates and products. This results in the chemical reaction being accelerated, i.e. the kinetics are enhanced. The thermodynamics, however, remain unaltered as the overall change in free energy is equal in both the catalytic reaction and the non-catalytic reaction. Due to these effects, catalysts can bring a variety of advantages to the table. Some of the most important advantages are: (1) catalysts enable processes that would otherwise not be possible due to thermodynamic limitations, (2) catalysts allow processes to take place under industrially and economically more feasible conditions, e.g. lower temperature or pressure, and (3) catalysts allow for different reaction pathways, herewith avoiding the use or production of toxic, hazardous, polluting or otherwise undesirable substances.¹⁵

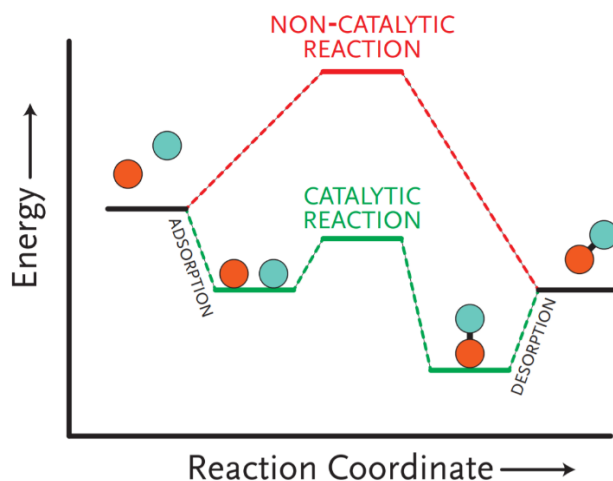


Figure 1.3: Visual representation of a reaction energy diagram of a combination reaction of two arbitrary compounds. The lower line shows the catalysed reaction pathway and the top line shows the uncatalyzed reaction pathway. Image was taken from dr.ir. I.A.W. Pilot, 2015¹⁶.

With so many possible advantages of using a catalyst, it should come as no surprise that catalysts are involved in 85 to 90% of all production processes in the chemical industry. However, catalysis does still have its issues to solve. As is demonstrated in Figure 1.4, our understanding of catalysis is lagging far behind the many applications on which we practise it today. The complex nature of catalysis results in major complications for the design of catalysts from first principles. This rational design, which is sometimes referred to as the ‘holy grail in catalysis’, is often seen as the end-goal of many catalysis-related studies, to which this research is no exception. In recent years, attention has been drawn to a modern concept in catalysis: mesoscale phenomena. These complex processes emanating as a result of changes in the surface adsorbed layer lead to an evolution of the catalyst structure. Examples are lateral interactions taking place between adsorbed

species on the surface, reconstruction of the surface atoms to a different coordination under the influence of adsorbates and surface deactivation due to (irreversible) deposition of atoms on the catalyst surface. The given examples of these so-called ‘dynamic surface processes’ will be of particular interest for this study. The word ‘dynamic’ is aptly chosen here, since it indicates a distinctive difference with the way in which catalyst functioning is often perceived in contemporary and past research and application. In many situations, catalysts are more often than not treated as static factors that influence the reaction. For instance, a black box which acts upon either the reactant coming in, conveniently turning it in a more desirable set of products, or upon a process, greatly enhancing the conditions in which it takes place. In reality, however, a catalyst is not static and the reaction taking place on the catalyst is most certainly influenced by dynamic surface processes. Understanding and describing these dynamic surface processes occurring on the mesoscale, and the effects they exercise on the reaction, is thought to make a notable contribution to the rational design of novel improved catalysts.

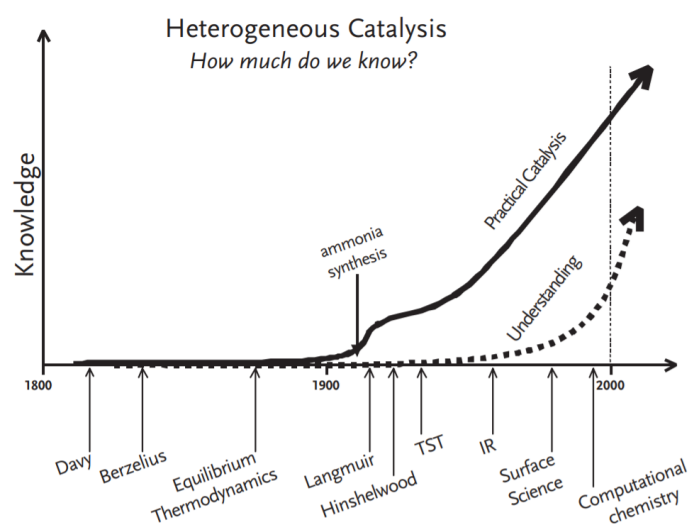


Figure 1.4: Schematic representation of practical catalysis and catalysis understanding over the past 200 years. *Imagine* was taken from *Concepts of Modern Catalysis and Kinetics* by I. Chorkendorff and J.W. Niemantsverdriet¹⁵.

1.3 THE ROLE OF FISCHER-TROPSCH SYNTHESIS

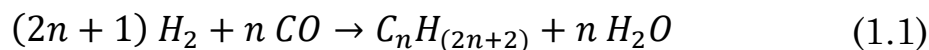
In quest of obtaining hydrocarbon molecules from coal-derived gas, suitable for the production of fuels and chemicals, the Fischer-Tropsch (FT) synthesis was developed by Franz Fischer and Hans Tropsch at the Kaiser Wilhelm Institute for Coal Research in Mülheim an der Ruhr, Germany.¹⁷ The development of this process stretched out over a period of roughly 20 years, mostly during the 1920s and 1930s, with the first publication on the synthesis being made in 1926 and the first industrial FT reactor, the Ruhrchemie atmospheric fixed bed reactor, opening in 1935.¹⁸ By the end of 1935, four more FT plants were under construction with an annual capacity of 100.000 to 120.000 metric tons and the industrial capacity would continue to grow to almost 600.000 metric tons by the end of World War II. This strong expansion of capacity resulted from strategic considerations such as petroleum independence, more so than from economic considerations.

After the Second World War, and especially after the discovery of large oil reserves in amongst others Alaska and Saudi Arabia, interest in the FT process declined. The notable

1.3 The Role of Fischer-Tropsch Synthesis

exception here is the Sasol FT industry in South Africa due to cheap domestic coal and the state policy at the time. In modern-day society, however, the FT process has seen a renewed interest. Significant reasons for the revival of the FT industry are a change in the fossil energy reserves and environmental demands. In relation to the change in energy reserves, the FT reaction allows the use of remotely located natural gas (also known as ‘stranded gas’) by converting it into shippable hydrocarbon liquids. This particular industry is often referred to as the Gas-to-Liquids (GTL) industry. In relation to the environmental demands, the FT process enables the production of ‘clean’ fuels from abundant and low-cost natural gas; the gas sometimes even being considered as a waste or by-product in some industries. These fuels are considered clean due to the absence or low presence of contaminants such as sulphur, nitrogen, heavy metals and aromatics. With the above-mentioned advantages of the FT industry and other advantages such as the utilization of co-products, production of high-quality chemicals or the production of biofuels from biomass¹⁹, the FT reaction can fulfil an important role in the world’s energy challenge.

The starting point of the FT reaction is synthetic gas (syngas), a mixture of H₂ and CO, which is turned into hydrocarbons of different chain lengths, described in Equation 1.1. In the context of this research, it is important to note that one of the elementary reaction steps in the FT reaction is the scission of the CO bond, resulting in free carbon atoms on the surface. These atoms then propagate to one of many options, such as being hydrogenated towards methane, reacting in a coupling reaction towards longer chains or leading to deposition on the catalyst surface, herewith deactivating the catalyst particle.



The FT reaction is carried out in different ways throughout the industry. Although process conditions vary a lot depending on feedstock and on what the FT plant is intended to produce, generally FT processes can be categorized in two classes. The Low Temperature Fischer-Tropsch (LTFT) process, which takes place at temperatures between 210 and 260 °C and is often carried out in a fixed-bed reactor, and the High Temperature Fischer-Tropsch (HTFT) process which ranges from 310 to 340 °C and frequently carried out in a fluidized bed reactor.²⁰ Designing an FT process comes with certain trade-offs. For example, increasing the temperature of the process favours undesirable effects such as methane formation, carbon deposition and other deactivation effects and it reduces the chain length of the product. In return, however, reaction rates are increased and steam quality from the reactor heat removal system is improved. Furthermore, an FT reactor cannot be designed without keeping the to-be-used catalyst in mind, as catalysts have certain advantages or restrictions based on feedstock and desired products, amongst other things.

Potential FT catalysts are based on iron, cobalt and ruthenium, although iron-based and cobalt-based catalysts are most common for industrial applications. Cobalt and ruthenium suffer from high methane selectivity at higher reaction temperatures, where methane selectivity remains low for iron-based catalysts. Ruthenium is the most active catalyst and can be used at the lowest temperature while still producing long hydrocarbon chains. Nevertheless, the high price of ruthenium bars it from being applied in industry.

With the information just supplied, it should not be a surprise that iron-based catalysts are most often, although not exclusively, used in HTFT processes. Its lower methane selectivity compared to cobalt at high temperature makes it a good candidate for HTFT processes, especially if you consider the susceptibility of iron-based catalysts to deactivation, which occurs more frequently in longer reactor runs. Cobalt-based catalysts, in comparison, have a higher conversion per pass due to a lack of water inhibition, as cobalt-based catalysts demonstrate no water gas shift activity in contrast to an iron-based catalyst. The higher conversion, combined with the lower methane selectivity at lower temperatures, are important reasons for the frequent use of cobalt-based catalysts in LTFT processes.

Two very important aspects that are usually first to be considered are the feedstock and the desired products. As syngas' ratios of H_2 to CO vary depending on the feedstock used, a certain catalytic material may be more preferential in particular cases than in others.²¹ Iron-based catalysts benefit from a syngas with low H_2 to CO ratios, due to the exhibited water gas shift activity, where cobalt-based catalysts prefer a higher H_2 to CO ratio. Low H_2/CO ratio syngas originates from coal gasification, where high H_2/CO syngas is derived from natural gas. On top of that, coal-derived syngas generally contains more impurities by which a cobalt-based catalyst is far more like to be poisoned than an iron-based catalyst. It is, therefore, that for coal-derived feedstock, iron is the catalytic material of choice, even more so when the higher price of cobalt compared to iron is taken into account. Finally, concerning the desired products, iron-based catalysts tend to favour olefin products where cobalt-based catalysts favour mainly paraffin products.

1.4 THE SCOPE OF THIS THESIS

As described previously, the world is facing an important energy challenge and it is undeniable that the rational design of the next-generation Fischer-Tropsch catalysts can have a valuable contribution to it. To make sure that catalysis and the FT reaction will play their role as optimal as possible, a greater understanding of catalyst design and the FT reaction mechanism is required. This research, therefore, focuses on elucidating the previously mentioned dynamic surface processes occurring during the FT reaction. More specifically, the deactivation effects of carbon deposition on the surface of a cobalt catalyst nanoparticle during the Fischer-Tropsch synthesis and the reconstruction of a cobalt catalyst surface in the presence of carbon adsorbates to a more favourable structure will be investigated.

Reconstruction effects on cobalt surfaces will be studied through careful analysis of energies and geometries acquired from density functional theory (DFT) calculations. In order to obtain more knowledge about deactivation effects on a cobalt nanoparticle, DFT calculations and grand canonical Monte Carlo (GCMC) simulations on the basis of a ReaxFF reactive force field will be utilized, as well as an in-house written piece of software to recognize the sites on which carbon is deposited. These methods will all be explained more extensively in the next chapter.

Through DFT, information can be obtained on the electronic structure of many-body systems consisting of cobalt, carbon or a combination of both atoms, a property that we use gratefully for the analysis of lateral interactions of adsorbates on the cobalt surface, as well as for the cobalt surface reconstruction, both presented in this thesis. DFT, being a quantum mechanics method, is limited to systems of a few hundred atoms. Therefore,

1.4 The Scope of This Thesis

as a method, it falls short to describe nanoparticles that contain well over a thousand atoms. Nonetheless, the information gained from DFT calculations can serve as a training set for a so-called reactive force field, an energy potential based on a mainly empirical set of parameters. With the help of an in-house developed ReaxFF force field fitting tool, the force field parameters will be adjusted to describe the data obtained from DFT as close as possible. This ReaxFF reactive force field can then be used as an input for the GCMC simulations, herewith describing the energetic environment of the simulation and enabling the molecular modelling of systems on a far larger scale. GCMC itself is a probabilistic method that will try to perform insertions, displacements or removals of carbon atoms on a cobalt nanoparticle.

The utilized cobalt nanoparticle, generated in previous research within the IMC group, was constructed in a similar fashion, using a ReaxFF reactive force field that was fit on cobalt DFT data (in fact, the same cobalt DFT data that was used in this research). After the creation of a suitable force field, the cobalt nanoparticle was created using a molecular dynamics technique, called simulated annealing. This method, however, will not be elaborated upon as this is outside the scope of this research. The ReaxFF reactive force field applied to attain the cobalt nanoparticle is also employed throughout this research, but in an altered form: the training set used to construct the force field has been extended with DFT data on carbon, cobalt carbide and cobalt surfaces with carbon adsorbates in order to accurately describe carbon and the various interactions it has with cobalt.

Once a cobalt nanoparticle has been successfully treated by the GCMC simulations based on this extended ReaxFF force field, a cobalt nanoparticle with carbon deposits should result, which will be subject to investigation. In this investigation, an in-house developed site recognition tool will be employed to recognize and link carbon deposits to distribution sites. The resulting distributions of the insertion sites will be evaluated and compared to the predictions of the ReaxFF reactive force fields used in the corresponding simulations. A visual representation of the research process is displayed in Figure 5.

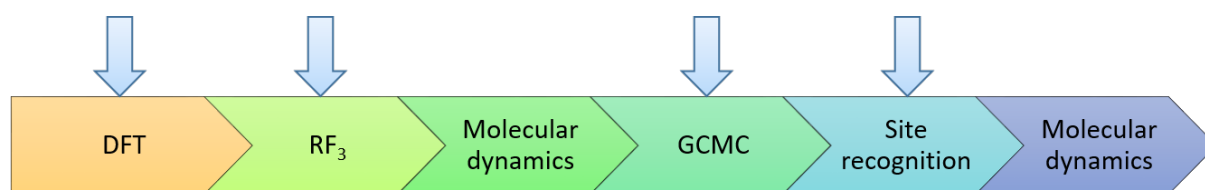


Figure 5: Visual representation of the flow of the different processes in this research. Arrows indicate in which processes this thesis is involved.

2 COMPUTATIONAL METHODS

2.1 DENSITY FUNCTIONAL THEORY

Ever since the discovery of the electron as a fundamental particle in the 1890s, scientists have tried to apply this knowledge on materials and phenomena and, in doing so, have developed important concepts of quantum mechanics and electronic structure theory.²² In recent decades, density functional theory has become the most popular electronic structure method in computational physics and chemistry.²³ The purpose of this section is to highlight, in simple words and terms, the key principles and approximations that form the foundation of DFT and, more importantly, to inform about the manner and conditions under which the computations in this report have been performed, for the purpose of reproducibility.

Since this section reflects only a very brief summary of electronic structure theory and DFT, the interested reader is highly recommended to consult far more elaborate sources on the topic, of which *Modern Quantum Chemistry: Introduction to Advanced Electronic Structure Theory* by Attila Szabo and Neil S. Ostlund and *Electronic Structure: Basic Theory and Practical Methods* by Richard M. Martin are prime examples.^{22,24}

The electronic problem

The main interest of electronic structure theory is finding a solution to the non-relativistic time-independent Schrödinger equation, seen in Equation 2.1.

$$H|\Phi\rangle = E|\Phi\rangle \quad (2.1)$$

Here, H is the Hamiltonian operator for a system of nuclei and electrons, Φ is the wave function and E is the energy. Using Equation 2.1, unfortunately, it is only possible to solve the rather small and simple case of a hydrogen atom exactly. Therefore, to be applicable for larger and more complex systems, it is required to simplify the problem, enabling us to find approximate solutions for the equation.

The Born-Oppenheimer approximation

The Hamiltonian operator described in Equation 2.1 is predominantly constituted by five contributions: the kinetic energies of the electrons and nuclei, the Coulomb attraction between electrons and nuclei, the repulsion between electrons and finally the repulsion between nuclei. Because nuclei have a significantly larger mass than electrons, they move considerably slower than electrons. Therefore, it is assumed within the Born-Oppenheimer approximation that the electrons are moving in a field of fixed nuclei. This assumption leads to approximating the second term of the Hamiltonian, the kinetic energy of the nuclei, as negligible, as well as to the approximation of the final term, the repulsion between the nuclei, as a constant.

Resulting from this, is the electronic Hamiltonian, as shown in Equation 2.2. This in turn results in the Schrödinger equation being simplified to Equation 2.3. In Equation 2.2, the number of electrons and nuclei are represented by N and M , respectively. ∇_i^2 is the

Laplacian operator, involving differentiation with respect to the coordinates of the i th electron. Z_A is the atomic number of nucleus A , r_{iA} is the distance between the i th electron and the A th nucleus and, finally, r_{ij} represents the distance between the i th and j th electron. The equation here is written in atomic units.

$$\mathcal{H}_{elec} = - \sum_{i=1}^N \frac{1}{2} \nabla_i^2 - \sum_{i=1}^N \sum_{A=1}^M \frac{Z_A}{r_{iA}} + \sum_{i=1}^N \sum_{j>1}^N \frac{1}{r_{ij}} \quad (2.2)$$

$$\mathcal{H}_{elec} \Phi_{elec} = \mathcal{E}_{elec} \Phi_{elec} \quad (2.3)$$

Hohenberg – Kohn theorems

Starting from the electronic Hamiltonian, Pierre Hohenberg and Walter Kohn derive two important theorems in their 1964 paper *Inhomogeneous Electron Gas*, which establish an important foundation for density functional theory to be built upon.²⁵ In *Electronic Structure: Basic Theory and Practical Methods*, Martin described the two theorems in a very clear way. The descriptions, although slightly paraphrased, are shown next.

1. The first theorem proves that for any system of interacting particles in an external potential, this potential is uniquely determined by the ground state particle density, with the exception of a constant.
2. The second theorem states that it is possible to define a universal functional for the energy in terms of the density, which is valid for any external potential. For any particular external potential, the exact ground state energy of the system is the global minimum value of this functional, and the density that minimizes the functional is the exact ground state density.

For a more comprehensive and more mathematical derivation of and the proof behind these theorems, it is strongly suggested to read through chapter 6 of Martin's *Electronic Structure: Basic Theory and Practical Methods* or through the original paper by Hohenberg and Kohn.^{22,25}

One can see that we encounter the core of density functional theory in these theorems: computing the electronic ground state. Furthermore, what results from these theorems is the fact that it is possible to reduce the electronic problem from a problem dependent on $3N$ degrees of freedom, with N being the number of electrons, to a problem that is dependent on the density within 3 spatial coordinates. Though Hohenberg and Kohn do not provide the functional for the energy in terms of density, this is not the end of the density functional story, as this is where continued work by Kohn and Lu Jeu Sham comes into view.

Kohn – Sham approach

The Kohn – Sham approach, also referred to as the ansatz, was proposed slightly over a year later than the Hohenberg – Kohn theorems. Published in 1965, the paper *Self-Consistent Equations Including Exchange and Correlation Effects* takes off with the

2.1 Density Functional Theory

ground-state energy of an interacting inhomogeneous electron gas in a static potential, as was derived by Hohenberg and Kohn.²⁶ This formula is presented in Equation 2.4, with $v(r)$ being the static potential, $n(r)$ the density and $G[n]$ the universal functional of the density, which is still undefined, as was mentioned previously.

$$E = \int v(r)n(r)dr + \frac{1}{2} \iint \frac{n(r)n(r')}{|r - r'|} drdr' + G[n] \quad (2.4)$$

Kohn and Sham then continue to define $G[n]$ as

$$G[n] \equiv T_s[n] + E_{xc}[n] \quad (2.5)$$

with $T_s[n]$ as the kinetic energy of a system of non-interacting electrons with density $n(r)$ and $E_{xc}[n]$ as the exchange and correlation energy of an interacting system with density $n(r)$. We will now continue the derivation in a likewise fashion as Kohn and Sham did in their original work.

If we hold Equation 2.1 subject to the condition that the overall density gradient is zero, as described in Equation 2.6, then we obtain Equation 2.7, in which the Coulomb potentials are represented by equation 2.8.

$$\int \delta n(r)dr = 0 \quad (2.6)$$

$$\int \delta n(r) \left\{ \varphi(r) + \frac{\delta T_s[n]}{\delta n(r)} + \mu_{xc}(n(r)) \right\} dr = 0 \quad (2.7)$$

$$\varphi(r) = v(r) + \int \frac{n(r')}{|r - r'|} dr' \quad (2.8)$$

The exchange and correlation contribution to the chemical potential of a uniform gas of density n is given by Equation 2.9 below.

$$\mu_{xc}(n) = d(n\epsilon_{xc}(n))/dn \quad (2.9)$$

From here, with a known φ and μ_{xc} , the density $n(r)$ can be obtained by solving the one-particle Schrödinger equation, shown in Equation 2.10.

$$\left\{-\frac{1}{2}\nabla^2 + [\varphi(r) + \mu_{xc}(n(r))]\right\}\psi_i(r) = \epsilon_i\psi_i(r) \quad (2.10)$$

Here, ϵ_i is the single-electron energy and the density is set to

$$n(r) = \sum_{i=1}^N |\psi_i(r)|^2 \quad (2.11)$$

with N being the number of electrons.

However, equations 2.8 to 2.11 have to be solved in a self-consistent way. With this, we mean that a value for $n(r)$ has to be assumed initially, from which $\varphi(r)$ and μ_{xc} are constructed and, in turn, a new value for $n(r)$ is obtained. From the Hohenberg-Kohn theorems, we have learned that the ground state is defined by the global energy minimum. Therefore, we continue this iterative process until we find no (significant) drop in energy anymore. The equation for the energy is shown in Equation 2.12, where ϵ_j and n and the self-consistent quantities.²⁷

$$E = \sum_1^v \epsilon_j - \frac{1}{2} \int \frac{n(r)n(r')}{|r-r'|} drdr' - \int v_{xc}(r)n(r)dr + E_{xc}[n(r)] \quad (2.12)$$

The exchange-correlation potential $v_{xc}(r)$ is described as

$$v_{xc}(r) = \delta E_{xc}[n(r)]/\delta n(r) \quad (2.13)$$

Still, there remains one problem to be solved: E_{xc} , the exchange-correlation energy, is still unknown. A brief overview of approximations in use to solve this problem is given in the next section.

Exchange-correlation functionals

To accommodate for the unknown value of the exchange-correlation energy, certain functionals and computational methods have been proposed in the past decades to approximate the value E_{xc} . A first relatively simple approximation is the so-called local density approximation (LDA) which can be seen in Equation 2.14. Here, ϵ_{xc} represents the exchange and correlation energy per electron of a uniform electron gas of density n . There are two limiting cases in which exact results can be achieved with the LDA, namely in the case of a slowly varying density and in the case of high density. These results are obtained through approximations that are well described in the Kohn-Sham paper.²⁶ An extension

2.1 Density Functional Theory

to the LDA can be made to adjust for magnetic properties. This approximation is named the local spin-density approximation.

$$E_{xc}^{LDA}[n(r)] \equiv \int \epsilon_{xc}(n(r))n(r)dr \quad (2.14)$$

Another class of functionals are the generalized gradient approximations (GGAs). They are of the shape represented in Equation 2.15, with $f(n, |\nabla n|)$ being a suitably chosen function of the density n and the absolute density gradient $|\nabla n|$.

$$E_{xc}^{GGA} = \int f(n(r), |\nabla n(r)|)dr \quad (2.15)$$

In general, the LDA and its extensions are used for systems that are strongly bound (with the exception of H bonds and van der Waals interactions) in order to obtain good data on molecular structures, vibrational frequencies and charge densities. GGAs are more commonly used to describe thermochemistry and are therefore more suitable to determine energies and structures of systems with strong chemical interactions, such as metals and hydrogen-bonded systems. In more recent times, many adaptations or combinations of these methods with other computational methods have been developed in order to improve on the accuracy or to suit DFT for systems where the mentioned methods fall short. Popular examples are meta-GGAs and hybrid functionals.²⁸

VASP settings

DFT calculations in this report have been performed using the Vienna Ab initio Simulation Package (VASP).^{29–33} In VASP, central quantities are expressed in plane wave basis sets. Interactions in the core regions of the nuclei are described using the projector-augmented wave (PAW) method in order to reduce the basis set size.³⁴ The cut-off energy of the plane waves was set to 400 eV. The criteria for electronic convergence and ionic convergence were set to 10^{-5} eV and 10^{-4} eV, respectively. Partial occupancies were determined using a first order Methfessel-Paxton scheme which employed a smearing width of 0.2 eV.³⁵ Spin polarized calculations were enabled. All the calculations throughout this report were performed with the use of the Perdew-Burke-Ernzerhof (PBE) approximation for the exchange-correlation energy, which is of the GGA type.^{36–38}

The number of points taken for the k -points integration grid was dependent on the size of the calculated structure and the material under study. More k -points generally result in higher accuracy, but this comes at the cost of computational time. Odd integer values between 3 and 13 for the Monkhorst-Pack k -points generation method were analysed in a bulk optimisation within unit cells of small volume.³⁹ The final amount of k -points was selected in such a fashion that a further increase in k -point-density would yield an increase in accuracy of less than 1 kJ/mol and it would thus be too computationally expensive to justify the extra gain in accuracy. Due to a larger length of the periodic box in the z direction, k -points for the z -coordinate were set to 1 for all surface slabs. Furthermore, k -

points were inversely scaled with the expansion of a unit cell and rounded up to the nearest odd integer. For example, increasing a 1x1 unit cell with a determined 9 k -points to a 2x2 unit cell, means that the k -points are scaled with a factor of $\frac{1}{2}$, resulting in 4.5 k -points, which will be rounded up to the nearest odd integer, i.e. 5 k -points.

With the above settings installed, DFT calculations were performed to acquire data on three types of materials, with the intended purpose of using the data to extend the ReaxFF reactive force field that is required for grand canonical Monte Carlo later in the process. These three materials are carbon, cobalt carbide and cobalt surfaces with adsorbed carbon atoms. The latter of these is also used to study lateral interactions, surface reconstruction effects and affinity of carbon for specific surface sites.

For the case of cobalt surfaces with carbon adsorbates, the surface sites of low-index facets of the face-centred cubic structure, resulting from earlier unpublished research within the IMC group, were edited with either a single carbon atom or a combination of two carbon atoms, in such a way that many different unique combination of sites were included. Only threefold and fourfold surface sites were evaluated for behaviour involving dynamic surface processes, as these sites are energetically preferred for atomic carbon deposition over onefold (top) and twofold (bridge) sites. Proof of this will be provided in the next chapter. This procedure was carried out on both the top and the bottom of the surface, with the atoms mirrored through point reflection in order to prevent dipole effects. The energy of the edited surfaces was subsequently calculated through DFT.

The procedure for the carbon and cobalt carbide structures are similar in design. After a k -point analysis for each bulk structure, i.e. diamond, graphene, graphite and cobalt carbide (Co_2C), the procedure was continued by doing bulk structure calculations by calculating a so-called equation of state. The equation of state means that the lattice constant of the crystal structure is varied and the corresponding energies of the resulting structures are calculated. This provides us with a good description of the bulk structure.

Once this has been achieved, we continue with the different types of surfaces for the materials. Using BIOVIA Materials Studio, sections were made on the bulk structure in order to obtain different surface slabs.⁴⁰ These surface slabs, which are subject to periodic boundary conditions, were placed between two vacuum layers of 7.5 Å in the z-direction to avoid undesired electronic interaction between these periodic systems. The energy of these resulting surfaces was calculated with DFT for a 1 by 1 (1x1), 2 by 2 (2x2), and if allowed by computational times a 3 by 3 (3x3) unit cell, in order to verify consistent energies. The calculated energies were compared through the surface energy, which is shown in Equation 2.16.

$$E_{surface} = \frac{E_{slab} - N * E_{bulk}}{2A} \quad (2.16)$$

Here, $E_{surface}$ is the surface energy, E_{slab} is the energy of the surface slab that resulted from the DFT calculation, N is the number of atoms in the system, E_{bulk} is the atom-based bulk energy of the corresponding structure and, finally, A is the surface area of the surface slab.

2.2 ReaxFF Reactive Force Field

If surface energies were consistent, 3x3 unit cells were used for diamond, graphite and graphene and 2x2 unit cells were used for carbon carbides for continued work, in order to have a large periodicity in the system. Surfaces with inconsistent surface energies, as well as surfaces for which the DFT calculations did not converge, are considered to be unstable and are therefore excluded from the data set provided to the ReaxFF reactive force field. These structures are not investigated any further with regards to dynamic surface processes, though a brief speculation on why these structures did not converge is included in the results & discussion chapter. The process continues by expanding the data set with surface defects and stacking faults that are manually introduced to the remaining surface slabs.

Finally, small clusters of atoms were added to the data set. These clusters were found to be stable, according to literature.^{41–45} For carbon, the size of the clusters included ranges from 2 to 19 atoms and also involves multiple isomers. For cobalt carbide, the clusters included are Co_nC_2 , with n ranging from 1 to 5. All calculations for carbon were performed in a unit cell of 17.04x17.04x17.04 Å, for cobalt carbide clusters the unit cell was 10x10x10 Å.

2.2 REAXFF REACTIVE FORCE FIELD

ReaxFF is a program for modelling chemical reactions with atomistic potentials.⁴⁶ It is based on the reactive force field approach developed by Adri C.T. van Duin and coworkers.^{47–49} The idea behind a force field is to use the results of quantum-mechanical calculations on small systems, in our case the data produced through density functional theory calculations, to determine an energy expression; an energy potential which is called the force field.⁵⁰ The force field can then calculate the forces directly for use in molecular dynamics calculations, which it does by solving coupled Newton's equations. The ReaxFF reactive force field, however, is different compared to traditional force fields as it allows for bond breaking and formation during the simulation. In other words: the ReaxFF reactive force field enables reactions to take place during the simulation. It does so by determining connectivity from bond orders calculated from interatomic distances that are updated in every molecular dynamics step. The way the bond order is determined is demonstrated in Equation 2.17.

$$\begin{aligned} BO_{ij} &= BO_{ij}^{\sigma} + BO_{ij}^{\pi} + BO_{ij}^{\pi\pi} \\ &= \exp \left[p_{bo,1} \cdot \left(\frac{r_{ij}}{r_0} \right)^{p_{bo,2}} \right] + \exp \left[p_{bo,3} \cdot \left(\frac{r_{ij}^{\pi}}{r_0} \right)^{p_{bo,4}} \right] \\ &\quad + \exp \left[p_{bo,5} \cdot \left(\frac{r_{ij}^{\pi\pi}}{r_0} \right)^{p_{bo,6}} \right] \end{aligned} \quad (2.17)$$

In this equation, BO_{ij} represents the bond order between atoms i and j , r_{ij} represents the interatomic distance and r_0 the equilibrium bond lengths. The bond parameters are represented by p_{bo} . These bond parameters are empirical as the ReaxFF reactive force field method, like most force field methods, is an empirical method. This also means that

the results can only be validated through extrapolation and comparison to quantum mechanical data or experimental results, as there are no first-principles to fall back on.

Finally, in a similar fashion to most empirical nonreactive force fields, the energy of the system is separated into various partial energy contributions. This is illustrated in Equation 2.18, where E_{system} is the system energy, E_{bond} the bond energy, E_{over} and E_{under} the energies due to over- and undercoordination, respectively, E_{val} is the valence angle energy, E_{pen} is the energy penalty introduced in order to reproduce the stability of systems with two double bonds sharing an atom in a valency angle, E_{tors} is the energy of torsion angles, E_{conj} is the contribution of conjugation effects to the molecular energy, $E_{vdWaals}$ is describing the van der Waals interactions and, lastly, $E_{Coulomb}$ describes the Coulomb interactions. The last two energies are used to describe the long range interactions for all atom pairs. All of the previously mentioned energies are defined by around 100 different parameters per type of atom.

$$E_{system} = E_{bond} + E_{over} + E_{under} + E_{val} + E_{pen} + E_{tors} + E_{conj} + E_{vdWaals} + E_{Coulomb} \quad (2.18)$$

2.3 REAXFF FITTER

To optimize the parameters that are used for the construction of the ReaxFF reactive force field, the ReaxFF Fitter (RF³) software tool was used.⁵¹ RF³ is an in-house developed program for fitting and testing ReaxFF potentials using a training set, which, in the case of this report, is made up from the DFT data calculated by VASP. The program is based on a genetic algorithm that uses Markov chain Monte Carlo iterations for the optimisation of the parameter set. As a starting point for the optimisation, the parameter set of the carbon-cobalt force field of Zhang *et al.* was used.⁵²

As was just mentioned, RF³ requires a training set which is based on DFT data. This data is included through geometries and expressions that have to be evaluated. Geometries are provided through geometry files and labelled in the settings file. With these labels, the expressions are drafted, also in the settings file. A settings file that contains all the geometry files included and all the expressions evaluated can be found in Appendix A. The expressions to be evaluated consist of a mathematical expression that calculates the difference in energy between two geometries, often with respect to the energy of a logically chosen optimum. The reason that there is being fit for energy differences instead of actual energies, is that in actual simulations in which the force field is employed, you will never be interested in electronic or bonding energy, for example. Naturally, we have already obtained this information through DFT. Therefore, to accurately describe chemical phenomena, the relative energy difference between geometries, especially the energy difference with respect to the equilibrium configuration, is much more valuable. Another important reason for this is the fact that the reference energy states for the DFT methods are mostly different from the ReaxFF reference state. Optimisation towards the shape of the potential energy surface is, therefore, much more important than optimisation for its absolute values

2.4 Grand Canonical Monte Carlo

The evaluation of the expressions for the optimisation of the parameter set is done through the minimization of a cost function. This cost function is described by the sum of the weighted squared error between the obtained data from the ReaxFF force field in the training set and the provided target energies based on DFT. The formula for the cost function is given in Equation 2.19.

$$e = \sum_i w_i \Delta_i^2 \quad (2.19)$$

Here, e is the total error, w_i is the weight factor and Δ_i is the difference between the energy of the expression obtained through the ReaxFF force field and the provided target energy based on DFT. Δ_i is more clearly described by Equation 2.20, in which $f_i(S, P)$ is the function as expressed in the settings file. The outcome of this expression is dependent on the systems in the dataset S and the current ReaxFF force field parameter set P . Finally, E_{target} represents the target energy attributed to the corresponding expression which is based on DFT calculations.

$$\Delta_i = f_i(S, P) - E_{target} \quad (2.20)$$

A detailed instruction for a procedure for the extension of a force field using RF₃, developed over the course of this research, is provided in Appendix B.

2.4 GRAND CANONICAL MONTE CARLO

Grand canonical Monte Carlo is a Monte Carlo simulation method that uses a grand canonical ensemble, also known as a μ VT ensemble.⁵³ It employs a fixed temperature, volume and chemical potential, whereas the number of particles is allowed to fluctuate during the simulation. This method is often used to model systems in thermodynamic equilibrium, such as multi-component sorption systems.⁵⁴ Conventional molecular dynamics methods cannot cope with the time-scales required for equilibration and struggle with other computational issues such as having to calculate a large number of computationally expensive gas phase properties, in which there is no interest for most cases. Due to the presence of an interfacial region with different properties than the bulk properties that are of interest, a large system has to be simulated in order to minimise the influence of the interfacial region. The use of a grand canonical ensemble solves most of these problems for sorption studies and it does so by imitating an experimental setup in which the adsorbed gas is in equilibrium with the gas outside of the adsorbent. The gas in contact with the adsorbent can be regarded as a reservoir which, in turn, imposes the equilibrium conditions of temperature and chemical potential on the adsorbed gas. Therefore, when the temperature and chemical potential of the reservoir are known, the equilibrium concentration inside the adsorbent can be determined with GCMC.

At the base of the method used throughout this research is a hybrid GCMC and molecular dynamics method for ReaxFF, originally developed by Thomas P. Senftle.^{55,56} It was later

adapted and added to the ADF-ReaxFF package by the SCM company. For this report, the unreleased ADF2019.102 version is used as the GCMC program. It should be noted that the program, and this version, in particular, is still under development and therefore the application is met with some limitations. As explained in the original paper by Senftle *et al.*, the program works by evaluating three possible Monte Carlo moves: inserting an atom in the system, removing an atom from the system or moving an atom inside the system. For this research, the atom under consideration is carbon. The selection of coordinates for insertion and move-steps, as well as the selection of atoms for removal and move-steps, occurred at random. Once equilibrated, the GCMC procedure results in a detailed balance, where the probabilities of a transition and its reverse transition should be equal. Equation 2.21 demonstrates this probability balance.

$$P_1^{Boltz} P_{1 \rightarrow 2}^{select} P_{1 \rightarrow 2}^{accept} = P_2^{Boltz} P_{2 \rightarrow 1}^{select} P_{2 \rightarrow 1}^{accept} \quad (2.21)$$

In here, P^{Boltz} is the Boltzmann probability that a microstate is occupied, P^{select} is the probability that a transition type is selected and, finally, P^{accept} is the probability that the transition is accepted. P^{select} is ensured to be equal on both sides of the equation by the generation of move types with equal frequency. The probability of accepting a transition, P^{accept} , is different for each Monte Carlo move. The equations of P^{accept} for insertions, removals and displacements (moves) are represented in Equation 2.22, 2.23 and 2.24, respectively.

$$P_{insert}^{accept} = \min \left[1, \frac{V}{\Lambda^3(N+1)} \exp[-\beta(E_2 - E_1 - \mu_{res})] \right] \quad (2.22)$$

$$P_{remove}^{accept} = \min \left[1, \frac{N\Lambda^3}{V} \exp[-\beta(E_2 - E_1 + \mu_{res})] \right] \quad (2.23)$$

$$P_{move}^{accept} = \min[1, \exp[-\beta(E_2 - E_1)]] \quad (2.24)$$

In these equations, N is the number of exchangeable particles in the system before the Monte Carlo move, V is the volume of the system, Λ is the thermal de Broglie wavelength of the exchanged particle, β is the Boltzmann factor given by $\beta = 1/k_b T$, with k_b as the Boltzmann constant and T as temperature, E_1 and E_2 are the potential energies calculated as a function of particle configurations the system before and after the Monte Carlo move, and μ_{res} is the chemical potential of the particle reservoir.

After a Monte Carlo has been executed, the program will carry out an energy minimisation step in order to relax the system and allow rearrangement of atoms. This should result in higher acceptance rates by opening up otherwise occupied positions in the system. However, by applying this relaxation, a bias is introduced to the Monte Carlo algorithm. Fortunately, this bias can be countered by replacing the system volume with an accessible volume for an inserted atom.

2.5 Site Recognition

In summary, the program’s Monte Carlo algorithm consists of three steps, the first being the execution of a Monte Carlo move, the second is the relaxation of atomic forces by energy minimisation and the third is the acceptance or rejection of the Monte Carlo move, which is determined by evaluating Equation 2.22, 2.23 or 2.24, depending on the Monte Carlo move in question, for the resulting geometry after relaxation. The algorithm is then iterated until equilibrium of the system is achieved.

For the data presented in the next chapter, two sets of 50 calculations were performed with exactly the same settings within the 50 calculations. The number 50 was chosen in order to have a large enough sample size for statistical averaging. The only difference between the two sets was the selected force field. In the first case, the force field resulting from the previous chapter was used. For the second set, the built-in force field named ‘CHONSSiPtZrNiCuCo.ff’, developed by Nielson *et al.*, was used for comparison.⁵⁷ Using the ADF ReaxFF program, GCMC calculations were run with bulk periodicity and enabled corrected torsions. GCMC iterations were set to 250 and the temperature was set to 500 K. The accessible volume for insertions was defined by the minimum and maximum distance settings, which were set to 1.0 Å and 2.3 Å, respectively. Energy minimisation was carried out through the FIRE (fast inertial relaxation engine) geometry optimisation method, with the maximum amount of iterations set to 2000. Finally, the chemical potential for carbon was found to be -0.02407931 Hartrees (-15.11 kcal/mol) by calculating the chemical potential for carbon resulting from the reaction shown in Equation 2.25 at equilibrium, based on data collected by the Eduard-Job-Foundation for Thermo- and Matterdynamics.⁵⁸ This seemed like a suitable choice, given the fact that this is the actual reaction occurring during the Fischer-Tropsch synthesis that is responsible for the presence of carbon on the catalyst surface.



2.5 SITE RECOGNITION

Once particles have been treated with the grand canonical Monte Carlo method, the resulting structures have to be inspected for the locations of the inserted carbon atoms. This is done through a two-step process: at first, an analysis of the original nanoparticle itself is performed, followed by an analysis of the inserted atoms using the output of the previous particle analysis. The analysis is carried out using an in-house developed program.

For the first analysis, a so-called common neighbour analysis (CNA) method is employed.⁵⁹ This method tries to identify local structure based on the topological relationships between nearby particles. The CNA algorithm starts off by defining a chosen cut-off radius and generating a neighbour list of particles that fall within range. For a particle i , the cut-off radius $r_{cut}(i)$ is defined as in Equation 2.26, with \vec{r}_{ij} being the displacement vector between the particles i and j . The sum is being applied over a sorted list of nearest neighbours. In this research, this results in a cut-off radius of approximately 3 Å.

$$r_{cut}(i) = \left(\frac{1 + \sqrt{2}}{2}\right) \left(\frac{1}{6} \sum_{j=1}^6 |\vec{r}_{ij}|\right) \quad (2.26)$$

To continue, for each of these particles, three characteristics are computed that compose a CNA index of a neighbouring particle, and, when all CNA indices are taken together, can be used to construct a CNA signature of the central particle. These three characteristics are the number of adjacent nodes, the number of edges between those nodes and the length of the longest path among only those edges. This will be explained more elaborately with the help of Figure 2.1. In the figure, part (I) describes the cut-off radius being applied to determine the positions of the neighbouring particles of the central particle '0'. Particle 0 is surrounded by nine other particles within the cut-off radius, meaning that the equation for the cut-off radius, Equation 2.26, is being evaluated once again for all of the nine particles in order to construct a binary adjacency matrix (II) of the neighbourhood. Note that the original particle, particle 0, does not take part in this neighbourhood and is, therefore, left out of this adjacency matrix. The adjacency matrix can then be converted to a more graphical illustration of the neighbour: the neighbourhood graph (III). From the neighbourhood graph, the CNA indices can be calculated. First, the number of adjacent nodes is evaluated by counting the number of nearest neighbour nodes. Then, the number of edges connecting these nodes to each other is evaluated and lastly, the length of the longest continuous path that can be constructed among those edges is looked at. The collection of all these indices is then bundled to create a set that makes up the CNA signature of particle 0.

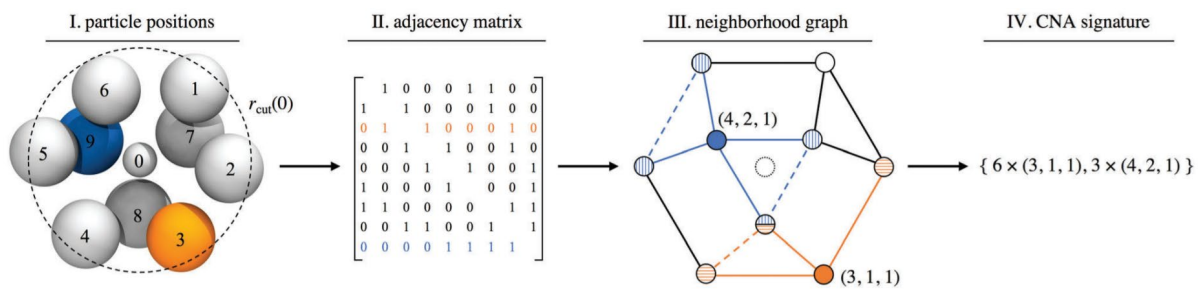


Figure 2.1: Schematic illustration of the CNA analysis. Image was taken from W.F. Reinhart et al., 2017. ⁵⁹

Fortunately, Figure 2.1 provides us with two examples to work out for acquiring a more deep understanding. The construction of an adjacency matrix for particle 3, the orange particle, and particle 9, the blue particle, is visualised. From part II and part III, the adjacency matrix and the neighbourhood graph, it can be seen that particle 3 and particle 9 are connected to three and four other particles, respectively. This can be observed either by counting the number 1 in the row of matched colour in part II or by counting the number of solid lines in their respective colours. Then, by counting the number of dashed lines between the connected particles, the number of connecting edges can be established, which results in one edge for particle 3 and two edges for particle 9. Finally, the length of the longest continuous path can be told by counting the number of connected dashed lines of the same colour, which, in this case, is one for both particles. As a result, the CNA indices for particle 3 and for particle 9 are $(3, 1, 1)$ and $(4, 2, 1)$, respectively. Upon further analysis, it would show that particles 1, 2, 4, 5 and 6 are equivalent to particle 3 and that particle 7 and 8 are equivalent to particle 9. This would result in a set of 6 indices of $(3, 1, 1)$ and 3 indices of $(4, 2, 1)$, together constructing the CNA signature of particle 0 to be $\{6 \times (3, 1, 1), 3 \times (4, 2, 1)\}$, as was shown in part IV of the image.

2.5 Site Recognition

Once the CNA analysis of the original nanoparticle has been completed. There can be continued with the second step of the process. The second step has a strong similarity to the first in that it also starts by applying the cut-off radius, this time by evaluating it for the inserted atoms to find only the nearest neighbours. By trial and error, it is found that 2.4 Å is a well-suited value for the cut-off radius in this step in order to include the nearest neighbours of the inserted atom, exclusively. In contrast to the first step, the second step does not construct an adjacency matrix in order to obtain CNA signatures for the inserted atoms. Instead, it uses the already determined CNA signatures, resulting from the previous analysis, of the particles within the cut-off range to construct a combination of signatures, which is then linked to a built-up library in order to determine the location of the inserted atom. Thus, in the case of this research, the carbon atoms inserted are coupled to the CNA signatures of the neighbouring cobalt atoms of the original nanoparticle. Regrettably, the library in use is fairly limited and can therefore only be employed to determine well-defined cases of 100, 110, 111 and 211 surfaces with a face-centred cubic crystal structure. This library includes a selection of top, bridge, threefold and fourfold sites on the previously mentioned low-index facets. Body-centred cubic structures and hexagonal close-packed structures, as well as poorly defined sites on the edges of the nanoparticle, are therefore mostly unrecognized by the program at the present stage. Hence, only a shallow analysis can be performed.

3 RESULTS & DISCUSSION

3.1 LATERAL INTERACTIONS AND SURFACE RECONSTRUCTION

In order to study dynamic surface processes involving lateral interactions and surface reconstruction effects, a careful analysis of data obtained through density functional theory was carried out. Within this study, a set of cobalt surface slabs with the face-centred cubic (fcc) crystal structure has been covered with one or two carbon atoms per side of the surface. These covered surfaces were then subject to DFT calculations after which the results were examined for energies and geometries. The surfaces investigated were the fcc(100), fcc(110), fcc(111) and fcc(211) surfaces. As important background information, the energies of these surfaces without adsorbates are given in Table 3.1.

Table 3.1: Energies of used cobalt surfaces without adsorbates.

Surface	fcc(100)	fcc(110)	fcc(111)	fcc(211)
System energy (eV)	-429.285	-422.783	-434.186	-788.223
Number of cobalt atoms	63	63	63	117
System energy per atom (eV)	-6.814	-6.711	-6.892	-6.737
Surface energy (eV/Å ²)	0.155	0.151	0.128	0.151

From this table, it can be seen that of the surfaces without adsorbates the fcc(111) is the most stable surface, as its surface energy is the lowest. This can easily be explained by the fact that out of the four different surfaces the surface atoms in the fcc(111) surface have the highest coordination numbers, which is a favourable situation. In general, coordination numbers of corrugated surfaces are slightly lower, which is in accordance with the resulting energies for fcc(110) and fcc(211) presented in Table 3.1. The surface energies of the fcc(110) and fcc(211) surfaces seem to be approximately equal and are, as a result, likely equally preferred. Albeit Table 3.1 is showing that the system energy per atom of fcc(100) is lower in energy than its fcc(110) and fcc(211) counterparts, this energy is apparently concentrated on a smaller surface which results in a higher surface energy for fcc(100) than for the other three surfaces. Based on this information, the fcc(100) appears to be the least stable. The difference, however, is only 0.004 eV/Å, which is rather small. Therefore, only a small preference for the fcc(110) and fcc(211) surfaces is expected and a larger preference for the fcc(111) can be anticipated. Thus, it is very likely that on a cobalt nanoparticle of sufficiently large size, the fcc(111) facets will be most present.

The research continues by inducing carbon atoms to surface sites for each of the surfaces. The sites were chosen in such a way that a wide range of unique combinations is covered for single carbon atoms and pairs of carbon atoms. Schematic illustrations of the chosen surface sites for the different surfaces can be found in Figures 3.1 to 3.6. In here, the blue circles represent the cobalt atoms forming the depicted surface, the smaller black circle represents a carbon atom adsorbed on a surface site that was evaluated for the single-atom case and the red circles represent the sites of carbon atoms that were covered to form a pair with the black carbon atom. For clarity, evaluated combinations always exist of the black-coloured carbon atom and one of the red-coloured carbon atoms. Combinations of red-coloured carbon atoms are not evaluated, although they might in some cases be identical to the black-red combinations evaluated due to the periodicity of the surface. It should also be noted that some combinations that could intuitively be expected based on

the figures presented, are, in fact, mirror images of evaluated combinations and are, therefore, energetically identical and are hence not included. A visualisation of all the geometries of the initial input state and the geometries resulting after DFT calculations, as well as the resulting energies, is included in Appendix C. To keep things simple, only the most relevant images and energies are included in the continuation of this section.

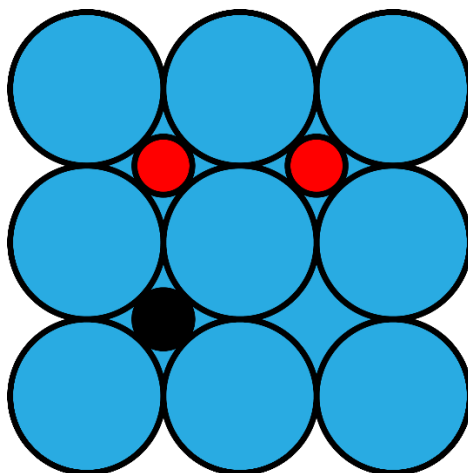


Figure 3.1: Schematic representation of combinations on an fcc(100) surface.

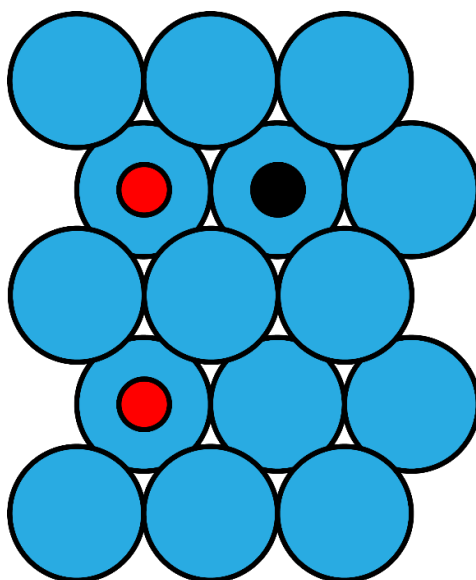


Figure 3.2: Schematic representation of the first set of combinations on an fcc(110) surface.

3.1 Lateral Interactions and Surface Reconstruction

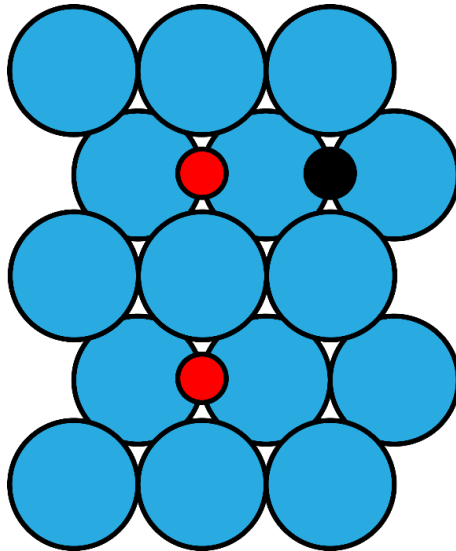


Figure 3.3: Schematic representation of the second set of combinations on an fcc(110) surface.

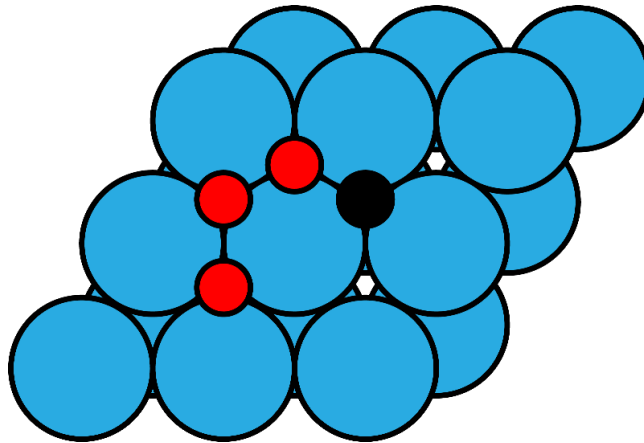


Figure 3.4: Schematic representation of combinations on an fcc(111) surface.

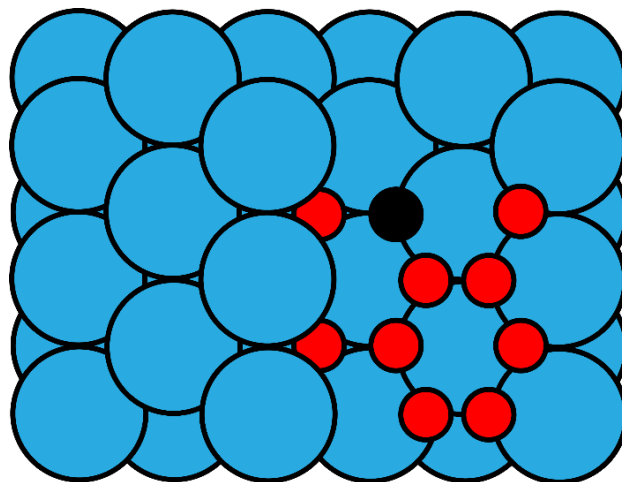


Figure 3.5: Schematic representation of the first set of combinations on an fcc(211) surface.

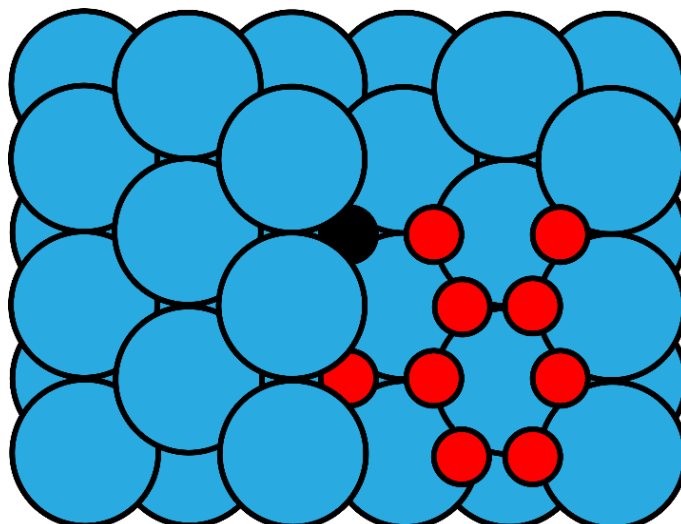


Figure 3.6: Schematic representation of the second set of combinations on an fcc(211) surface.

Evaluation of site and surface affinity

Before more detailed results are considered, it is good practice to confirm assumptions about preferential binding sites. It is expected that a fourfold site will be the most favourable site for a carbon atom to be adsorbed on, due to the fact that carbon endeavours to have a coordination number of 4. Subsequently, it is anticipated that lower coordination results in a less favourable site, resulting in preference of threefold sites over twofold sites and twofold sites over onefold sites. To verify this assumption, the adsorption energies for different sites are compared in Table 3.2. System energies for onefold and twofold sites are calculated through DFT by only evaluating the initial input geometry in a single run since it is expected that longer DFT runs will converge towards a different, supposedly more stable result. The adsorption energy is defined as the difference between the system energies of the system with one adsorbate on the surface and the empty surface plus the energy of one gas-phase carbon ion. It should be noted that, unfortunately, not all surfaces contain (stable) three- or fourfold sites and therefore comparisons between different surfaces will have to be made. As an incidental coincidence, this enables the comparison of adsorption on different surfaces as well.

Table 3.2: Comparison of adsorption energies for different sites and surfaces.

Surface	Adsorption energy (eV)			
	onefold	twofold	threefold	fourfold
Fcc(100)	-3.383	-5.011	-	-8.062
Fcc(110) set 1	-3.362	-4.342	-	-7.397
Fcc(110) set 2	-	-	-	-7.295
Fcc(111)	-3.499	-5.148	-6.724	-
Fcc(211)	-1.778	-3.087	-	-7.700

From the results in Table 3.2, it can be concluded that the assumption about the preference towards binding sites with a higher coordination number for carbon is correct. There is a clear trend noticeable in decreasing adsorption energies for sites resulting in lower coordination numbers. What can also be concluded from these results, is that the fcc(111)

3.1 Lateral Interactions and Surface Reconstruction

surface seems to be less prone to adsorption in general, due to the absence of more favourable fourfold sites. Finally, there also seems to be an energetic difference between adsorptions on different fourfold-containing surfaces, where the fcc(100) appears to be the most favourable and fcc(110) the least favourable to adsorb upon.

Fcc(100)

DFT calculations show that the two fcc(100) combinations evaluated are somewhat similar in energy. These combinations, which will further be addressed to as ‘100A’ and ‘100B’ are visualised in Figure 3.7 and 3.8. Their system energies, based on a system of sixty-three cobalt atoms and four carbon atoms, two on each side of the surface slab, can be found in Table 3.3.

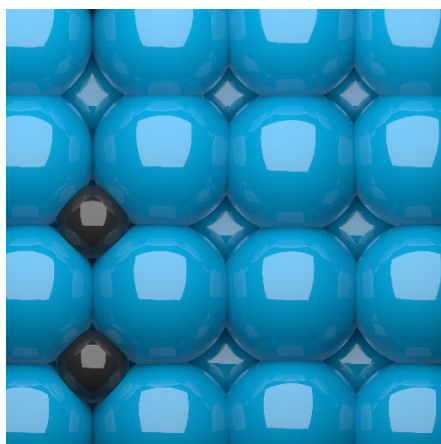


Figure 3.7: Combination 100A.

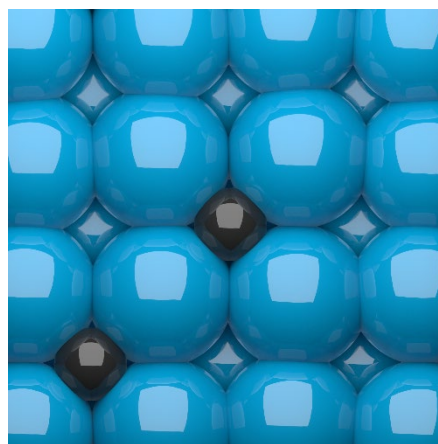


Figure 3.8: Combination 100B.

Table 3.3: System energies of cobalt fcc(100) surfaces with different combinations of carbon atoms adsorbed.

Combination	100A (Figure 3.7)	100B (Figure 3.8)
System energy (eV)	-466.660	-466.986

With a difference of approximately 0.32 eV in energy, it can be assumed that there is a prevalence of the 100B combination to be expected. This difference in energy can most likely be explained by the fact that the adsorbed carbon atoms ‘sink’ a little into the fourfold sites of the surface. This is expected to cause a small surface tension, which in the case of combination 100B, might be slightly lower due to the fact that the displacement energy caused by the carbon atoms can be distributed over eight different cobalt-cobalt bonds. For the case of 100A, there are only seven cobalt-cobalt bonds available for the displacement energy to be distributed over. An additional energetic effect that might play a role is a lateral interaction between the carbon adsorbates. Both adsorbates have already bound to four atoms, which is the favoured configuration for carbon, and therefore, it would be expected that the presence of an additional carbon atom would lead to a repulsive effect in order to prevent the formation of a fifth bond. If this repulsive effect plays a role, it is presumably less expressed for combination 100B due to the larger distance between the carbon adsorbates. With this being said, neither 100A nor 100B display any further observable mesoscale phenomena.

Fcc(110)

For the fcc(110) surfaces, two sets of DFT calculations were performed in the manner demonstrated in Figures 3.2 and 3.3. To start, the set of calculations shown in Figure 3.2 will be discussed, as this yields particularly interesting results. Both resulting geometries are displayed in Figure 3.9 and 3.10 and will be further referred to as '110A' and '110B', respectively. From these figures, it can be seen that both 110A and 110B exhibit fascinating behaviour. In both figures, it is clearly visible that some sort of contraction of cobalt atoms occurs around the adsorbed carbon atoms. What is more interesting, however, is that due to this contraction, the surface around the carbon adsorbates starts to resemble the previously inspected fcc(100) surface, which is a sign of surface reconstruction. To further the understanding of the cause and probability of occurrence for this dynamic surface process, the remaining combinations, given in Figure 3.11 and 3.12 and designated '110C' and '110D', will be investigated first.

When first examined, it can be seen that similar contractions are not present in 110C and 110D. As there are no other anomalies detectable, a logical next step is to compare system energies. From Table 3.4, we can conclude that the energy difference between 110C and 110D is approximately 0.3 eV, which is, surprisingly, almost equal to the energy difference that was found for combinations 100A and 100B. Given the similarities between the geometries of 100A and 100B compared to 110C and 110D, it is no strange idea to employ the same reasoning that was used in the fcc(100) section. Once again, the more favourable system has more bonds available to effectively incorporate the displacement caused by the carbon adsorbates. Additionally, repulsive interactions between carbon adsorbates might play a role once more, especially for the 110C case. When the comparison of the system energies is extended to combinations 110A and 110B, it can be observed that 110A is lowest in energy and, therefore, supposed to be the most stable combination, whereas 110B is apparently the least stable combination. If it is assumed that the observed contraction is an energetically favourable effect, which is not an unreasonable assumption to make, considering the system energies obtained through DFT, then the argument could be made that the same effect that is creating stability for the 110D case, is adversely affecting the stability of the 110B combination. To explain this further: in this case, the displacement caused by the carbon adsorbates seems to have an energetically favourable effect, which can be expected, given the favourable configuration of carbon that results. So far, however, the fact that this displacement effect can be distributed over multiple bonds has been assumed to be favourable, but when applying the same logic to this situation, it is essentially counteracting an effect that has been proven by DFT to be energetically favourable. This also seems to be somewhat observable in Figure 3.10. If this logic endures, it would serve to be an acceptable justification for the lower system energy encountered. Nonetheless, with the results provided and the explanation presented above, there are reasonable grounds to believe that surface reconstruction of an fcc(110) surface towards an fcc(100) surface under the influence of carbon adsorbates might occur for certain areas of the fcc(110) surface.

3.1 Lateral Interactions and Surface Reconstruction

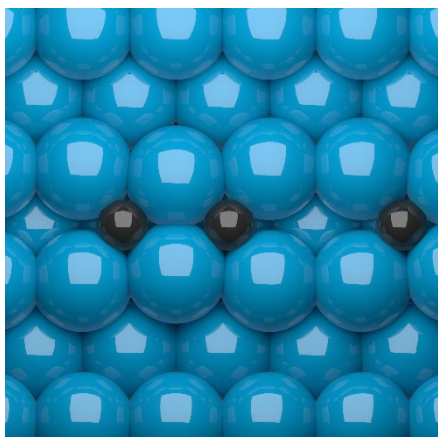


Figure 3.9: Combination 110A.

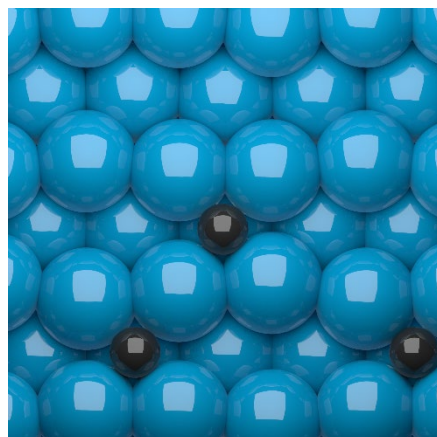


Figure 3.10: Combination 110B.

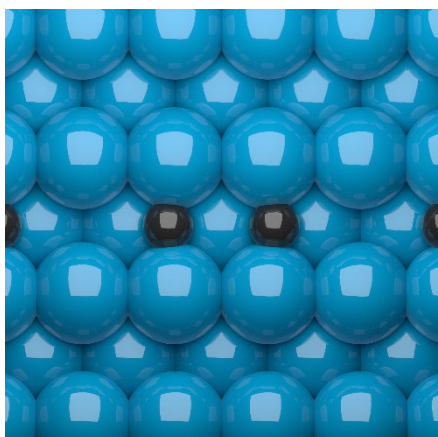


Figure 3.11: Combination 110C.

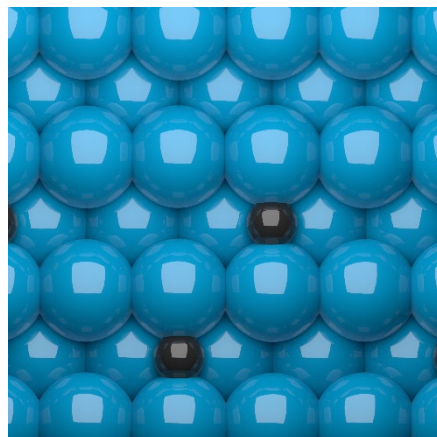


Figure 3.12: Combination 110D.

Table 3.4: System energies of cobalt fcc(110) surfaces with different combinations of carbon atoms adsorbed.

Combination	110A (Figure 3.9)	110B (Figure 3.10)	110C (Figure 3.11)	110D (Figure 3.12)
System energy (eV)	-457.965	-456.668	-456.823	-457.127

In addition to the previously presented results, there are two combinations left that call for some more explanation, as they were unintentionally left out of the set of combinations calculated. These combinations are illustrated in Figure 3.13 and 3.14 and will be named 110E and 110F, respectively. Although DFT calculations have not been performed for these structures, assumptions can be made based on the behaviour that we have seen for the structures 110A, 110B, 110C and 110D. Proving these assumptions to be right with follow-up DFT calculations would be a good demonstration of progressing catalytic understanding based on previously obtained knowledge and therefore it would be worthwhile to investigate these assumptions in further research. Concluding from the previous combinations, it is predicted that some kind of contraction will occur for 110E, but will not occur for 110F. Furthermore, when we employ the already applied logic of more stable combinations when the displacement can be distributed over multiple bonds, assumptions can be made for the system energies relative to the known combinations. Since it was observed that a configuration with more bonds available worked adversely for combination 110B, but to an advantage of combination 110D, it is expected that combinations 110E and 110F are influenced in the same respective ways. To start off with

110E, the amount of cobalt-cobalt bonds available is most likely equal to the situation of 110A, but since the carbon atoms, as well as the cobalt atoms are spread further apart, the contraction effect is most likely less pronounced in 110E. Therefore, the structure of 110E is expected to be less stable than 110A, but it is difficult to predict whether or not it is more stable than 110B. Although there are more bonds available, it can also be reasoned that the contraction effect is impeded more severely since in the case of 110E two atoms are prevented from contracting. So far, the contraction effect has been seen as the main cause of stability and therefore, the assumption is made that 110E will be less stable than 110B. Now, for the case of 110F, the problem simplifies due to the absence of contraction effects and so only bonds have to be counted. From this, it can be concluded that there are fewer bonds available for 110F than there are for 110D and thus, 110F is most likely less stable than 110D. The same amount of bonds are available for 110C and 110F, the main difference being a cobalt atom located between the carbon atoms. Although the effect of this is probably minor, it might help in reducing repulsive interactions between the carbon atoms and hence it can be expected that the stabilities of 110C and 110F are similar with a slight energetic advantage for 110F.

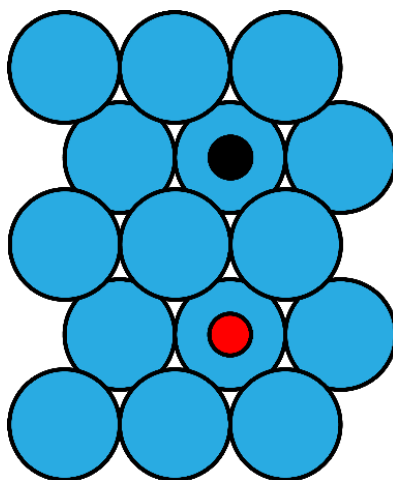


Figure 3.13: Schematic representation of combination 110E.

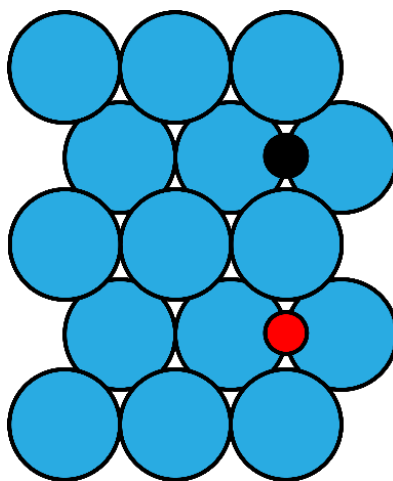


Figure 3.14: Schematic representation of combination 110F.

3.1 Lateral Interactions and Surface Reconstruction

Fcc(111)

Visualisations of the resulting geometries of the three combinations that were illustrated in Figure 3.4 can be found in Figure 3.15, 3.16 and 3.17. The combination displayed in Figure 3.15 will be named '111A'; the combination in Figure 3.16 '111B'; and the combination in Figure 3.17 will be named '111C'.

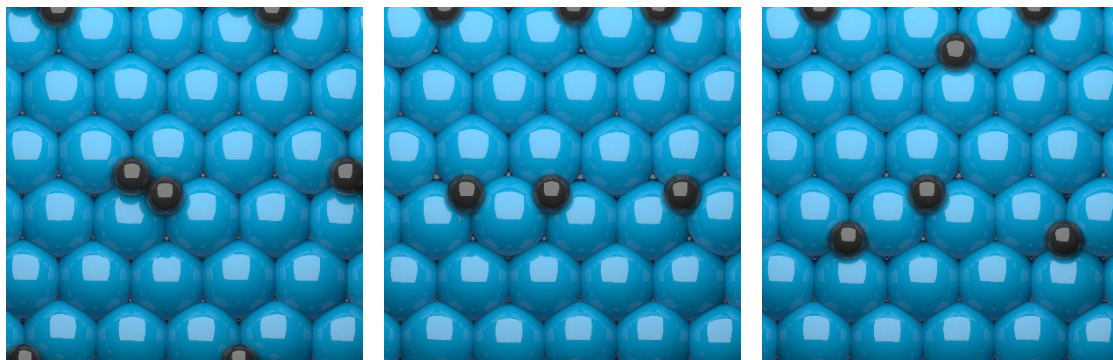


Figure 3.15: Combination 111A. Figure 3.16: Combination 111B. Figure 3.17: Combination 111C.

From these figures, it can be observed that despite the different combinations of carbon adsorbates, the cobalt surfaces seem to remain unaltered. Recalling from Table 3.1 that the fcc(111) surface was the most stable surface of the investigated selection, it is very much possible that this stability is the reason the surface stays unaffected by the carbon adsorbates. As a rule of thumb, the carbon atoms would bind ideally to four cobalt atoms. Be that as it may, but there is no option for carbon to obtain this configuration without severely disrupting the surface, an option that seems highly unlikely given the stable and highly coordinated configuration in which the cobalt atoms are in. Carbon will, therefore, have to conform to a less favourable configuration. Interestingly enough, carbon can find another way to achieve its optimal configuration. Upon closer inspection of Figure 3.15, it can be seen that carbon finds its fourth bond through a lateral interaction with the other carbon adsorbate on the surface, stabilising the carbon adsorbates in the process. This is also supported by Table 3.5, which demonstrates that of the three combinations evaluated, 111A has the lowest energy and is, therefore, the most stable combination. It might also be a possible origin of the formation of graphene layers on the surface, although further research would have to be conducted in order to prove this. The difference in energy between 111A and the other two combinations is also significant, with a difference of around 2.0 eV compared to 111B and 1.3 eV compared to 111C. Comparing 111B and 111C, it is clear that they are similar in the fact that they are both not able to form a lateral interaction. Considering that the carbon atoms in 111B and 111C are respectively 2.96 Å and 3.16 Å apart, and given that the bond length of sp^3 - sp^3 carbon-carbon bonds is 1.54 Å, it is improbable that the carbon atoms are within a close enough range of each other to have a stabilizing effect. This, therefore, means that the attractive forces of the carbon adsorbates resulting from the missing bond will have to be directed towards the cobalt surface. As was encountered many times throughout this section, it is often more favourable to spread out energetic effects over a larger surface area and this is therefore expected to be the most reasonable explanation for the lower energy of 111C compared to 111B.

Table 3.5: System energies of cobalt fcc(111) surfaces with different combinations of carbon atoms adsorbed.

Combination	111A (Figure 3.13)	111B (Figure 3.14)	111C (Figure 3.15)
System energy (eV)	-467.998	-465.927	-466.678

Fcc(211)

As was illustrated in Figure 3.5 and Figure 3.6, a much larger number of different combinations of the fcc(211) surface were evaluated in comparison to the other surfaces, seventeen combinations to be exact. For clarity's sake, only selected geometries will be discussed, but it is highly suggested to consult Appendix C during parts of this section to compare initial and final states of other unmentioned combinations. The geometries that will be discussed are the geometries with the highest and lowest system energy, one additional interesting case, as well as and the single-adsorbate case, which will be discussed first.

For the case of a single carbon adsorbate on the surface, two situations were evaluated: a carbon adsorbate on a fourfold site and a carbon adsorbate on a threefold site. As was expected, the fourfold site has proven to be the more stable adsorption site. Not so much expected, however, was the migration of the carbon adsorbate from the threefold site to the fourfold site. To demonstrate this migration, Figure 3.18 and Figure 3.19 display the initial input geometry and the result after DFT calculations, respectively. This migration of the carbon atom has not been encountered in results for other surfaces, but it is oft-recurring for the results on the fcc(211) surface.

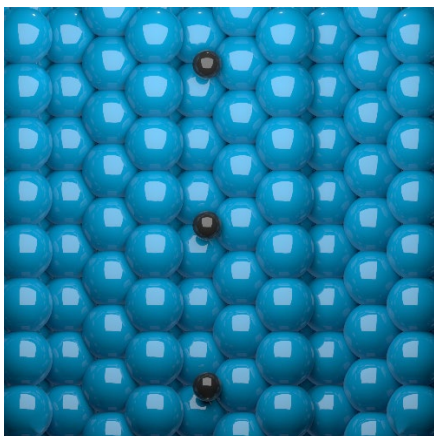


Figure 3.18: Initial input geometry.

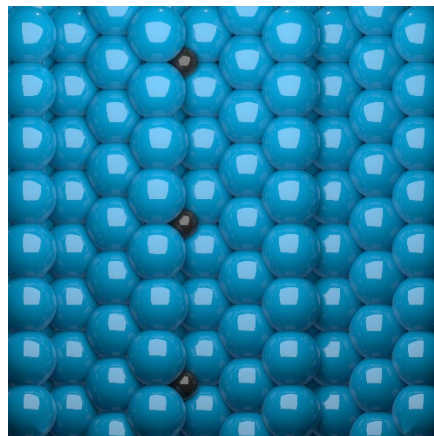


Figure 3.19: Geometry after DFT calculation.

The next case to be discussed is the case of the lowest system energy, i.e. the most stable case. It will be referred to as '211A' and can be seen in Figure 3.20. It is interesting to see, that out of seventeen evaluated cases, four converge to this same result. This means that there have been three combinations for which at least one carbon adsorbate has migrated towards the fourfold sites. The reason that this combination is the most stable is fairly simple to explain: it is the only combination that can accommodate two adsorbates in the energetically most favourable fourfold sites. The system energy is given in Table 3.6, together with the energies of the yet to be discussed combinations '211B' and '211C'.

3.1 Lateral Interactions and Surface Reconstruction

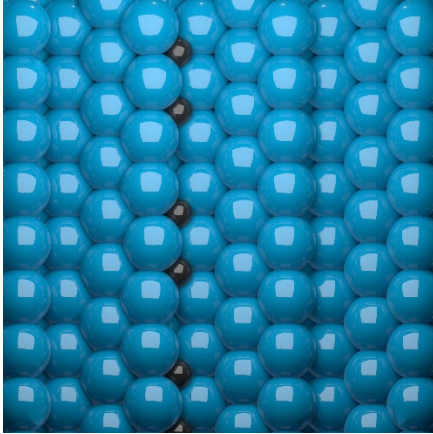


Figure 3.20: Combination 211A.

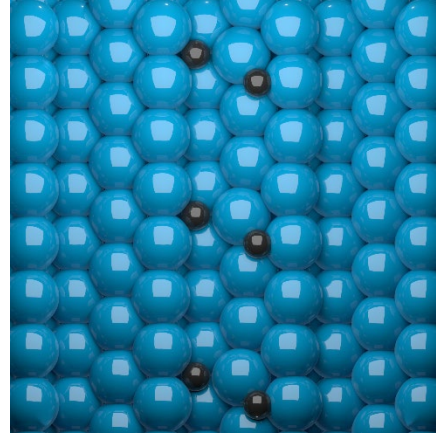


Figure 3.21: Combination 211B.

Table 3.6: System energies of cobalt fcc(211) surfaces with different combinations of carbon atoms adsorbed.

Combination	211A (Figure 3.18)	211B (Figure 3.19)	211C (Figure 3.20)
System energy (eV)	-824.087	-821.467	-823.638

Combination 211B represents the combination that is highest in system energy and therefore the least stable. It is displayed in Figure 3.21. Out of seventeen combinations, a result like 211B only occurred once. The suggested explanation for its lower stability is an interesting trade-off between the stability of both carbon adsorbates. Naturally, the carbon atom bound to the threefold site is looking for a more favourable configuration. The solution it has found is to ‘dig in’ the threefold site, herewith displacing the cobalt atoms forming the threefold. One particular cobalt atom is affected by a large displacement, which is observable in Figure 3.21. Although this displacement is energetically favourable for the threefold-bound carbon atom, it results in a less favourable configuration for the fourfold-bound carbon atom due to the fact that the displaced cobalt atom is driven towards it. This effectively raises the coordination number of the fourfold-bound carbon atom to a less ideal coordination number of five, and one could, therefore, argue that it is no longer fourfold-bound but fivefold-bound.

Combination 211C is a combination found in two out of seventeen. It is the structure lowest in system energy, save for the 211A combination. The geometry of 211C can be found in Figure 3.22. The solution it has found to stabilise the energy is similar to 211B, as it does so by making a trade-off between decreasing the energy of the threefold-bound carbon atom at the cost of increasing the energy of the fourfold-bound carbon atom. It is also similar to the case of 111A, as it decreases the energy of the threefold-bound carbon by engaging in a lateral interaction with the other carbon atom. However, unlike 211B, it stabilises the threefold-bound carbon without displacing the cobalt atoms of the surface. The lack of displacement, combined with the lateral interaction to attain a favourable configuration for the threefold-bound atom, presumably accounts for the majority of the energy difference between the system energies of 211B and 211C.

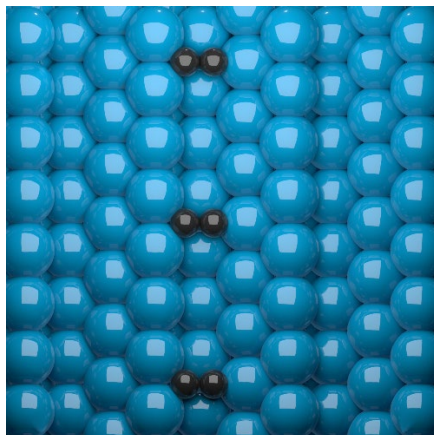


Figure 3.22: Combination 211C.

Evaluation of unconverged calculations

In the process of doing numerous DFT calculations, plenty of calculations have gone wrong due to a wide variety of reasons. Often, this would be caused by human-made mistakes, for example, wrong settings in the input files. Sometimes, calculations would not converge within reasonable times as they were computationally demanding. More interestingly, there were cases where convergence was not reached because DFT had determined an alternative energetic pathway. From all these outcomes, lessons could be learned, some more useful than others. Conveniently, the type of situations encountered can be roughly classified within three categories that coincide with the materials we have worked with: carbon, cobalt carbide and carbon-adsorbed cobalt surfaces.

With regards to carbon, it has been experienced that carbon DFT calculations within the settings used in this research are very sensitive to small deviations. A slightly misplaced atom in the input file could result in an entirely unintended structure, whereas the intended structure could be obtained by correcting these misplacements. This was especially the case for carbon clusters. Calculations of surfaces, surface defects and stacking faults have also been troublesome at times and would oftentimes converge towards strange, amorphous structures. Possibly, this could be reduced by altering the settings of the calculations, such as the smearing.

Considering cobalt carbide, a brief statement can be made about failed calculations. The majority of these calculations involve stacking faults. Out of twenty-five stacking faults considered, eighteen have failed to deliver a useful result. This can either signify that stacking faults for cobalt carbide are frequently unstable, perhaps due to an accumulation of cobalt or carbon atoms in a particular region, or that the method used to construct these stacking faults, mirroring through the centre of the surface slabs, was unviable.

The most interesting lessons have been learned from the unconverged carbon-adsorbed cobalt surfaces. Besides the results that have been discussed above, attempts on fully carbon-covered surfaces were performed. Most of these calculations would, however, end up with a floating layer of carbon, often graphene-like, on top of the surface slab. Many surface reconstruction effects were often involved before this carbon layer started to construct and release itself from the surface. A remarkable case occurred for the fully carbon-covered fcc(100) surface, where carbon atoms would sink deep in the fourfold sites, eventually leading to the displacement of cobalt atoms outside of the surface lattice. These cobalt atoms would pop-up and remain on top of the surface, from where they would lift

3.2 Evaluation and Comparison of a Created Force Field

the remaining carbon atoms, having formed a layer, from the surface. This compelling phenomenon indicates that only a small step towards the unravelling of dynamic surface processes has been made and there remains a whole lot left to be discovered.

3.2 EVALUATION AND COMPARISON OF A CREATED FORCE FIELD

While developing and using the procedure described in Appendix B, an intermediate force field has been constructed to employ in grand canonical Monte Carlo simulations, which will be discussed in the next section. In this section, the constructed force field will be evaluated on its predictive accuracy. This evaluation will take place for the constructed carbon force field, as well as the force field extensions of cobalt carbide and cobalt surfaces with carbon adsorbates. Ideally, the evaluation would be done by comparing the results to the expressions listed in Appendix A. However, since it is often difficult to explain the physical interpretation of an expression (if there is one at all), these expressions have been ‘translated’ into a more easily understandable format: the system energy. This ‘translation’ has been carried out by calculating the energies of the presented structures with the use of the energy difference of the expressions, resulting from the force field prediction, and energies of optima calculated with density functional theory. Nevertheless, the original results of the fitting procedure using the original expressions can be found in Appendix D.

Furthermore, the constructed force field will also be compared to the ‘CHONSSiPtZrNiCuCo.ff’ force field provided by SCM and developed by Nielson *et al.*⁵⁷ As the name suggests, this is a multi-component force field consisting of hydrogen, oxygen, nitrogen, sulphur, silicon, platinum, zirconium, nickel, copper and most importantly carbon and cobalt. It is the same force field that will be used for the comparative GCMC simulation in the next section. From now on, hoping to avoid confusion, this force field will be referred to as the SCM force field (SCMFF). If SCM is not specified, then the constructed force field resulting from this research is referred to. The parameter sets of both force fields can be found in Appendix E.

Finally, it should be noted that since the force field was trained using the same set of geometries that are now being evaluated, the force field has an inherent advantage over the SCMFF, as this was undoubtedly trained using a different training set with a different purpose in mind. Therefore, this comparison is by no means intended to prove the superiority of one force field over the other, but merely to expose the behaviour of both force fields in order to lay a foundation of knowledge that can be accessed to explain the results in the next section.

Carbon force field

First off, the carbon force field constructed throughout this research will be evaluated. To start, the equations of state of some of the many allotropes of carbon will be inspected. Figure 3.23 shows the results for diamond, Figure 3.24 for graphene and Figure 3.25 and Figure 3.26 both show equations of state for graphite. The latter has, in contrast to the former two, a lattice constant that can change in two dimensions independently of one another. Therefore, the change in the x- and y-direction is presented with two of the more favourable lattice parameter of z being kept constant, which are 5.539 Å for Figure 3.25 and 5.875 Å for Figure 3.26. Throughout these figures, it can be observed that there is a clear agreement of the energies predicted by the force field and predicted by DFT. Not only are the differences relatively small, especially near the more-important data points near

the optimum, but also the general trend is very similar. A fit is considered to be a good fit when both the trend is met and the resulting energies per atom are within a range of 10 kJ/mol (or approximately 0.1 eV) of the DFT data, as the accuracy of DFT is generally assumed to be around 10 kJ/mol. There are exceptions, however, depending on the information that should be conveyed. That being said, the just-presented fits are examples of good fits. The predicted energies of the SCMFF, however, are somewhat less in agreement with the energies predicted by DFT, especially for the cases of a lower-than-optimal lattice parameter, where the differences in energy start to increase rapidly. For the structures with a larger lattice parameter, the SCMFF results follow the trend fairly well, except for interpreting the point to the right of the optimum as more favourable than is actually the case for diamond and graphene.

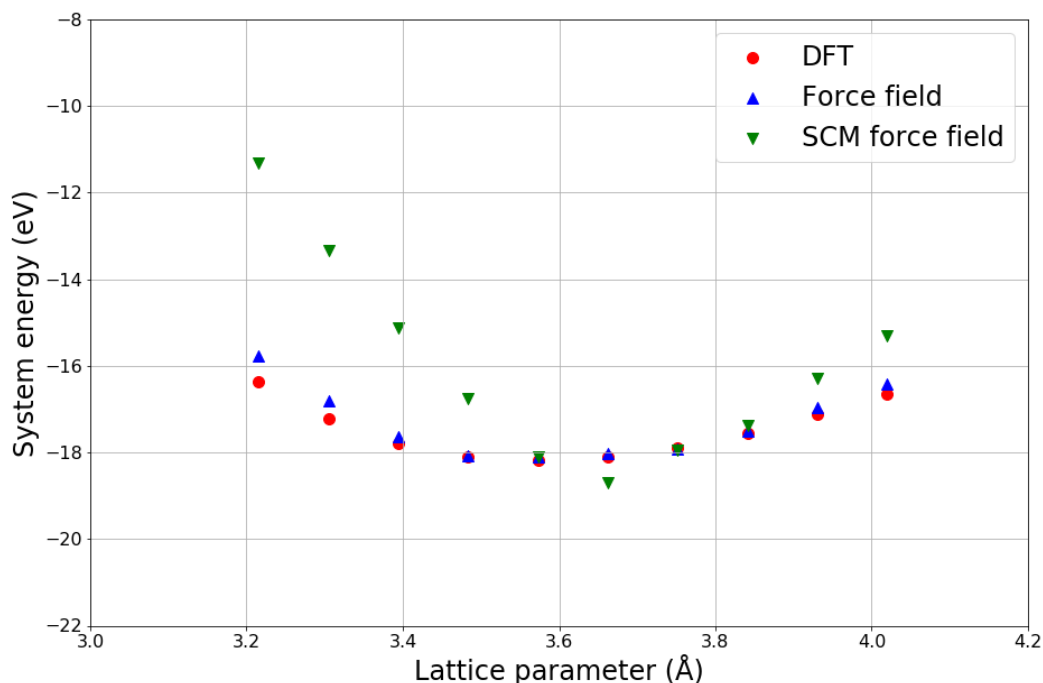


Figure 3.23: Force field results of the equation of state for diamond.

3.2 Evaluation and Comparison of a Created Force Field

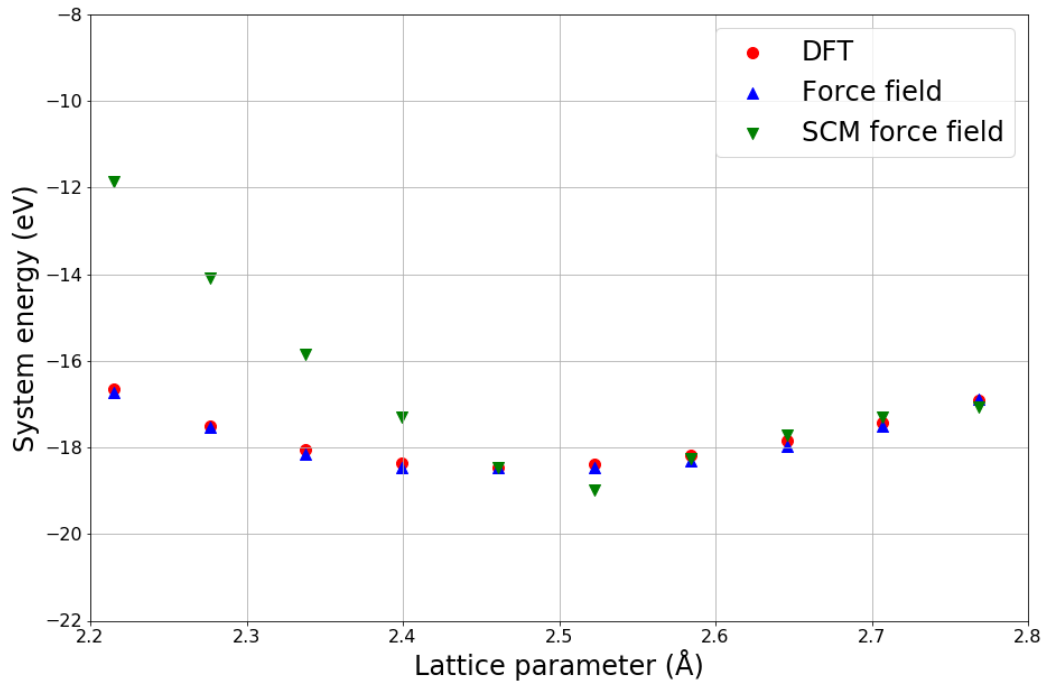


Figure 3.24: Force field results of the equation of state for graphene.

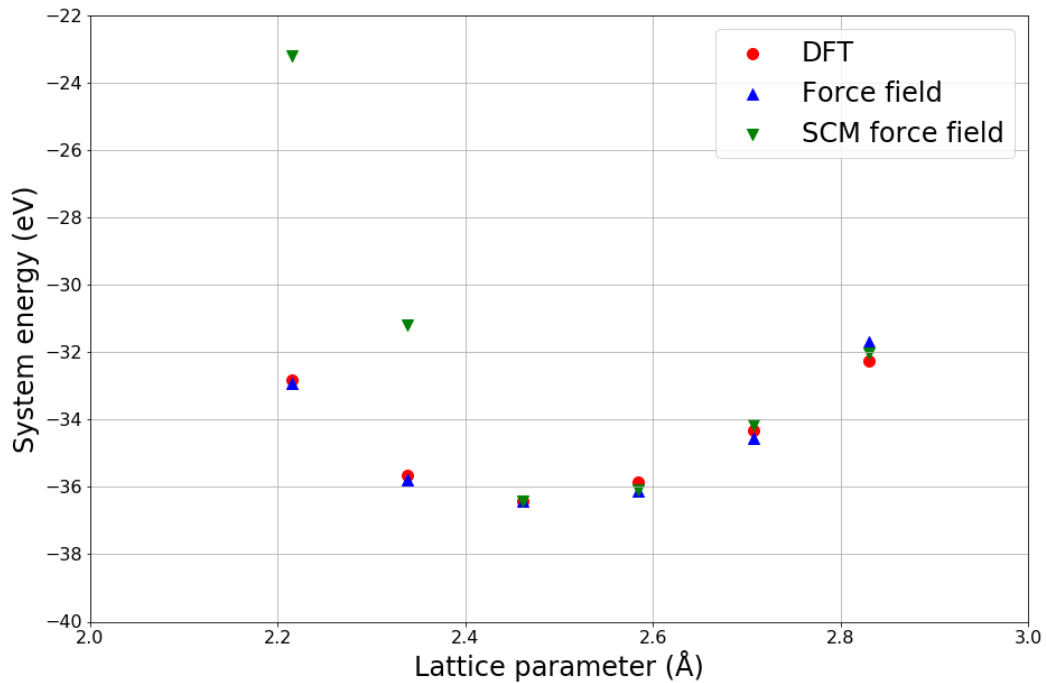


Figure 3.25: Force field results of the equation of state for graphite, with a constant lattice parameter in the z-direction of 5.539 Å.

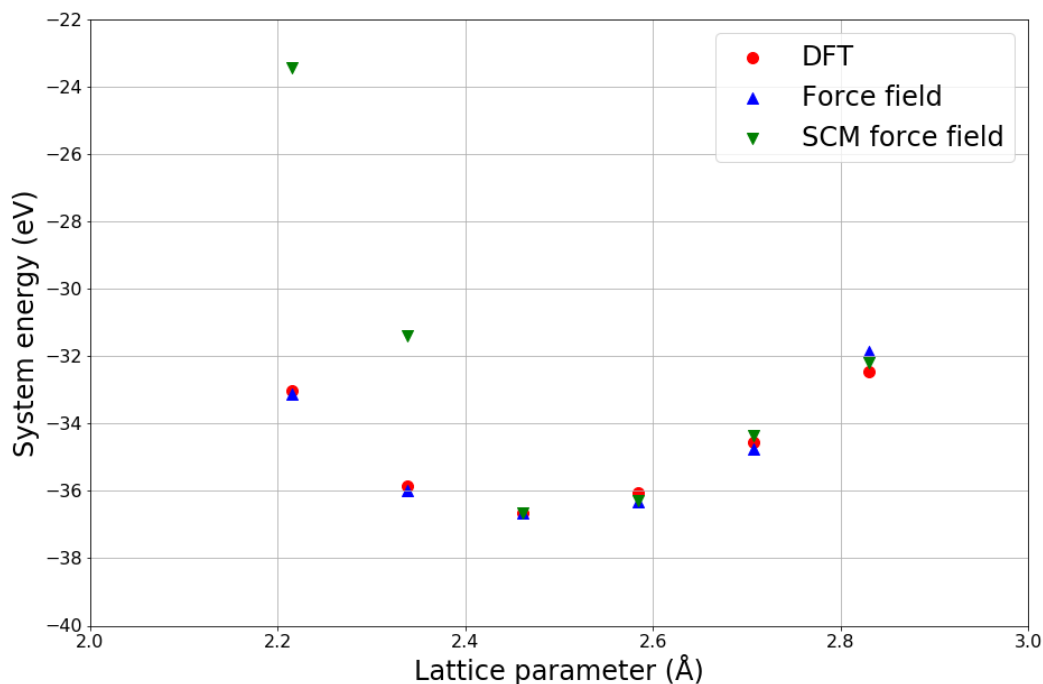


Figure 3.26: Force field results of the equation of state for graphite, with a constant lattice parameter in the z -direction of 5.875 Å.

In Figure 3.27, the few obtained surface structures of diamond are presented. At first sight, it can be seen that the force field shows results relatively similar to the DFT data for all six structures, whereas the SCMFF gives results of the same similarity in three of the six cases. However, it should be noted that since the difference on the scale is very large, a small discrepancy in the graph equals an already significant difference. So, upon closer inspection of the atom-based energies, it turns out that the energy of the diamond 111 surface and its accompanying stacking fault are not within the 0.1 eV range, although the latter falls just barely out of range. For the SCMFF, all atom-based energies fall outside of the 0.1 eV range except for the diamond fcc(110) surface defect.

Figure 3.28 displays the energies of small carbon clusters including carbon atoms in the range of two to nineteen atoms. For clusters consisting of three, four, five or six atoms, multiple different cluster structures have been taken into account. It can be seen that both force fields follow the trend of decreasing energy especially well. The accuracy of prediction is high for the force field created in this research. The SCMFF seems to have a tendency to predict the cluster energies somewhat less favourable than is predicted by DFT, which would likely lead to an even lower formation of clusters than would already be the expected.

In conclusion, it can be assumed that the constructed carbon force field is capable of predicting most of the included results with high accuracy and it should, therefore, form a strong foundation for future research on carbon using (extended) force fields. The SCMFF has been shown to predict with acceptable accuracy in some cases, but based on the presented results, it is not suitable for predicting diamond, graphene or graphite bulk structures with high accuracy.

3.2 Evaluation and Comparison of a Created Force Field

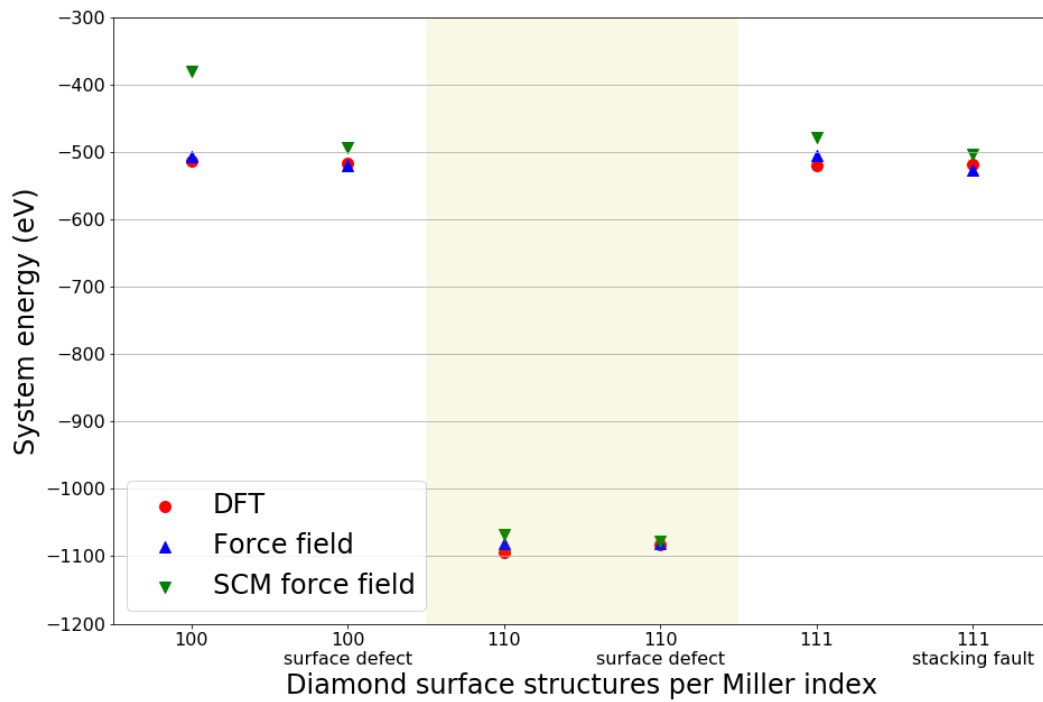


Figure 3.27: Force field results of diamond surface structures for different Miller indices.

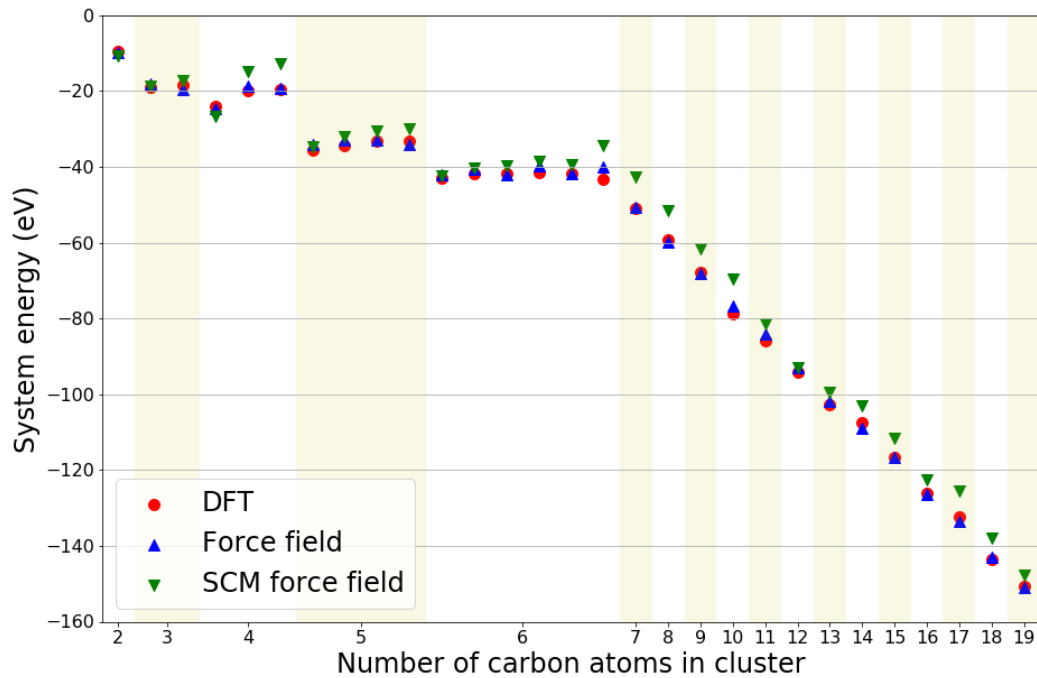


Figure 3.28: Force field results of multiple carbon clusters with atoms ranging from two to nineteen.

Cobalt carbide extension of the force field

As one of the next steps, the force field was extended with structures consisting of both cobalt and carbon atoms, in this case forming the compound of cobalt carbide (Co_2C). Co_2C was found to be the only stable phase composition. Like with carbon, it was started by evaluating the equation of state. The force field results of this are illustrated in Figure 3.29. From here, it can be observed that although the system energy at the optimum lattice parameter is predicted correctly, both force fields have increasing difficulty with accurately predicting the system energies for lattice parameters distanced further from the lattice parameter optimum, especially for higher values of the lattice parameter. For lower lattice parameters, the constructed force field predicts somewhat higher values where the SCMFF predicts slightly lower values. The SCMFF, however, predicts the energy to go even lower with an increasing lattice parameter, herewith falling out of trend with the DFT data. The constructed force field follows the trend considerably better but still fails to predict some data points with sufficient accuracy. A crucial inaccuracy is the data point directly to the right of the optimum, which the force field predicts to be more energetically favourable. In further simulations, this would result in the prediction of cobalt carbide bulk structures with a greater than ideal lattice parameter. Although the constructed force field appears to be the more accurate force field, both force fields are, as of yet, deemed unsuitable for predicting cobalt carbide bulk structures with high accuracy, since based on these force fields GCMC might accept carbon inserts in the bulk structure with higher lattice parameters than the optimum, leading to unrealistic results.

To continue, cobalt carbide surfaces with different low-index Miller indices were evaluated. The derived energies are shown in Figure 3.30. At first sight, the results seem to be quite similar to the DFT values, but it should be noted that since the scale of the system energy is large, a small deviation already results in a large energy discrepancy. On average, the energy difference compared to the DFT data per atom is almost 0.9 eV for the constructed force field and close to 0.4 eV for the SCMFF. Only five out of fifty values, all from the SCMFF results, fall within the desired accuracy ranged of 0.1 eV, specified earlier. Both force fields are thus insufficient for correctly predicting absolute values for the system energy. However, the general trend observed throughout the data points is matched fairly well, especially by the SCMFF. The SCMFF could, therefore, have potential applications in cases where it is important to correctly predict the relative energies between different surface slabs, without needing correct absolute energy values.

Figure 3.31 demonstrates the results of the same cobalt surfaces presented in Figure 3.30, but with created surface defects. Although there are no new conclusions to make based on this information, since the conclusions made for the regular surfaces uphold also in this case, it is good to see that there is at least a form of consistency within the estimates of the force fields.

3.2 Evaluation and Comparison of a Created Force Field

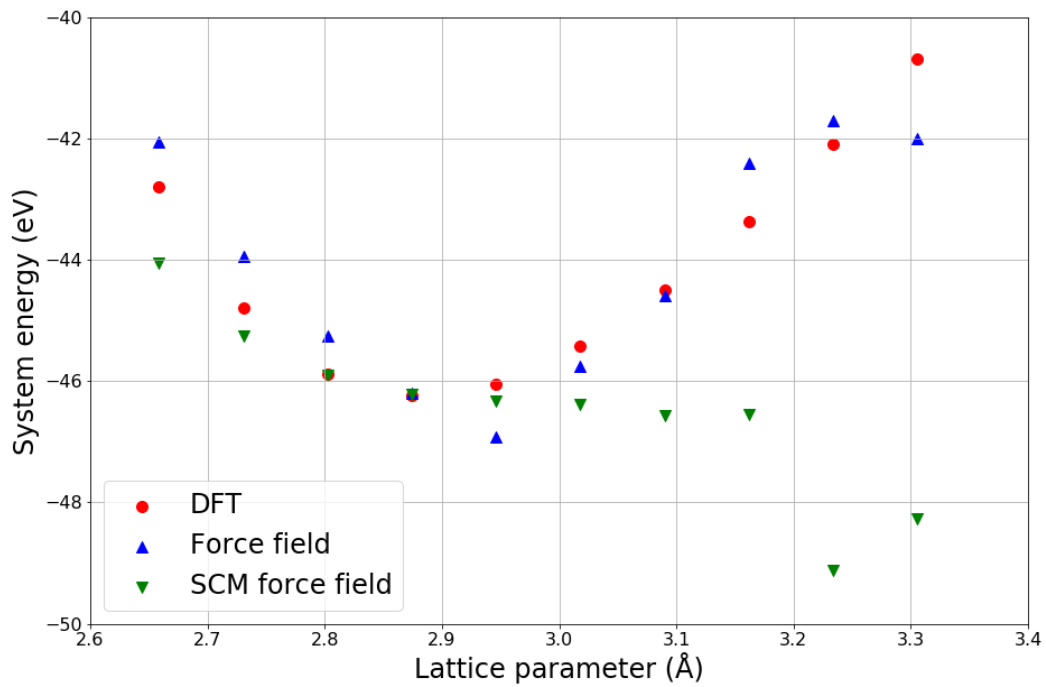


Figure 3.29: Force field results of the equation of state for cobalt carbide.

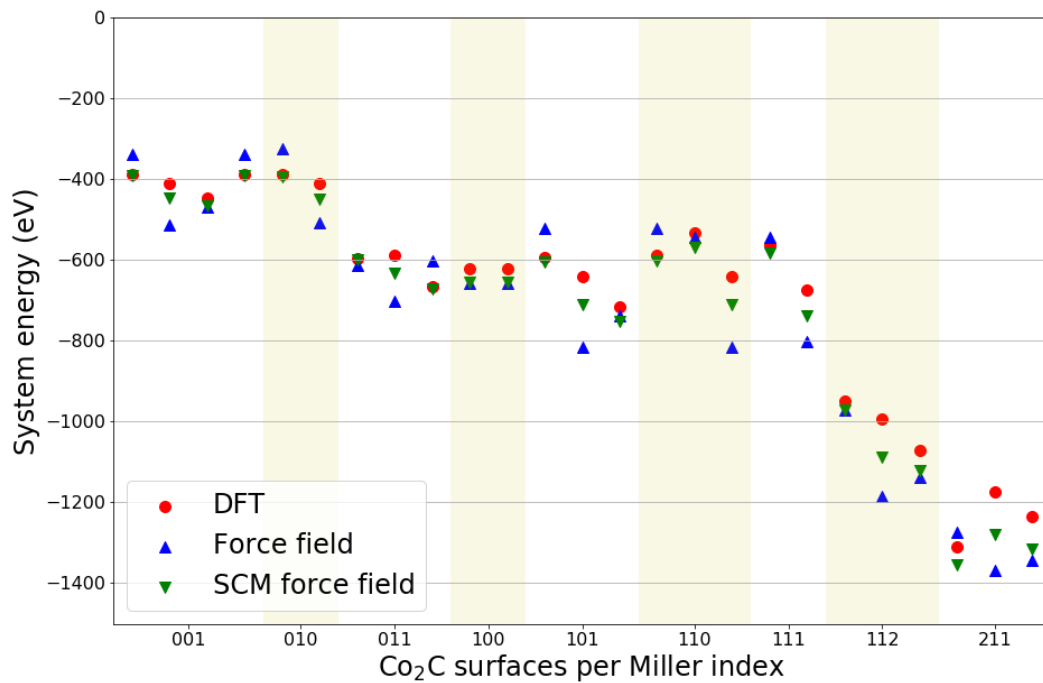


Figure 3.30: Force field results of cobalt carbide surfaces for different Miller indices. Note that there are different options per Miller index, which result from a difference in the top layer of the surface slab, i.e. variations in carbon-cobalt compositions in the top layer result in multiple options.

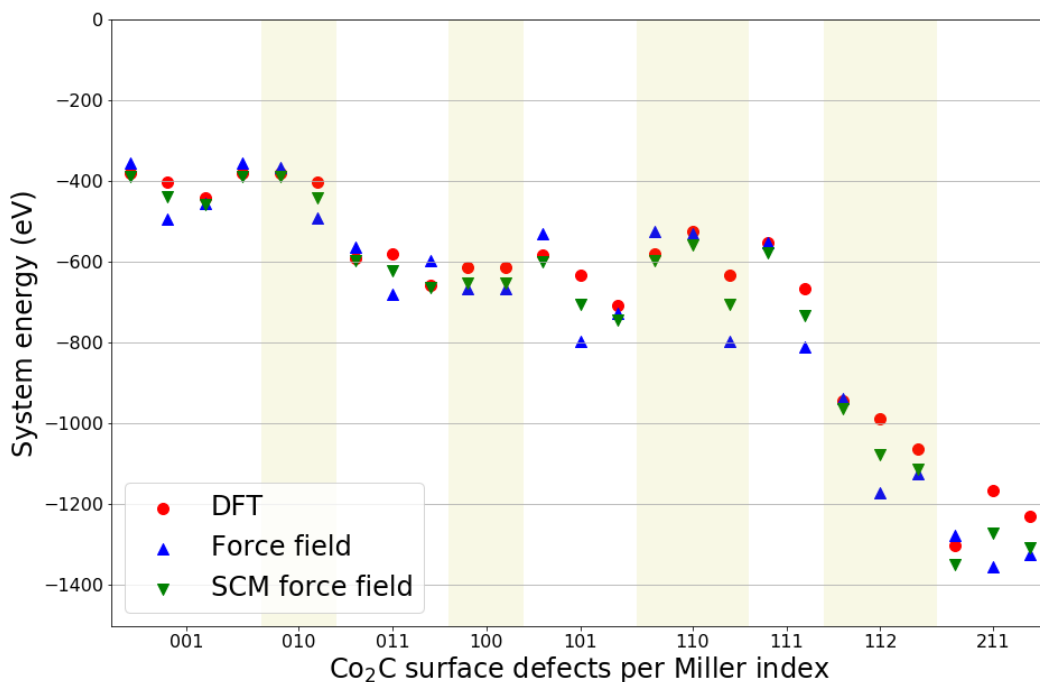


Figure 3.31: Force field results of cobalt carbide surface defects for different Miller indices.

In Figure 3.32, the few successful results of cobalt carbide surfaces with introduced stacking faults are presented. It can be seen that the results for the SCMFF match the DFT data quite well, except for the 111 case. The force field from this research has a large energy difference compared to the DFT data, aside from the second option of the 001 surface. The SCMFF would, therefore, be the preferred force field to use in force field calculations involving cobalt carbide stacking faults.

Finally, in Figure 3.33 the energies of cobalt carbide clusters with different molecular formulas are demonstrated. The constructed force field matches the DFT data relatively well, whereas the SCMFF tends to portray the cobalt carbide clusters as significantly more favourable than is actually the case. Although the SCMFF is not accurate enough to predict absolute energy levels correctly, and the constructed force field most likely is not accurate enough either, they both do convey the message that it is energetically more favourable to create larger clusters or, ideally, nanoparticles, if the trend continues. This is something that can provide useful information to simulations done under the influence of a force field.

Concluding from the illustrated results of cobalt carbide, it can be said that both force fields are far from a desirable accuracy and should thus not be used in situations where this is required. There are, however, some specific niches where both force fields could be of value. These are cases where the absolute energy levels are not important, but rather the relative stabilities are evaluated. Most evident examples encountered were the cobalt carbide surfaces for the SCMFF and the cobalt carbide clusters for the force field constructed throughout this research.

3.2 Evaluation and Comparison of a Created Force Field

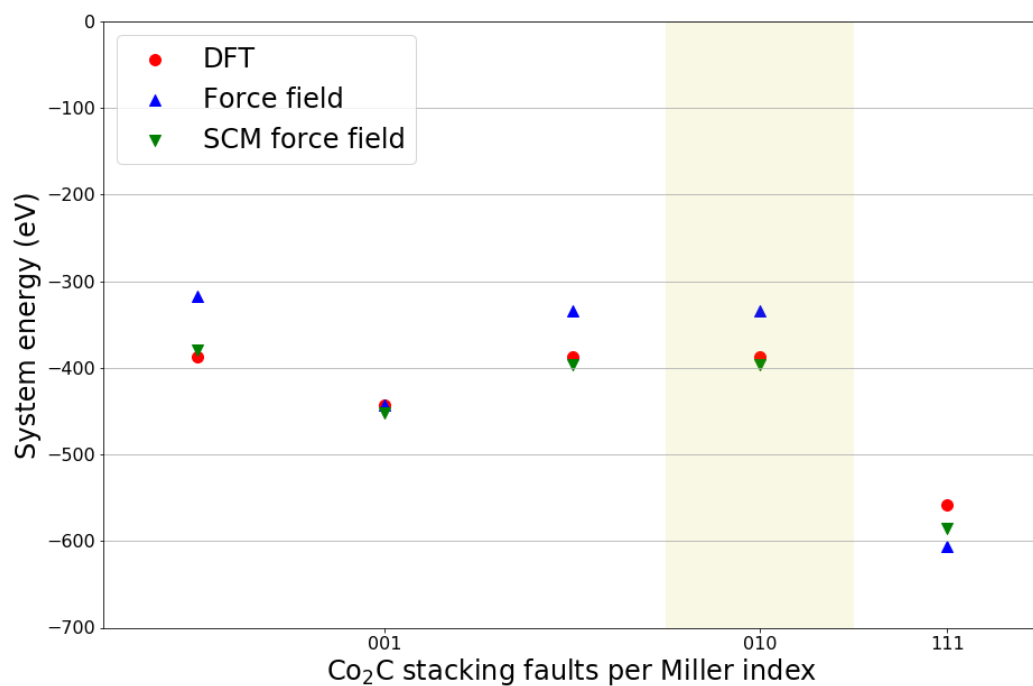


Figure 3.32: Force field results of cobalt carbide stacking faults for different Miller indices.

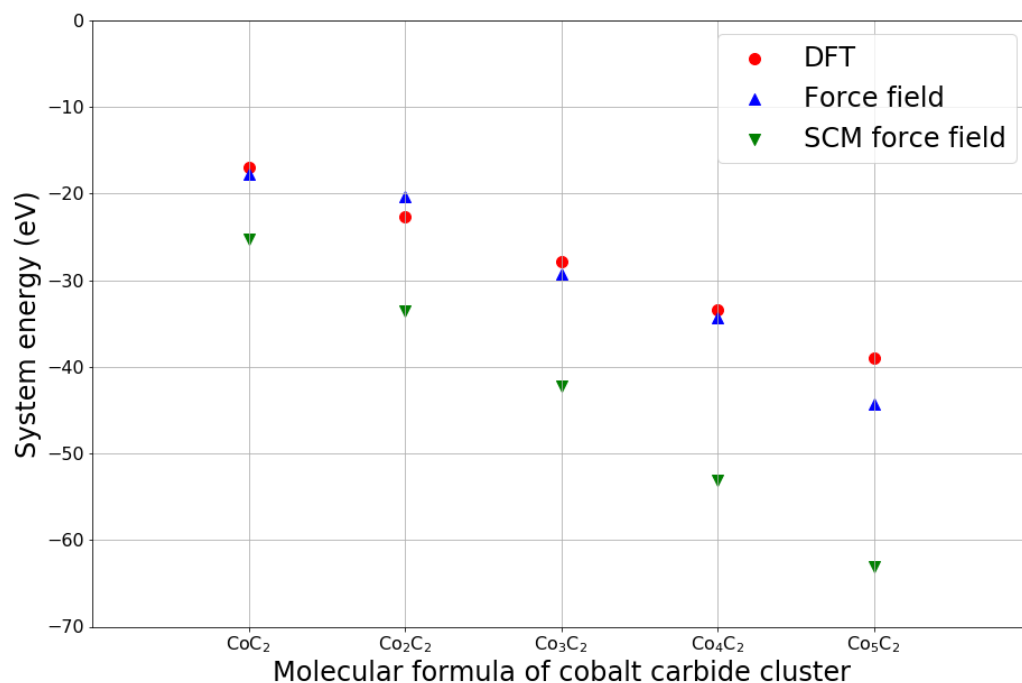


Figure 3.33: Force field results of cobalt carbide clusters of different molecular formulas.

Extension of the force field with carbon-adsorbed cobalt surfaces

Another extension to the force field was done with cobalt surfaces including carbon adsorbates. This extension is particularly interesting since the expressions evaluated here are predominantly responsible for the results that will be discussed in the next section about GCMC. Many of the evaluated structures in this section have already been encountered during the DFT results on lateral interactions and surface reconstruction. However, the continuation of these results towards GCMC is what is needed to make this information applicable for gathering information about carbon insertions and, as an extension thereof, carbon deposition. The results to be discussed are separated in three figures: Figure 3.34 for the visualisation of surfaces with one adsorbate, Figure 3.35 for presenting two-adsorbate surfaces and Figure 3.36 for all one- and two-adsorbate combinations on cobalt fcc(211) surfaces. The last set of results has been separated from the rest in order to improve the clarity of the graphs presented, as the system energies of fcc(211) surfaces are roughly 400 eV apart from the other surfaces.

For the one-adsorbate cases of fcc(100), fcc(110) and fcc(111) surfaces, it can be seen from Figure 3.34 that in general structures are estimated by both force fields to be less stable than it is predicted by DFT calculations. The exceptions here are the cases for repulsive interactions, which have been evaluated for the fcc (111) surface. These repulsive interaction cases are situations in which carbon atoms have been placed so close to the cobalt atom that the distance between them is too close, resulting in an unfavourable interaction and therefore repulsive behaviour. There is a rather significant difference in energy between the force field calculations and the DFT calculations, implying that the structures experiencing repulsive interactions are regarded as more stable than is actually the case. Fortunately, they are not portrayed as more stable than the most energetically favourable threefold and fourfold sites, as determined by DFT. There are two cases, namely fcc(100) and fcc(110), where the constructed force field predicts the configurations of these surfaces with a carbon adsorbate on a bridge site to be less stable than a repulsive interaction on a bridge site of the fcc(111) surface, which is, of course, not something that should be expected to happen based on physical knowledge. It might, therefore, be expected that the force field erroneously prefers bond lengths shorter than desired, which might lead to some odd insertions happening in the GCMC simulations. Looking at the constructed force field, it can also be expected that inserts will be less readily accepted in general due to the higher system energies. The SCMFF seems to do a better job regarding the accuracy of energies, but also here a worrisome trend is visible. The SCMFF predicts energies that increase with the number of cobalt atoms the carbon is bound to in all cases except for the repulsive interactions. This is exactly the opposite of what DFT shows to be true. Due to this, it can be expected that the GCMC simulations using the SCMFF will most likely reveal to have a large amount of onefold binding sites.

In continuing the evaluation of the force fields by investigating Figure 3.35, one sees results that differ quite a bit from the one-adsorbate examples. The constructed force field shows a far better agreement with the DFT data, except for the fcc(111) surfaces. Based on this, it can be expected that with the occurrence of combinations of carbon atoms on the surface, combinations on fcc(110) surfaces are mistakenly preferred over fcc(111) surfaces. This expectation is even more reinforced by the fact that when differences in energy between one atom cases and combinations are calculated, the energy decreasements of fcc(100) and fcc(110) surfaces, and therefore the increasements in stability, far exceed the energy decreasement of the fcc(111) surfaces. Although the SCMFF demonstrated a better

3.2 Evaluation and Comparison of a Created Force Field

similarity for one-adsorbate cases, the same cannot be said about two-adsorbate cases. The energy differs with approximately 30 eV, or approximately 0.45 eV per atom, for all points except one. Due to this portrayal of combinations of two carbon atoms on the surface as less energetically favourable, a tendency to avoid combinations, and therefore a tendency to spread out the insertions over the nanoparticle, can be expected.

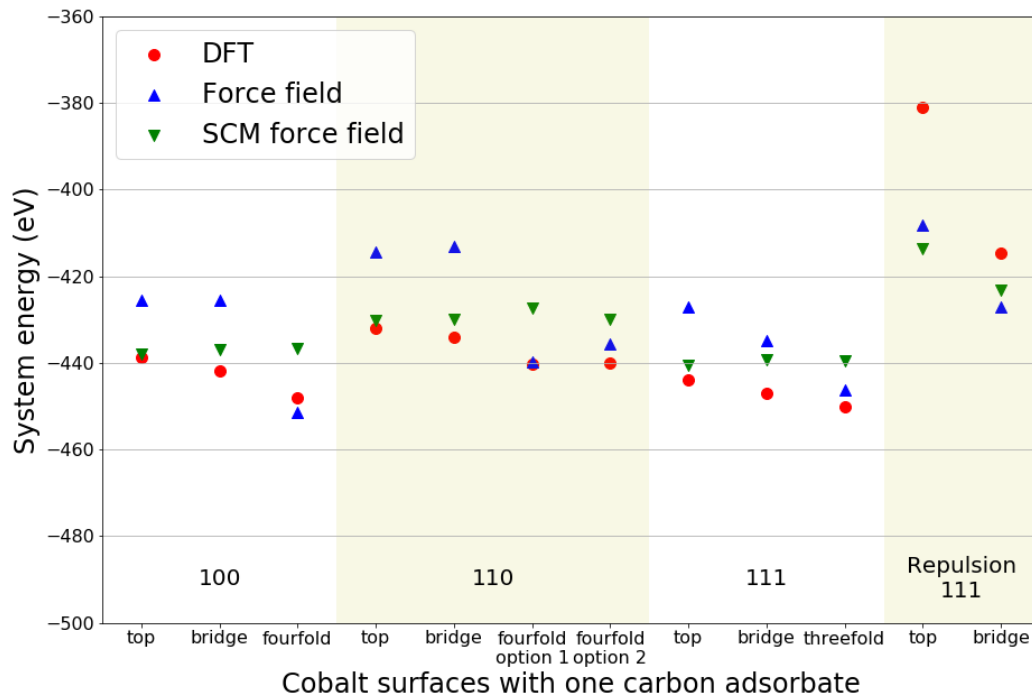


Figure 3.34: Force field results of cobalt surfaces with one carbon adsorbate for different sites and Miller indices.

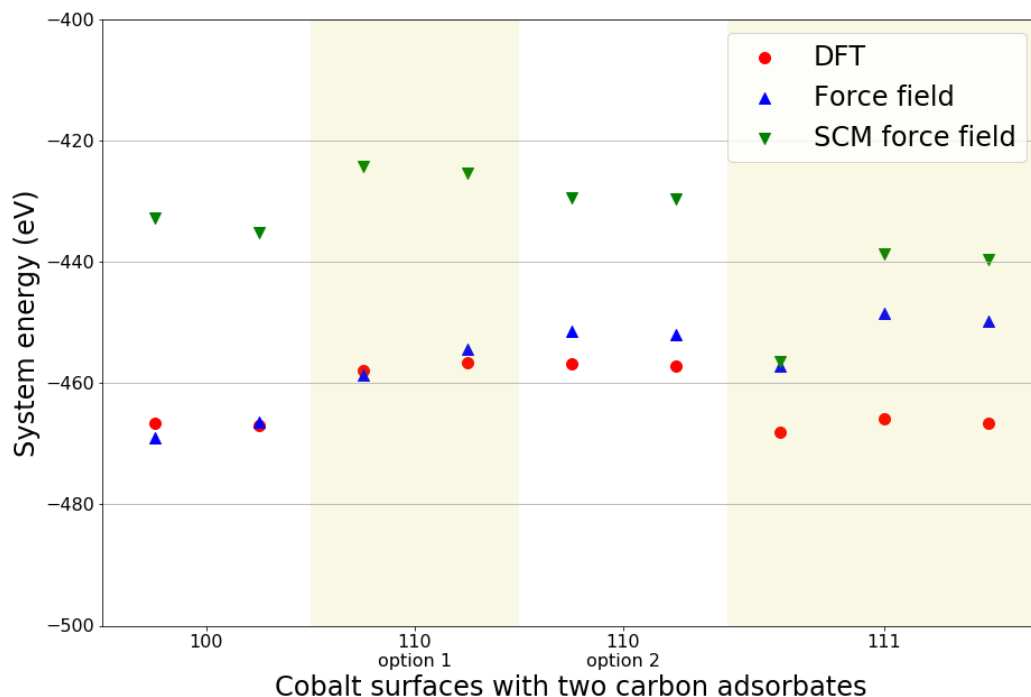


Figure 3.35: Force field results of cobalt surfaces with two carbon adsorbates for different sites and Miller indices.

The final figure to evaluate is Figure 3.36. In here, for a large part, the same trends are encountered as in the previous two figures. The SCMFF once again shows a tendency to portray two-adsorbate cases less favourable than they truly are but it is closer in its prediction for one- and twofold one-adsorbate cases. Many of the predicted values of the constructed force field are also less favourable than expected, but most of them are closer to the DFT value than the SCMFF values. With all cases having been evaluated, Table 3.7 provides an overview where these cases are listed based on their relative system energies as predicted by the force fields. Since a lower system energy corresponds with a higher stability, it is also expected for an adsorption site that a higher ranking on this list will result in a stronger presence of the site in the GCMC results of the respective force field.

To conclude, it can be stated that both force fields have significant flaws in predicting interactions of carbon adsorbates on cobalt surfaces. Although the constructed force field has better accuracy for combinations of two adsorbates, it is of little use if the first insertion is mispredicted, as there will be worked with an incorrect interim result, which will inevitably leave its mark to the simulation. The SCMFF has shown to be substantially more accurate for one- and twofold-bound sites in cases with one adsorbate, but since it incorrectly assumes these sites to be more stable than the three- and fourfold sites of most surfaces, it is bound to predict physically unlikely structures. It is also likely to avoid the formation of combinations on the surfaces to a greater degree than is justified based on the DFT. Therefore, in order to suit the goals of this research, improvements will be needed for either force field to function accordingly.

3.2 Evaluation and Comparison of a Created Force Field

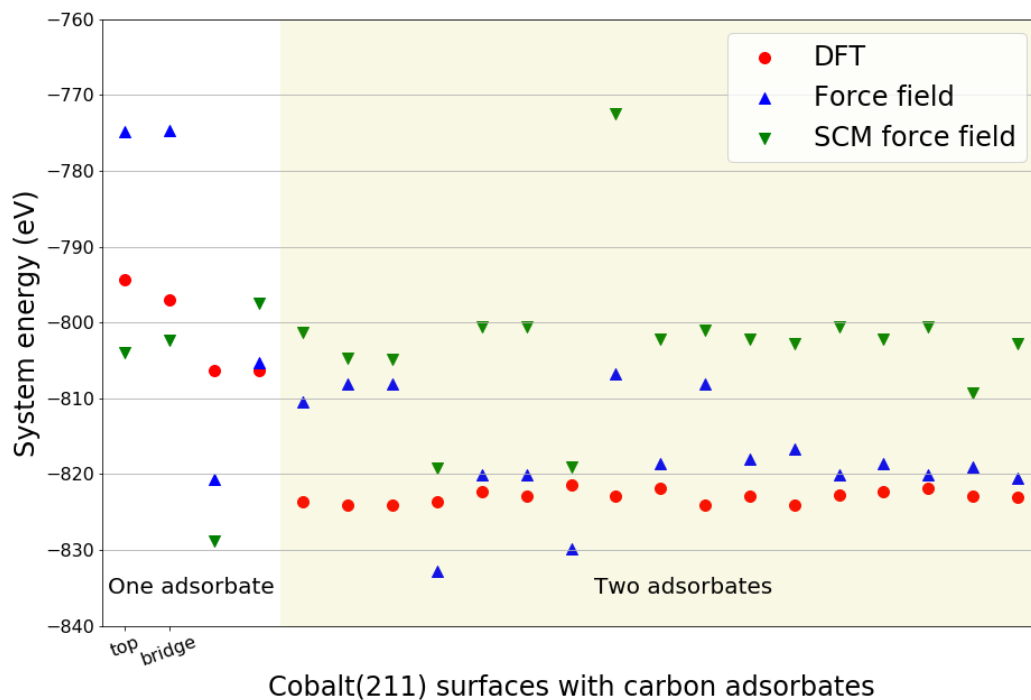


Figure 3.36: Force field results of cobalt fcc(211) surfaces with one (left, white half) or two (right, yellow half) carbon adsorbates for different sites and Miller indices.

Table 3.7: Schematic distribution of relative system energy and stability of adsorption sites.

Constructed force field	SCM force field
<i>Lowest relative system energy / Highest stability</i>	
Fcc(100) fourfold	Fcc(211) fourfold option 1
Fcc(211) fourfold option 1	Fcc(111) top
Fcc(111) threefold	Fcc(111) threefold
Fcc(211) fourfold option 2	Fcc(111) bridge
Fcc(110) fourfold set 1	Fcc(211) top
Fcc(110) fourfold set 2	Fcc(211) bridge
Fcc(111) bridge	Fcc(100) top
Fcc(111) bridge repulsion	Fcc(100) bridge
Fcc(111) top	Fcc(100) fourfold
Fcc(100) top	Fcc(211) fourfold option 2
Fcc(100) bridge	Fcc(110) top
Fcc(211) top	Fcc(110) bridge
Fcc(211) bridge	Fcc(110) fourfold set 2
Fcc(110) top	Fcc(110) fourfold set 1
Fcc(110) bridge	Fcc(111) bridge repulsion
Fcc(111) top repulsion	Fcc(111) top repulsion
<i>Highest relative system energy / Lowest stability</i>	

3.3 GRAND CANONICAL MONTE CARLO SIMULATIONS

With the force fields evaluated in the previous section, grand canonical Monte Carlo simulations have been performed, resulting in cobalt nanoparticles with carbon inserts. An example of one such particle is given in Figure 3.37. For each force field, a set of 50 simulations has been carried out. Unfortunately, due to an error being triggered in the GCMC software tool, not all simulations were successful. The error, which is accompanied with the message “Atoms are too close”, is believed to be a bug in the program as it is believed that in a system where atoms really are too close, the GCMC program would simply reject the move and continue towards the next step. Since the chances of this error being triggered increase with the number of iterations, simulations could not be run until convergence and therefore the presented results are interim results that have all been produced in 250 iterations. For the constructed force field, 47 simulations were successful where the number of successful simulations was 41 for the SCM force field. In order to have the same statistical averaging, the last six successful simulations with the constructed force field were discarded in order to have both averages be based on 41 samples.

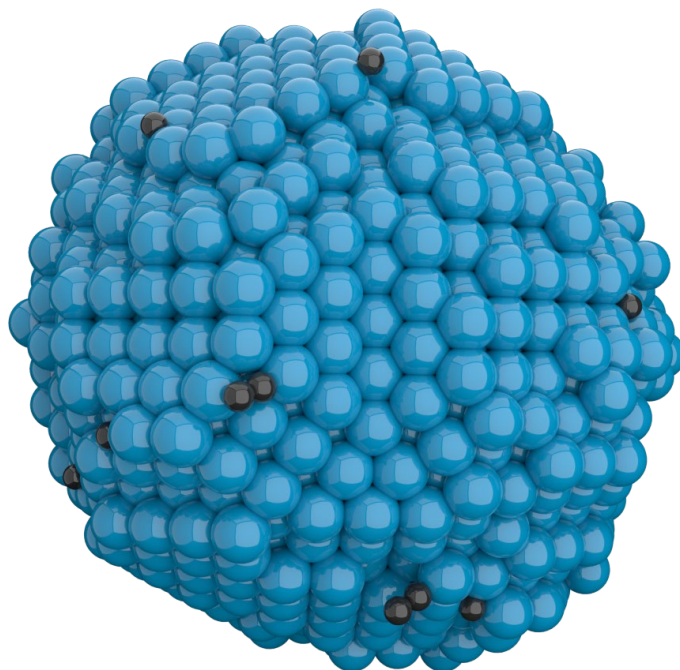


Figure 3.37: Cobalt nanoparticle with inserted carbon atoms, resulting from GCMC simulation.

Figure 3.38 and Figure 3.39 show the results of the statistically averaged site distribution on particles simulated with the constructed force field and the SCMFF, respectively. For the constructed force field, on average there have been 8.7 inserts per simulation, with a minimum of 5 and a maximum of 18 carbon atoms inserted. The SCMFF appears to insert carbon atoms more readily with on average 31.9 inserts. The minimum amount of carbon atoms inserted was 19 where the maximum was 48. This rather large gap in the number of inserts between the two force fields can most likely be explained by the fact that the energies of almost all one-adsorbate cases were observed to be more favourable for the SCMFF than for the constructed force field.

3.3 Grand Canonical Monte Carlo Simulations

To continue with the results presented in Figure 3.38 on the force field created throughout this research, it can at first be seen that a little less than half of the sites remain unrecognized and a large percentage of 36% of the inserted atoms is inserted at a distance too far from the surface. 18.20% of the inserted carbon is deposited on one of the four different recognized sites. By far the largest category is the fcc(111) threefold sites, which is a good thing, considering that these sites would be expected to have a fair presence in a real system and the threefold site on the fcc(111) surface is the preferable site for carbon deposition. The rest of the sites are divided between two types of twofold sites, making up approximately 30% of the recognized sites, and fcc(211) onefold sites representing slightly less than 20% of the recognized sites.

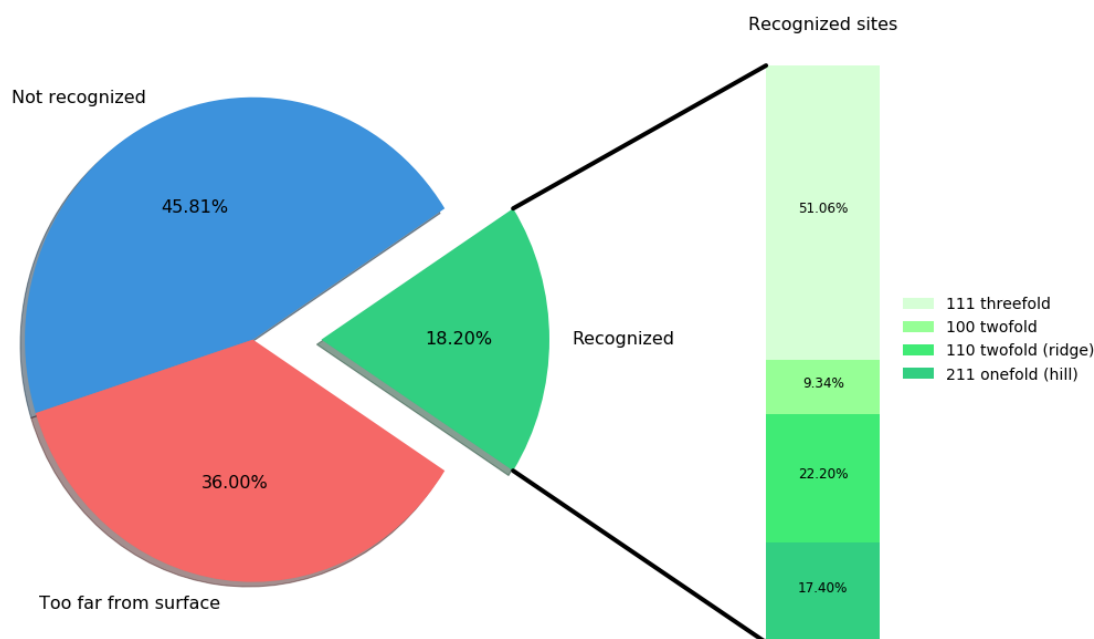


Figure 3.38: Site distribution of inserted carbon atoms after GCMC simulations with the constructed force field.

The SCMFF results in Figure 3.39 show a very different picture from the results in Figure 3.38. The largest observable change is seen in the sites remaining unrecognized, which comprises over 80% of the inserted atoms. Also, the inserts accepted at larger distances from the surface have, with a difference of around 30%, changed drastically compared to the results of the previously demonstrated force field. The relative amount of atoms recognized is with 13.23% slightly lower for the SCMFF. This group of recognized sites is made up for 55.68% out of four different onefold sites, of which the presence was already predicted based on the force field evaluation. The remainder of the recognized sites consists of almost equal parts of twofold and threefold inserted atoms, with a slight predominance of the threefold sites.

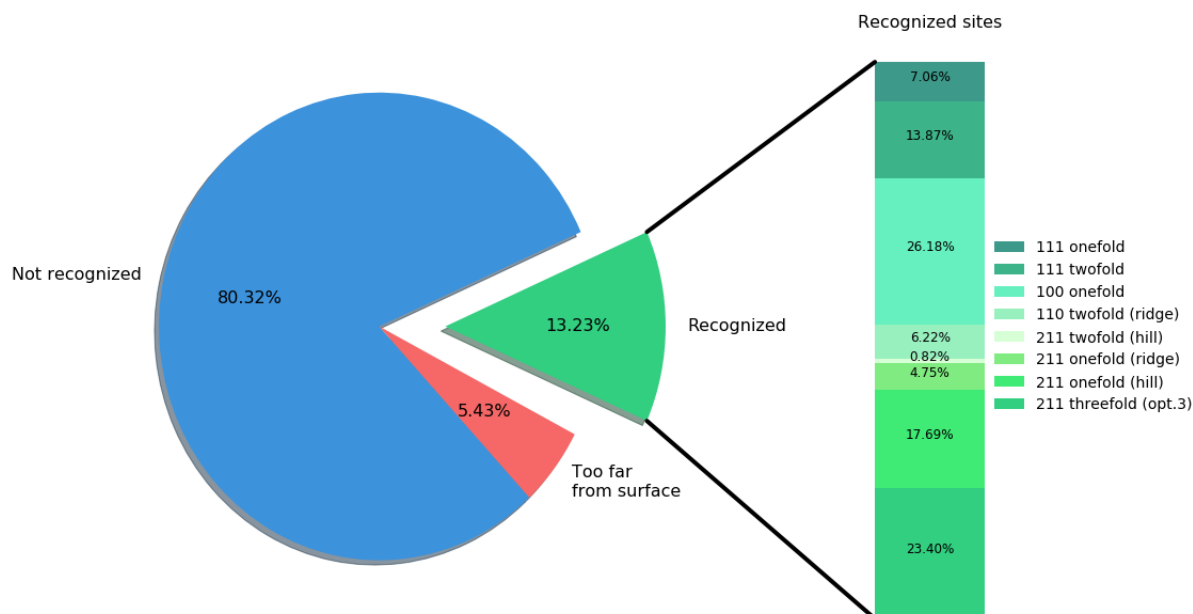


Figure 3.39: Site distribution of inserted carbon atoms after GCMC simulations with the SCM force field.

So, with these results having been presented, the conclusion can be divided into three aspects. First and foremost, the results of the GCMC simulations reinforce the conclusion drawn from the previous section that the constructed force field is, at the present moment, insufficient for the goals pursued within this study and therefore further improvement of the force field is needed. Secondly, once the force field has been improved to a satisfactory level, it should be made possible to run GCMC simulations until convergence. When it is confirmed that the force field works properly and the ‘atoms are too close’-error continues to be triggered, it is a strong indication that the error is indeed a bug of the GCMC program, in which case it will require an investment from the SCM company into their GCMC program in order to avoid or prevent the bug from being triggered. An alternative would be to develop an in-house program for GCMC simulations. Once satisfying GCMC results have been achieved, the site recognition library should be enlarged to assure that it contains a high amount of different sites or, at the very least, most of the expected sites. Adding cobalt hexagonal close-packed surfaces with carbon adsorbates to the force field and the surface recognition library would probably account for a major improvement at the cost of a relatively low effort and would, therefore, be a good first suggestion towards achieving better results. Another suggestion that might prove to be helpful in achieving improved GCMC results, is starting out with force fields trained and tested on smaller systems. A worked example is explained in the next paragraph.

Figure 3.40 provides the force field predictions compared to DFT, after fitting the force field for high accuracy on cobalt fcc(100) surfaces. Characteristic for this fit is that it has made use of a variation of bond lengths for the fourfold one-adsorbate case on the fcc(100) surface by taking images from different steps of the geometry optimisation trajectory, along with their corresponding system energies. By training for various bond lengths, an accurate description of the ideal bond length can be described by the force field, especially if this is combined with the equation of state for cobalt carbide, which also provides information about bond lengths. The results for the equation of state are illustrated in

3.3 Grand Canonical Monte Carlo Simulations

Figure 3.41. The force field has resulted in a strong fit for the equation of state as well: all but two points are within the range of an energy difference compared to DFT of 0.1 eV per atom, and the two less accurate points are located at the far, less important ends of the optimum. All data points presented in Figure 3.40 are within the accuracy range of 0.1 eV per atom. The sought-after relative trend between surface sites is mostly present and the small inaccuracy in the trend of the last three length variations is expected to be negligible. A predominance of an illogical option is therefore not anticipated. The result after submitting the force field to a GCMC simulation on a cobalt fcc(100) surface slab is illustrated in Figure 3.42. The figure shows an fcc(100) surface with a number of carbon atoms inserted on the most energetically favourable fourfold sites. Both the combinations included in the force field are also present. Although useful results have not yet been obtained on larger systems, the cobalt fcc(100) system presented in Figure 3.42 has proven the concept to be possible.

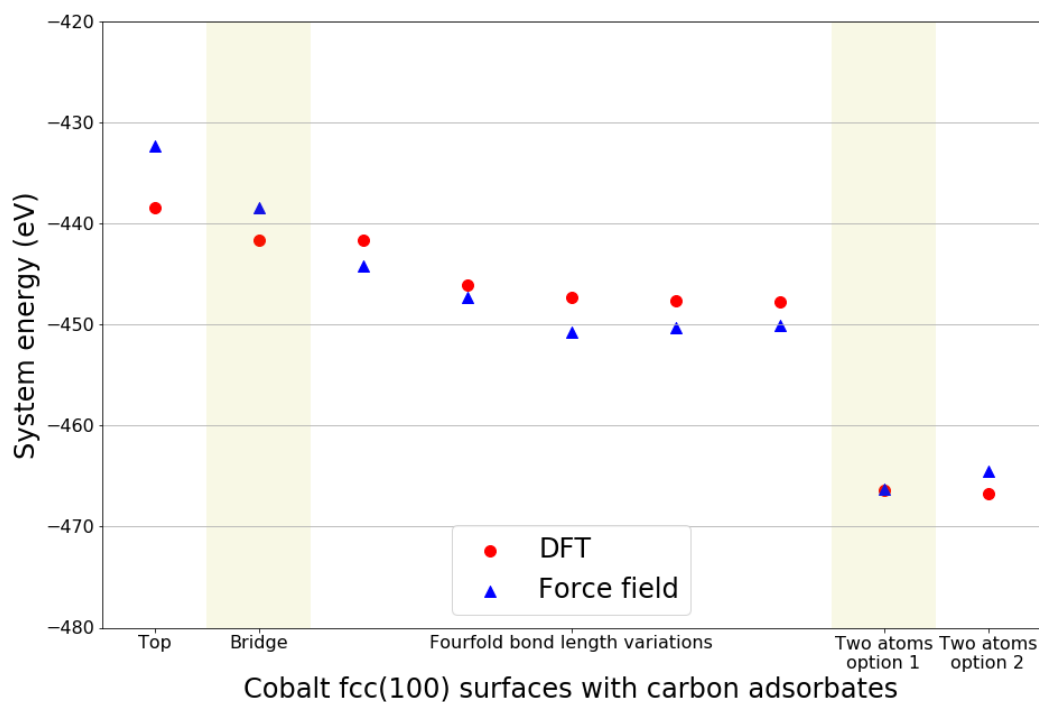


Figure 3.40: Force field results of cobalt fcc(100) surfaces with carbon adsorbates.

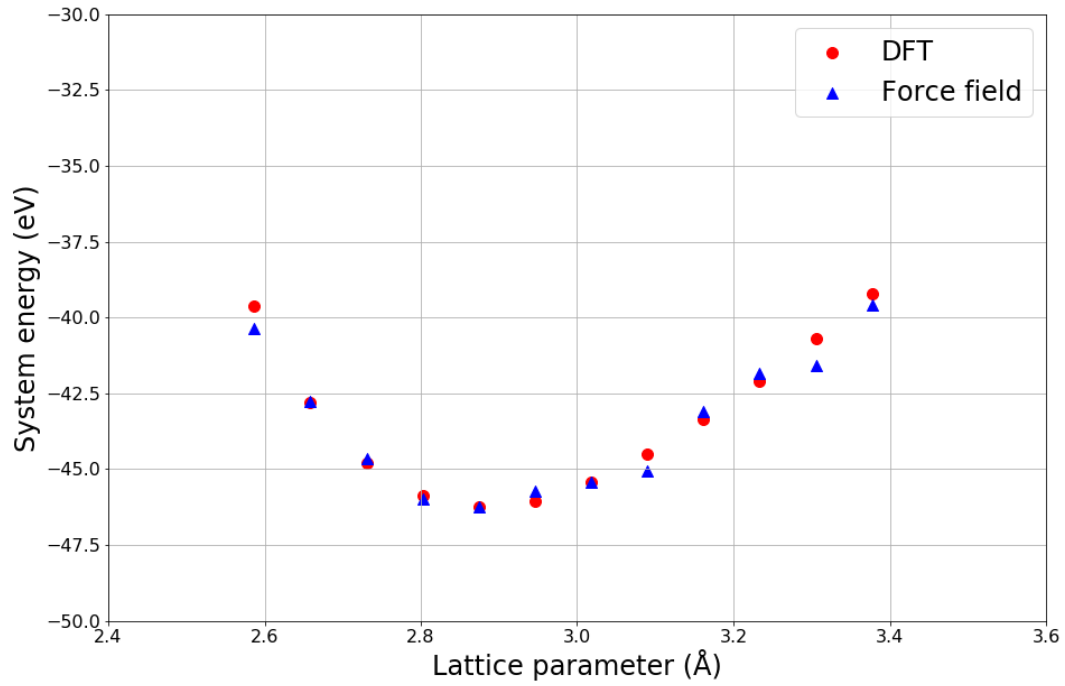


Figure 3.41: Force field results of the equation of state for cobalt carbide.

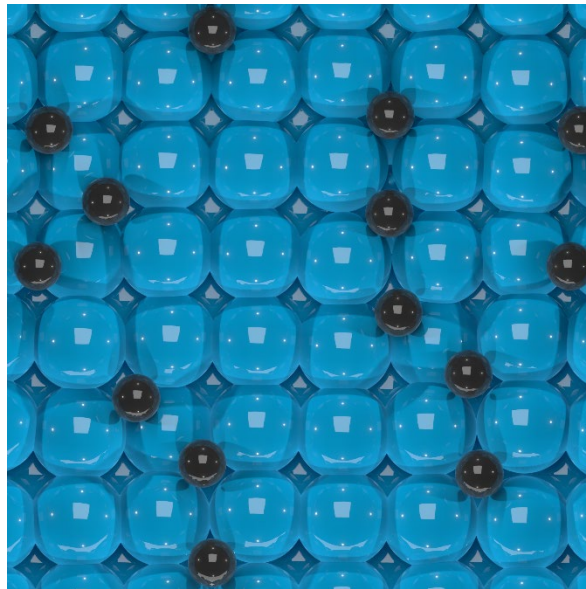


Figure 3.42: Cobalt fcc(100) surface with inserted carbon atoms, resulting from GCMC simulation.

4 CONCLUSION

Throughout this research, many progressive methods have been employed in order to study dynamic surface processes on the cobalt nanoparticle surface during Fischer-Tropsch synthesis. Although only a glimpse has been revealed of the behaviour of the carbon atoms on the surface, the phenomena observed encourage to continue with more extensive research on the subject.

Through studies using density functional theory, many energies and stabilities of systems involving cobalt and carbon have been determined. Fourfold sites were demonstrated to be the most stable binding sites for carbon atoms on cobalt surfaces, followed by threefold, twofold and onefold sites, respectively. In line with this, cobalt fcc(111) surfaces were shown to be the least energetically favourable surfaces to adsorb on since they lack the energetically preferred fourfold sites, but are expected to be present most frequently on cobalt nanoparticles due to the higher surface stability compared to their fcc(100), fcc(110) and fcc(211) counterparts. Upon inspection of the geometries, surface reconstruction effects were sighted for cobalt fcc(110) surfaces, as well as stabilizing lateral interactions for fcc(111) and fcc(211) surfaces, resulting in carbon-carbon bonds. Further investigation through more elaborate DFT calculations is required in order to develop a more coherent explanation for the observed behaviours.

Existing DFT data for cobalt was combined with discussed DFT data on systems of carbon, cobalt carbide and carbon adsorbate on cobalt surfaces, all produced in this study, in order to create a force field. For this, the in-house developed program RF₃ was used, for which a strategy has been developed for extending an existing force field towards a multi-elemental force field.

The predictions of the produced force field have been evaluated and compared to another force field supplied with the ADF-ReaxFF program. Both force fields have been compared to the results of DFT and based on this, predictions were made on the results of grand canonical Monte Carlo simulations in the next step of this research. The constructed force field was evaluated to be an adequate tool, capable of predicting energies for the carbon systems included with high accuracy through its force field calculations. For use in cobalt carbide systems, significant improvements will have to be made before it becomes viable, as very few situations could be described with sufficient accuracy. Situations of a carbon atom or a combination of carbon atoms, on the cobalt surface, were evaluated and although combinations matched fairly well with DFT results, one-adsorbate cases were too far out of line with the DFT results to produce useful results after force field calculations. In a consecutive step, the scale of the system under investigation was downsized. GCMC simulations were performed on a cobalt fcc(100) surface slab with a force field specifically fit for this purpose. The force field was ensured to have good predictions on the cobalt carbide equation of state and a variety of options of fcc(100) surfaces with adsorbates. Promising results from these fcc(100) simulations were obtained, implying that further optimisation of the force fields is possible and can lead to desired results. However, for larger systems, the force field will need considerable improvement, especially for the one-adsorbate cases on cobalt surfaces.

GCMC simulations have confirmed the predictions made from the force field evaluations and have shown that both the constructed force field, as well as the SCM force field it was compared to, are at present stage not capable of delivering realistic and desirable results in the context of this research, as carbon atoms were mainly inserted on positions that are known to be energetically less favourable, such as top and bridge positions. In addition to the shortcomings of the force field, the GCMC program itself also faces issues that need to be solved, while used settings could benefit from further optimisation. Finally, the library in use for the site recognition is at present too limited and needs a further expansion of recognized sites included, such as hexagonal close-packed surface sites, accompanied with the required additional DFT calculations.

5 OUTLOOK & RECOMMENDATION

This study has tried to unravel the effects of dynamic surface processes during the Fischer-Tropsch reaction, specifically with regards to the placement and behaviour of carbon atoms on the cobalt surface. Throughout this research, many obstacles have been stumbled upon along the way. Although some have been overcome, it has not been possible to solve all of the problems encountered, unfortunately, due to the time restrictions of the project. Nevertheless, ways to resolve the remaining issues, as well as perspectives on how to approach continued research on the topic, have been developed and will be shared within this section.

Interesting results have emerged from the density functional theory studies, as has been presented in the previous chapters. To increase understanding of these phenomena and to establish a more solid foundation of knowledge on the topic, it is recommended to carry out a number of follow-up calculations. Calculations carried out with a larger unit cell could confirm that atoms that were adsorbed over a distance further apart do not influence each other, a behaviour that has been assumed so far. Furthermore, it would be interesting to see what happens when there are more adsorbates present on the surface. Calculations could be performed with combinations of three or four carbon atoms on the surface, for example, to observe whether the structures behave in line with the expectations that have been created based on the current results. The last suggestion would be to add adsorbates in a linear fashion in order to create lines of adsorbates over the surface. Evaluating this directional periodicity for enhanced, or perhaps reduced, effects could tell more about whether certain combinations are expected to be more confined to a local area, or that they will reinforce a propagating behaviour. One could also extend this towards a purposeful attempt at deactivating a single line on the transition between two sites, for example, the fcc(111) and fcc(100) structures, which are favourable for hydrogenation and CO dissociation, respectively. The effects of this deactivation on the Fischer-Tropsch reaction can then be studied.

Considering the force field and grand canonical Monte Carlo simulations, many improvements have to be made. Firstly, the force field needs further optimising towards both cobalt carbide and cobalt surfaces with carbon adsorbates. To achieve this, more time is required for fitting using RF_3 . Also, the parameter set used to fit the data could be enlarged slightly more to help with this. During the project, overambitious decisions were made often, as a result of which the switch was made too quickly to continue with GCMC simulations. There has thus been learned to practise more patience and to test the effects of a force field first on a smaller system, for example, a specific surface slab. Once results in GCMC are satisfying on these smaller systems, they can be scaled to larger systems such as the nanoparticles under investigation. A next step is to enlarge the library used to recognize the GCMC results in order to have a more thorough analysis of the sites where insertions have occurred. Once desirable results for the face centred-cubic structures have been achieved, a logical step to continue with is to expand the training set with DFT data of hexagonal close-packed surfaces with carbon adsorbates. Inclusion of this data in the force field and structure recognition library is anticipated to have a considerable impact on the comprehensiveness of this research. Finally, to round up the process up to GCMC, the structure recognition library could be expanded with the last, difficult to identify insertion sites.

In future work, the particles resulting from GCMC can be used as input geometries for molecular dynamics simulations to study the effect these insertions have on the particle. Possibly, the formation of small cobalt carbide phases can be witnessed, if the force field can be sufficiently optimised towards this goal. Surface reconstruction effects could be studied in more depth and their potential positive or negative influence on the activity of certain (more difficult) reaction steps can be evaluated. It could also be evaluated which surfaces are more prone to deactivation, perhaps due to the formation of deactivating carbon chains or graphene layers on the nanoparticle surface. A further upgrade to this research could be the inclusion of oxygen and hydrogen in the force field, in order to describe the complete Fischer-Tropsch process and its associated effects such as CO dissociation, chain formation, migration and so forth. As was demonstrated in this chapter and throughout this report, there is still a vast field left to unravel on the topic of dynamic surface processes.

6 ACKNOWLEDGEMENTS

Having arrived at the end of this master thesis, a couple of words remain unspoken: words of gratitude for all the people who have enabled this project and helped me throughout various stages of my research. I could not have done this all by myself. So, to make these words of gratitude spoken, I would like to start off by thanking Emiel Hensen for the opportunity to carry out my graduation project in the IMC group. I would also like to thank Maïke Baltussen for her time and effort in taking place in my graduation committee. I very much appreciate it! Ivo, thank you for sparking my interest in this research area, the opportunities you have created for me and for your guidance along the way. A further word of thanks goes out to all the members of the IMC group who have made my stay more enjoyable, either by their delightful presence and pleasant conversations or by their valuable assistance. A special mention goes out to Bart Klumpers for his help and discussions on the subject of density functional theory; to Bart Zijlstra for his help in creating beautiful images and animations; and to Dennis, Francesco and Michel for making our office a pleasant place. On top of the previous mention, as my daily supervisor for nine months and another two months in a different project before, an additional line or two go out to Michel. Michel, thank you for your close guidance, fruitful discussions and valuable advice during the past months. I have greatly enjoyed all this, as well as the memorable moments that were accompanied with it. It was a genuine pleasure working for and with you!

Finally, the last word of thanks goes out to my family, who have supported me not only throughout the project and my studies but in all the moments leading up to this. Your trust and support are truly treasured.

7 BIBLIOGRAPHY

- (1) Hulme, M. *Why We Disagree About Climate Change: Understanding Controversy, Inaction, and Opportunity*; Cambridge University Press: Cambridge, 2009.
- (2) Büntgen, U.; Tegel, W.; Nicolussi, K.; McCormick, M.; Frank, D.; Trouet, V.; Kaplan, J. O.; Herzig, F.; Heussner, K. U.; Wanner, H.; et al. 2500 Years of European Climate Variability and Human Susceptibility. *Science (80-.)*. **2011**, *331* (6017), 578–582.
- (3) Agassiz, J. L. R. *Études Sur Les Glaciers*; Jent et Gassmann: Neuchâtel, 1840.
- (4) Tyndall, J. *The Glaciers of the Alps. Being a Narrative of Excursions and Ascents, an Account of the Origin and Phenomena of Glaciers and an Exposition of the Physical Principles to Which They Are Related*; Ticknor and Fields: Boston, 1861.
- (5) Arrhenius, S. On the Influence of Carbonic Acid in the Air upon the Temperature of the Ground. *Philos. Mag. J. Sci. Ser.* **1896**, *41*, 237–276.
- (6) Arrhenius, S.; Translated by Borns, H. *Worlds in the Making; the Evolution of the Universe*; Harper & Brothers Publishers: New York, London, 1908.
- (7) Marx, W.; Haunschild, R.; Thor, A.; Bornmann, L. Which Early Works Are Cited Most Frequently in Climate Change Research Literature? A Bibliometric Approach Based on Reference Publication Year Spectroscopy. *Scientometrics* **2017**, *110* (1), 335–353.
- (8) Intergovernmental Panel on Climate Change. *Climate Change: The IPCC Scientific Assessment*; 1990.
- (9) United Nations. *Paris Agreement*; 2015.
- (10) United Nations Treaty Collection
https://treaties.un.org/Pages/ViewDetails.aspx?src=TREATY&mtdsg_no=XXVII-7-d&chapter=27&clang=_en (accessed May 7, 2019).
- (11) Abas, N.; Kalair, A.; Khan, N. Review of Fossil Fuels and Future Energy Technologies. *Futures* **2015**, *69*, 31–49.
- (12) U.S. Energy Information Administration - EIA - Independent Statistics and Analysis <https://www.eia.gov/outlooks/aeo/data/browser/#/?id=2-IEO2017®ion=0-0&cases=Reference&start=2010&end=2050&f=A&linechart=~~~~~Reference-d082317.76-2-IEO2017~Reference-d082317.77-2-IEO2017~Reference-d082317.78-2-IEO2017~Reference-d0823> (accessed May 10, 2019).
- (13) Tortajada, A.; Juliá-Hernández, F.; Börjesson, M.; Moragas, T.; Martin, R. Transition-Metal-Catalyzed Carboxylation Reactions with Carbon Dioxide. *Angew. Chemie Int. Ed.* **2018**, *57* (49), 15948–15982.
- (14) IUPAC Compendium of Chemical Terminology, Electronic version
<http://goldbook.iupac.org/C00876.html> (accessed May 10, 2019).
- (15) Chorkendorff, I.; Niemantsverdriet, J. W. *Concepts of Modern Catalysis and*

- Kinetics*; WILEY-VCH Verlag GmbH & Co. KGaA: Weinheim, 2003.
- (16) Filot, I. Quantum Chemical and Microkinetic Modeling of the Fischer-Tropsch Reaction, Technische Universiteit Eindhoven, 2015.
 - (17) Steynberg, A. P. Introduction to Fischer-Tropsch Technology. In *Studies in Surface Science and Catalysis*; Elsevier, 2004; Vol. 152, pp 1–63.
 - (18) Schulz, H. Short History and Present Trends of Fischer-Tropsch Synthesis. *Appl. Catal. A Gen.* **1999**, *186* (1–2), 3–12.
 - (19) Dominković, D. F.; Bačeković, I.; Pedersen, A. S.; Krajačić, G. The Future of Transportation in Sustainable Energy Systems: Opportunities and Barriers in a Clean Energy Transition. *Renewable and Sustainable Energy Reviews*. Pergamon February 1, 2018, pp 1823–1838.
 - (20) Leckel, D. Diesel Production from Fischer - Tropsch: The Past, the Present, and New Concepts. *Energy and Fuels* **2009**, *23* (5), 2342–2358.
 - (21) Van Santen, R. A.; Markvoort, A. J.; Filot, I. A. W.; Ghouri, M. M.; Hensen, E. J. M. Mechanism and Microkinetics of the Fischer-Tropsch Reaction. *Phys. Chem. Chem. Phys.* **2013**, *15* (40), 17038–17063.
 - (22) Martin, R. M. *Electronic Structure Basic Theory and Practical Methods*; Cambridge University Press: New York, 2004.
 - (23) Becke, A. D. Perspective: Fifty Years of Density-Functional Theory in Chemical Physics. *J. Chem. Phys.* **2014**, *140* (18), 18A301.
 - (24) Szabo, A.; Ostlund, N. S. *Modern Quantum Chemistry: Introduction to Advanced Electronic Structure Theory*, First Edit.; Dover Publications, Inc.: Mineola, New York, 1996.
 - (25) Hohenberg, P.; Kohn, W. Inhomogeneous Electron Gas. *Phys. Rev.* **1964**, *136* (3B), B864–B871.
 - (26) Kohn, W.; Sham, L. J. Self-Consistent Equations Including Exchange and Correlation Effects. *Phys. Rev.* **1965**, *140* (4A), A1133–A1138.
 - (27) Kohn, W.; Becke, A. D.; Parr, R. G. Density Functional Theory of Electronic Structure. *J. Phys. Chem.* **1996**, *100* (31), 12974–12980.
 - (28) Mardirossian, N.; Head-Gordon, M. Thirty Years of Density Functional Theory in Computational Chemistry: An Overview and Extensive Assessment of 200 Density Functionals. *Molecular Physics*. Taylor & Francis October 2, 2017, pp 2315–2372.
 - (29) Kresse, G.; Hafner, J. Ab Initio Molecular Dynamics for Liquid Metals. *Phys. Rev. B* **1993**, *47* (1), 558.
 - (30) Kresse, G.; Furthmüller, J. Efficient Iterative Schemes for Ab Initio Total-Energy Calculations Using a Plane-Wave Basis Set. *Phys. Rev. B* **1996**, *54* (16), 11169–11186.
 - (31) Kresse, G.; Furthmüller, J. The VASP site <https://www.vasp.at/> (accessed Nov 6, 2018).
 - (32) Kresse, G.; Furthmüller, J. Efficiency of Ab-Initio Total Energy Calculations for Metals and Semiconductors Using a Plane-Wave Basis Set. *Comput. Mater. Sci.* **1996**, *6* (1), 15–50.

- (33) Kresse, G.; J. Hafner. Ab Initio Molecular-Dynamics Simulation of the Liquid-Metal-Amorphous-Semiconductor Transition in Germanium. *Phys. Rev. B* **1994**, *49* (20), 14251.
- (34) Kresse, G.; Joubert, D. From Ultrasoft Pseudopotentials to the Projector Augmented-Wave Method. *Phys. Rev. B* **1999**, *59* (3), 1758–1775.
- (35) Methfessel, M.; Paxton, A. T. High-Precision Sampling for Brillouin-Zone Integration in Metals. *Phys. Rev. B* **1989**, *40* (6), 3616–3621.
- (36) Perdew, J. P.; Burke, K.; Ernzerhof, M. Generalized Gradient Approximation Made Simple. *Phys. Rev. Lett.* **1996**, *77* (18), 3865–3868.
- (37) Perdew, J. P.; Burke, K.; Ernzerhof, M. ERRATA - Generalized Gradient Approximation Made Simple [Phys. Rev. Lett. 77, 3865 (1996)]. *Phys. Rev. Lett.* **1997**, *78* (7), 1396.
- (38) Perdew, J. P.; Burke, K.; Ernzerhof, M. Generalized Gradient Approximation for the Exchange-Correlation Hole of a Many-Electron System. *Phys. Rev. B* **1996**, *54* (23), 16533–16539.
- (39) Monkhorst, H. J.; Pack, J. D. Special Points Fro Brillouin-Zone Integrations. *Phys. Rev. B* **1976**, *13* (12), 5188–5192.
- (40) Materials Studio Materials Modeling & Simulation Application | Dassault Systèmes BIOVIA <https://www.3dsbiovia.com/products/collaborative-science/biovia-materials-studio/> (accessed Jun 6, 2019).
- (41) Yuan, J.-Y.; Xu, H.-G.; Zheng, W.-J. Photoelectron Spectroscopy and Density Functional Study of ConC₂⁻ (n = 1–5) Clusters. *Phys. Chem. Chem. Phys.* **2014**, *16*, 5434–5439.
- (42) Van Orden, A.; Saykally, R. J. Small Carbon Clusters: Spectroscopy, Structure, and Energetics. *Chem. Rev.* **2002**, *98* (6), 2313–2358.
- (43) Ngandjong, A. C.; Mezei, J. Z.; Mougnot, J.; Michau, A.; Hassouni, K.; Lombardi, G.; Seydou, M.; Maurel, F. Structural Stability and Growth Mechanism of Neutral and Anionic Small Carbon Clusters: Density Functional Study. *Comput. Theor. Chem.* **2017**, *1102*, 105–113.
- (44) Lai, S. K.; Setiyawati, I.; Yen, T. W.; Tang, Y. H. Studying Lowest Energy Structures of Carbon Clusters by Bond-Order Empirical Potentials. *Theor. Chem. Acc.* **2017**, *136* (1), 20.
- (45) Raghavachari, K.; Binkley, J. S. Structure, Stability, and Fragmentation of Small Carbon Clusters. *J. Chem. Phys.* **1987**, *87* (4), 2191–2197.
- (46) ReaxFF Manual 2019 — ReaxFF 2019 documentation <https://www.scm.com/doc/ReaxFF/index.html> (accessed Jun 7, 2019).
- (47) Van Duin, A. C. T.; Dasgupta, S.; Lorant, F.; Goddard, W. A. ReaxFF: A Reactive Force Field for Hydrocarbons. *J. Phys. Chem. A* **2001**, *105* (41), 9396–9409.
- (48) Chenoweth, K.; Van Duin, A. C. T.; Goddard, W. A. ReaxFF Reactive Force Field for Molecular Dynamics Simulations of Hydrocarbon Oxidation. *J. Phys. Chem. A* **2008**, *112* (5), 1040–1053.
- (49) Van Duin, A. C. T.; Goddard, W. A.; Islam, M. M.; van Schoot, H.; Trnka, T.; Yakovlev, A. L. ReaxFF 2019, SCM, Theoretical Chemistry, Vrije Universiteit,

- Amsterdam, The Netherlands <http://www.scm.com> (accessed Jun 7, 2019).
- (50) Van Duin, A. Reactive Force Fields: Concepts of ReaxFF. In *Computational Methods in Catalysis and Materials Science: An Introduction for Scientists and Engineers*; Van Santen, R. A., Sautet, P., Eds.; WILEY-VCH Verlag GmbH & Co. KGaA: Weinheim, 2009; pp 167–181.
- (51) Filot, I. ReaxFF Fitter (RF3) — RF3 0.9.5.1-alpha documentation <https://www.rf3.nl/> (accessed Nov 6, 2018).
- (52) Zhang, X. Q.; Van Santen, R. A.; Hensen, E. J. M. Carbon-Induced Surface Transformations of Cobalt. *ACS Catal.* **2015**, *5* (2), 596–601.
- (53) Frenkel, D.; Smit, B. *Understanding Molecular Simulation: From Algorithms to Applications*, Second edi.; Frenkel, D., Klein, M., Parrinello, M., Smit, B., Eds.; Academic Press: San Diego, San Francisco, New York, Boston, London Sydney, Tokyo, 2002.
- (54) Carstensen, O.; Goumans, F. Grand-Canonical Monte-Carlo NSCCS ADF/ReaxFF Workshop. 2016.
- (55) Senftle, T. P.; Meyer, R. J.; Janik, M. J.; van Duin, A. C. T. Development of a ReaxFF Potential for Pd/O and Application to Palladium Oxide Formation. *J. Chem. Phys.* **2013**, *139* (4), 044109.
- (56) Senftle, T. P.; van Duin, A. C. T.; Janik, M. J. Determining in Situ Phases of a Nanoparticle Catalyst via Grand Canonical Monte Carlo Simulations with the ReaxFF Potential. *Catal. Commun.* **2014**, *52*, 72–77.
- (57) Nielson, K. D.; Van Duin, A. C. T.; Oxgaard, J.; Deng, W. Q.; Goddard, W. A. Development of the ReaxFF Reactive Force Field for Describing Transition Metal Catalyzed Reactions, with Application to the Initial Stages of the Catalytic Formation of Carbon Nanotubes. *J. Phys. Chem. A* **2005**, *109* (3), 493–499.
- (58) C | Eduard-Job-Foundation for Thermo- and Matterdynamics <https://www.job-stiftung.de/index.php?id=54,147,0,0,1,0> (accessed Jun 17, 2019).
- (59) Reinhart, W. F.; Long, A. W.; Howard, M. P.; Ferguson, A. L.; Panagiotopoulos, A. Z. Machine Learning for Autonomous Crystal Structure Identification. *Soft Matter* **2017**, *13* (27), 4733–4745.

8 APPENDICES

8.1 APPENDIX A – RF₃ SETTINGS FILE

```
#
# Author: Ivo Filot <i.a.w.filot@tue.nl>
#
# This file describes how a basic run file for POGO should look
#
# Lines starting with a # are treated as comments
#

#
# REAXFF PARAMETER INITIALIZATION
#
# Always put the filename between quotes and make sure the path does not contain
# any quotes.
#
# Put here the path for the file containing the lower bounds for the parameters
LOWER_BOUND_FILE = "low.tpl"
# Put here the path for the file containing the upper bounds for the parameters
UPPER_BOUND_FILE = "high.tpl"
# Put here the path for the file containing the initial values for the parameters
INITIAL_VALUES_FILE = "CoCnew3.ff"

STRATEGY=GA-MCMC

#
# GEOMETRIES
#

# Co2C Equation of State
GEOM "geom/Geo_Co2C_5.geo"    Co2C_5    f
GEOM "geom/Geo_Co2C_6.geo"    Co2C_6    f
GEOM "geom/Geo_Co2C_7.geo"    Co2C_7    f
GEOM "geom/Geo_Co2C_8.geo"    Co2C_8    f
GEOM "geom/Geo_Co2C_9.geo"    Co2C_9    f
GEOM "geom/Geo_Co2C_10.geo"   Co2C_10   f
GEOM "geom/Geo_Co2C_11.geo"   Co2C_11   f
GEOM "geom/Geo_Co2C_12.geo"   Co2C_12   f
GEOM "geom/Geo_Co2C_13.geo"   Co2C_13   f
GEOM "geom/Geo_Co2C_14.geo"   Co2C_14   f
GEOM "geom/Geo_Co2C_opt.geo"   Co2C_opt  f

# Diamond Equation of State
GEOM "geom/C_4.geo"           C_4       f
GEOM "geom/C_5.geo"           C_5       f
GEOM "geom/C_6.geo"           C_6       f
GEOM "geom/C_7.geo"           C_7       f
GEOM "geom/C_opt.geo"         C_opt     f
GEOM "geom/C_9.geo"           C_9       f
GEOM "geom/C_10.geo"          C_10      f
GEOM "geom/C_11.geo"          C_11      f
GEOM "geom/C_12.geo"          C_12      f
GEOM "geom/C_13.geo"          C_13      f

# Graphene Equation of State
GEOM "geom/Ce_4.geo"          Ce_4       f
GEOM "geom/Ce_5.geo"          Ce_5       f
GEOM "geom/Ce_6.geo"          Ce_6       f
GEOM "geom/Ce_7.geo"          Ce_7       f
GEOM "geom/Ce_opt.geo"        Ce_opt     f
GEOM "geom/Ce_9.geo"          Ce_9       f
GEOM "geom/Ce_10.geo"         Ce_10      f
GEOM "geom/Ce_11.geo"         Ce_11      f
```

```

GEOM "geom/Ce_12.geo"    Ce_12    f
GEOM "geom/Ce_13.geo"    Ce_13    f

# Graphite Equation of State
GEOM "geom/Ci_4_1.geo"    Ci_4_1    f
GEOM "geom/Ci_4_3.geo"    Ci_4_3    f
GEOM "geom/Ci_6_1.geo"    Ci_6_1    f
GEOM "geom/Ci_6_3.geo"    Ci_6_3    f
GEOM "geom/Ci_8_1.geo"    Ci_8_1    f
GEOM "geom/Ci_8_3.geo"    Ci_8_3    f
GEOM "geom/Ci_10_1.geo"   Ci_10_1   f
GEOM "geom/Ci_10_3.geo"   Ci_10_3   f
GEOM "geom/Ci_12_1.geo"   Ci_12_1   f
GEOM "geom/Ci_12_3.geo"   Ci_12_3   f
GEOM "geom/Ci_14_1.geo"   Ci_14_1   f
GEOM "geom/Ci_14_3.geo"   Ci_14_3   f

# FCC Equation of State
GEOM "geom/Co_FCC_2.geo"   Co_FCC_2   f
GEOM "geom/Co_FCC_3.geo"   Co_FCC_3   f
GEOM "geom/Co_FCC_4.geo"   Co_FCC_4   f
GEOM "geom/Co_FCC_5.geo"   Co_FCC_5   f
GEOM "geom/Co_FCC_6.geo"   Co_FCC_6   f
GEOM "geom/Co_FCC_7.geo"   Co_FCC_7   f
GEOM "geom/Co_FCC_8.geo"   Co_FCC_8   f
GEOM "geom/Co_FCC_9.geo"   Co_FCC_9   f
GEOM "geom/Co_FCC_10.geo"  Co_FCC_10  f
GEOM "geom/Co_FCC_11.geo"  Co_FCC_11  f
GEOM "geom/Co_FCC_12.geo"  Co_FCC_12  f
GEOM "geom/Co_FCC_opt.geo" Co_FCC_opt f

# BCC Equation of State
GEOM "geom/Co_BCC_3.geo"   Co_BCC_3   f
GEOM "geom/Co_BCC_5.geo"   Co_BCC_5   f
GEOM "geom/Co_BCC_7.geo"   Co_BCC_7   f
GEOM "geom/Co_BCC_9.geo"   Co_BCC_9   f
GEOM "geom/Co_BCC_11.geo"  Co_BCC_11  f
GEOM "geom/Co_BCC_13.geo"  Co_BCC_13  f
GEOM "geom/Co_BCC_15.geo"  Co_BCC_15  f
GEOM "geom/Co_BCC_opt.geo" Co_BCC_opt f

# HCP Equation of State
GEOM "geom/Co_HCP_1_3.geo" Co_HCP_1_3 f
GEOM "geom/Co_HCP_2_3.geo" Co_HCP_2_3 f
GEOM "geom/Co_HCP_3_1.geo" Co_HCP_3_1 f
GEOM "geom/Co_HCP_3_2.geo" Co_HCP_3_2 f
GEOM "geom/Co_HCP_3_3.geo" Co_HCP_3_3 f
GEOM "geom/Co_HCP_3_4.geo" Co_HCP_3_4 f
GEOM "geom/Co_HCP_3_5.geo" Co_HCP_3_5 f
GEOM "geom/Co_HCP_4_3.geo" Co_HCP_4_3 f
GEOM "geom/Co_HCP_5_3.geo" Co_HCP_5_3 f
GEOM "geom/Co_HCP_6_3.geo" Co_HCP_6_3 f
GEOM "geom/Co_HCP_opt.geo" Co_HCP_opt f

#Surfaces of cobalt carbide
GEOM "geom/Co2C_001_1.geo" Co2C_001_1 f
GEOM "geom/Co2C_001_2.geo" Co2C_001_2 f
GEOM "geom/Co2C_001_3.geo" Co2C_001_3 f
GEOM "geom/Co2C_001_4.geo" Co2C_001_4 f
GEOM "geom/Co2C_010_1.geo" Co2C_010_1 f
GEOM "geom/Co2C_010_2.geo" Co2C_010_2 f
GEOM "geom/Co2C_011_1.geo" Co2C_011_1 f
GEOM "geom/Co2C_011_2.geo" Co2C_011_2 f
GEOM "geom/Co2C_011_3.geo" Co2C_011_3 f
GEOM "geom/Co2C_100_1.geo" Co2C_100_1 f
GEOM "geom/Co2C_100_2.geo" Co2C_100_2 f
GEOM "geom/Co2C_101_1.geo" Co2C_101_1 f
GEOM "geom/Co2C_101_2.geo" Co2C_101_2 f

```

8.1 Appendix A – RF3 Settings File

```
GEOM "geom/Co2C_101_3.geo" Co2C_101_3 f
GEOM "geom/Co2C_110_1.geo" Co2C_110_1 f
GEOM "geom/Co2C_110_2.geo" Co2C_110_2 f
GEOM "geom/Co2C_110_3.geo" Co2C_110_3 f
GEOM "geom/Co2C_111_1.geo" Co2C_111_1 f
GEOM "geom/Co2C_111_2.geo" Co2C_111_2 f
GEOM "geom/Co2C_112_1.geo" Co2C_112_1 f
GEOM "geom/Co2C_112_2.geo" Co2C_112_2 f
GEOM "geom/Co2C_112_3.geo" Co2C_112_3 f
GEOM "geom/Co2C_211_1.geo" Co2C_211_1 f
GEOM "geom/Co2C_211_2.geo" Co2C_211_2 f
GEOM "geom/Co2C_211_3.geo" Co2C_211_3 f

#Surfaces of diamond
GEOM "geom/C_surf_100.geo" C_surf_100 f
GEOM "geom/C_surf_110.geo" C_surf_110 f
GEOM "geom/C_surf_111.geo" C_surf_111 f

# Surfaces of cobalt
GEOM "geom/Co_FCC_100.geo" Co_FCC_100 f
GEOM "geom/Co_FCC_110.geo" Co_FCC_110 f
GEOM "geom/Co_FCC_111.geo" Co_FCC_111 f
GEOM "geom/Co_FCC_211.geo" Co_FCC_211 f
GEOM "geom/Co_BCC_100.geo" Co_BCC_100 f
GEOM "geom/Co_BCC_110.geo" Co_BCC_110 f
GEOM "geom/Co_HCP_001.geo" Co_HCP_001 f
GEOM "geom/Co_HCP_100.geo" Co_HCP_100 f
GEOM "geom/Co_HCP_111.geo" Co_HCP_111 f

#Cobalt carbide surface defects
GEOM "geom/Co2C_SD_001_1.geo" Co2C_SD_001_1 f
GEOM "geom/Co2C_SD_001_2.geo" Co2C_SD_001_2 f
GEOM "geom/Co2C_SD_001_3.geo" Co2C_SD_001_3 f
GEOM "geom/Co2C_SD_001_4.geo" Co2C_SD_001_4 f
GEOM "geom/Co2C_SD_010_1.geo" Co2C_SD_010_1 f
GEOM "geom/Co2C_SD_010_2.geo" Co2C_SD_010_2 f
GEOM "geom/Co2C_SD_011_1.geo" Co2C_SD_011_1 f
GEOM "geom/Co2C_SD_011_2.geo" Co2C_SD_011_2 f
GEOM "geom/Co2C_SD_011_3.geo" Co2C_SD_011_3 f
GEOM "geom/Co2C_SD_100_1.geo" Co2C_SD_100_1 f
GEOM "geom/Co2C_SD_100_2.geo" Co2C_SD_100_2 f
GEOM "geom/Co2C_SD_101_1.geo" Co2C_SD_101_1 f
GEOM "geom/Co2C_SD_101_2.geo" Co2C_SD_101_2 f
GEOM "geom/Co2C_SD_101_3.geo" Co2C_SD_101_3 f
GEOM "geom/Co2C_SD_110_1.geo" Co2C_SD_110_1 f
GEOM "geom/Co2C_SD_110_2.geo" Co2C_SD_110_2 f
GEOM "geom/Co2C_SD_110_3.geo" Co2C_SD_110_3 f
GEOM "geom/Co2C_SD_111_1.geo" Co2C_SD_111_1 f
GEOM "geom/Co2C_SD_111_2.geo" Co2C_SD_111_2 f
GEOM "geom/Co2C_SD_112_1.geo" Co2C_SD_112_1 f
GEOM "geom/Co2C_SD_112_2.geo" Co2C_SD_112_2 f
GEOM "geom/Co2C_SD_112_3.geo" Co2C_SD_112_3 f
GEOM "geom/Co2C_SD_211_1.geo" Co2C_SD_211_1 f
GEOM "geom/Co2C_SD_211_2.geo" Co2C_SD_211_2 f
GEOM "geom/Co2C_SD_211_3.geo" Co2C_SD_211_3 f

#Diamond surface defects
GEOM "geom/C_surfDef_100.geo" C_surfDef_100 f
GEOM "geom/C_surfDef_110.geo" C_surfDef_110 f

#Cobalt surface defects
GEOM "geom/Co_FCC_100_SD2.geo" Co_FCC_100_SDf
GEOM "geom/Co_FCC_110_SD2.geo" Co_FCC_110_SDf
GEOM "geom/Co_FCC_111_SD2.geo" Co_FCC_111_SDf
GEOM "geom/Co_FCC_211_SD2.geo" Co_FCC_211_SDf
GEOM "geom/Co_BCC_100_SD2.geo" Co_BCC_100_SDf
GEOM "geom/Co_HCP_001_SD2.geo" Co_HCP_001_SDf
GEOM "geom/Co_HCP_100_SD2.geo" Co_HCP_100_SDf
```



```

#Cobalt carbide stacking faults
GEOM "geom/Co2C_SF_001_1.geo" Co2C_SF_001_1f
GEOM "geom/Co2C_SF_001_3.geo" Co2C_SF_001_3f
GEOM "geom/Co2C_SF_001_4.geo" Co2C_SF_001_4f
GEOM "geom/Co2C_SF_010_1.geo" Co2C_SF_010_1f
GEOM "geom/Co2C_SF_111_1.geo" Co2C_SF_111_1f

#Diamond stacking faults
GEOM "geom/C_stackF_111.geo" C_stackF_111 f

#Cobalt stacking faults
GEOM "geom/Co_FCC_111_SF2.geo" Co_FCC_111_SFf
GEOM "geom/Co_HCP_001_SF2.geo" Co_HCP_001_SFf
GEOM "geom/Co_HCP_100_SF2.geo" Co_HCP_100_SFf

# Cobalt carbide clusters
GEOM "geom/CoC2.geo" CoC2 f
GEOM "geom/Co2C2.geo" Co2C2 f
GEOM "geom/Co3C2.geo" Co3C2 f
GEOM "geom/Co4C2.geo" Co4C2 f
GEOM "geom/Co5C2.geo" Co5C2 f

#Carbon clusters
GEOM "geom/C_clus2.geo" C_clus2 f
GEOM "geom/C_clus3_linear.geo" C_clus3_linear f
GEOM "geom/C_clus3_cyclic.geo" C_clus3_cyclic f
GEOM "geom/C_clus4_linear.geo" C_clus4_linear f
GEOM "geom/C_clus4_lincyc.geo" C_clus4_lincyc f
GEOM "geom/C_clus4_cluster.geo" C_clus4_cluster f
GEOM "geom/C_clus5_linear.geo" C_clus5_linear f
GEOM "geom/C_clus5_lincyc.geo" C_clus5_lincyc f
GEOM "geom/C_clus5_linclus.geo" C_clus5_linclus f
GEOM "geom/C_clus5_cluster.geo" C_clus5_cluster f
GEOM "geom/C_clus6_linear.geo" C_clus6_linear f
GEOM "geom/C_clus6_lincyc.geo" C_clus6_lincyc f
GEOM "geom/C_clus6_linclus.geo" C_clus6_linclus f
GEOM "geom/C_clus6_bicyc.geo" C_clus6_bicycf
GEOM "geom/C_clus6_cluster.geo" C_clus6_cluster f
GEOM "geom/C_clus6_cyclic.geo" C_clus6_cyclic f
GEOM "geom/C_clus7.geo" C_clus7 f
GEOM "geom/C_clus8.geo" C_clus8 f
GEOM "geom/C_clus9.geo" C_clus9 f
GEOM "geom/C_clus10.geo" C_clus10 f
GEOM "geom/C_clus11.geo" C_clus11 f
GEOM "geom/C_clus12.geo" C_clus12 f
GEOM "geom/C_clus13.geo" C_clus13 f
GEOM "geom/C_clus14.geo" C_clus14 f
GEOM "geom/C_clus15.geo" C_clus15 f
GEOM "geom/C_clus16.geo" C_clus16 f
GEOM "geom/C_clus17.geo" C_clus17 f
GEOM "geom/C_clus18.geo" C_clus18 f
GEOM "geom/C_clus19.geo" C_clus19 f

# Cobalt clusters
GEOM "geom/Co3.geo" Co3 f
GEOM "geom/Co4.geo" Co4 f
GEOM "geom/Co5.geo" Co5 f
GEOM "geom/Co6.geo" Co6 f
GEOM "geom/Co7.geo" Co7 f
GEOM "geom/Co13.geo" Co13 f
GEOM "geom/Co55.geo" Co55 f

#Carbon on cobalt surfaces
GEOM "geom/Co_C100_1.geo" Co_C100_1 f
GEOM "geom/Co_C100_2_1.geo" Co_C100_2_1 f
GEOM "geom/Co_C100_2_2.geo" Co_C100_2_2 f
GEOM "geom/Co_C110_1.geo" Co_C110_1 f

```

8.1 Appendix A – RF3 Settings File

```

GEOM "geom/Co_C110_2_1.geo" Co_C110_2_1 f
GEOM "geom/Co_C110_2_2.geo" Co_C110_2_2 f
GEOM "geom/Co_C110b_1.geo" Co_C110b_1 f
GEOM "geom/Co_C110b_2_1.geo" Co_C110b_2_1 f
GEOM "geom/Co_C110b_2_2.geo" Co_C110b_2_2 f
GEOM "geom/Co_C111_1.geo" Co_C111_1 f
GEOM "geom/Co_C111_2_1.geo" Co_C111_2_1 f
GEOM "geom/Co_C111_2_2.geo" Co_C111_2_2 f
GEOM "geom/Co_C111_2_3.geo" Co_C111_2_3 f
GEOM "geom/Co_C211_1_1.geo" Co_C211_1_1 f
GEOM "geom/Co_C211_1_2.geo" Co_C211_1_2 f
GEOM "geom/Co_C211_2_1.geo" Co_C211_2_1 f
GEOM "geom/Co_C211_2_2.geo" Co_C211_2_2 f
GEOM "geom/Co_C211_2_3.geo" Co_C211_2_3 f
GEOM "geom/Co_C211_2_4.geo" Co_C211_2_4 f
GEOM "geom/Co_C211_2_5.geo" Co_C211_2_5 f
GEOM "geom/Co_C211_2_6.geo" Co_C211_2_6 f
GEOM "geom/Co_C211_2_7.geo" Co_C211_2_7 f
GEOM "geom/Co_C211_2_8.geo" Co_C211_2_8 f
GEOM "geom/Co_C211_2_9.geo" Co_C211_2_9 f
GEOM "geom/Co_C211_2_10.geo" Co_C211_2_10 f
GEOM "geom/Co_C211_2_11.geo" Co_C211_2_11 f
GEOM "geom/Co_C211_2_12.geo" Co_C211_2_12 f
GEOM "geom/Co_C211_2_13.geo" Co_C211_2_13 f
GEOM "geom/Co_C211_2_14.geo" Co_C211_2_14 f
GEOM "geom/Co_C211_2_15.geo" Co_C211_2_15 f
GEOM "geom/Co_C211_2_16.geo" Co_C211_2_16 f
GEOM "geom/Co_C211_2_17.geo" Co_C211_2_17 f
GEOM "geom/C_gas.geo" C_gas f
GEOM "geom/Co_C100_top.geo" Co_C100_top f
GEOM "geom/Co_C110_top.geo" Co_C110_top f
GEOM "geom/Co_C111_top.geo" Co_C111_top f
GEOM "geom/Co_C211_top.geo" Co_C211_top f
GEOM "geom/Co_C100_bridge.geo" Co_C100_bridge f
GEOM "geom/Co_C110_bridge.geo" Co_C110_bridge f
GEOM "geom/Co_C111_bridge.geo" Co_C111_bridge f
GEOM "geom/Co_C211_bridge.geo" Co_C211_bridge f
GEOM "geom/repulsie_top.geo" repulsie_top f
GEOM "geom/repulsie_bridge.geo" repulsie_bridge f

# Co2C Equation of State
EXPR "Co2C_5/6 - Co2C_opt/6" 0.574044273333333 3
EXPR "Co2C_6/6 - Co2C_opt/6" 0.240000119999999 5
EXPR "Co2C_7/6 - Co2C_opt/6" 0.06037091 8
EXPR "Co2C_8/6 - Co2C_opt/6" 0.000427123333333 10
EXPR "Co2C_9/6 - Co2C_opt/6" 0.033078496666667 8
EXPR "Co2C_10/6 - Co2C_opt/6" 0.13570338 5
EXPR "Co2C_11/6 - Co2C_opt/6" 0.289497496666667 3
EXPR "Co2C_12/6 - Co2C_opt/6" 0.478617958333333 1
EXPR "Co2C_13/6 - Co2C_opt/6" 0.692720945 1
EXPR "Co2C_14/6 - Co2C_opt/6" 0.924873221666667 1

# Diamond Equation of State
EXPR "C_4/2 - C_opt/2" 0.916668735 1
EXPR "C_5/2 - C_opt/2" 0.480059445 1
EXPR "C_6/2 - C_opt/2" 0.1990128 3
EXPR "C_7/2 - C_opt/2" 0.046405595 5
EXPR "C_opt/2 - C_opt/2" 0 10
EXPR "C_9/2 - C_opt/2" 0.04232616 5
EXPR "C_10/2 - C_opt/2" 0.15279381 3
EXPR "C_11/2 - C_opt/2" 0.319038285 1
EXPR "C_12/2 - C_opt/2" 0.529722815 1
EXPR "C_13/2 - C_opt/2" 0.774573615 1

# Graphene Equation of State
EXPR "Ce_4/2 - Ce_opt/2" 0.907028089999999 1
EXPR "Ce_5/2 - Ce_opt/2" 0.47999394 1
EXPR "Ce_6/2 - Ce_opt/2" 0.202067305 3

```

```

EXPR "Ce_7/2 - Ce_opt/2" 0.048980275 5
EXPR "Ce_opt/2 - Ce_opt/2" 0 10
EXPR "Ce_9/2 - Ce_opt/2" 0.036921385 5
EXPR "Ce_10/2 - Ce_opt/2" 0.14630872 3
EXPR "Ce_11/2 - Ce_opt/2" 0.311608735 1
EXPR "Ce_12/2 - Ce_opt/2" 0.52274255 1
EXPR "Ce_13/2 - Ce_opt/2" 0.770532164999999 1

# Graphite Equation of State
EXPR "Ci_4_1/4 - Ci_8_1/4" 0.898275877500002 3
EXPR "Ci_4_3/4 - Ci_8_3/4" 0.905292380000001 3
EXPR "Ci_6_1/4 - Ci_8_1/4" 0.197845922500001 5
EXPR "Ci_6_3/4 - Ci_8_3/4" 0.200840492500001 5
EXPR "Ci_8_1/4 - Ci_8_1/4" 0 10
EXPR "Ci_8_3/4 - Ci_8_3/4" 0 10
EXPR "Ci_10_1/4 - Ci_8_1/4" 0.14846771 5
EXPR "Ci_10_3/4 - Ci_8_3/4" 0.147097882500001 5
EXPR "Ci_12_1/4 - Ci_8_1/4" 0.52509139 3
EXPR "Ci_12_3/4 - Ci_8_3/4" 0.524128055 3
EXPR "Ci_14_1/4 - Ci_8_1/4" 1.0461736775 1
EXPR "Ci_14_3/4 - Ci_8_3/4" 1.0467145875 1

# FCC Equation of State
EXPR "Co_FCC_2 - Co_FCC_opt" 0.698514 1
EXPR "Co_FCC_3 - Co_FCC_opt" 0.339284 1
EXPR "Co_FCC_4 - Co_FCC_opt" 0.111951 3
EXPR "Co_FCC_5 - Co_FCC_opt" 0.012921 5
EXPR "Co_FCC_6 - Co_FCC_opt" 0.009946 10
EXPR "Co_FCC_7 - Co_FCC_opt" 0.075904 5
EXPR "Co_FCC_8 - Co_FCC_opt" 0.195321 3
EXPR "Co_FCC_9 - Co_FCC_opt" 0.352775 1
EXPR "Co_FCC_10 - Co_FCC_opt" 0.539964 1
EXPR "Co_FCC_11 - Co_FCC_opt" 0.744822 1
EXPR "Co_FCC_12 - Co_FCC_opt" 0.961518 1

# BCC Equation of State
EXPR "Co_BCC_3 - Co_BCC_opt" 0.474932 3
EXPR "Co_BCC_5 - Co_BCC_opt" 0.113423 5
EXPR "Co_BCC_7 - Co_BCC_opt" 0.002578 10
EXPR "Co_BCC_9 - Co_BCC_opt" 0.057325 5
EXPR "Co_BCC_11 - Co_BCC_opt" 0.223985 3
EXPR "Co_BCC_13 - Co_BCC_opt" 0.461114 1
EXPR "Co_BCC_15 - Co_BCC_opt" 0.740740 1

# HCP Equation of State
EXPR "Co_HCP_1_3 - Co_HCP_opt" 0.859482 1
EXPR "Co_HCP_2_3 - Co_HCP_opt" 0.128836 3
EXPR "Co_HCP_3_1 - Co_HCP_opt" 0.343554 3
EXPR "Co_HCP_3_2 - Co_HCP_opt" 0.076270 5
EXPR "Co_HCP_3_3 - Co_HCP_opt" 0.012672 10
EXPR "Co_HCP_3_4 - Co_HCP_opt" 0.088784 5
EXPR "Co_HCP_3_5 - Co_HCP_opt" 0.254424 3
EXPR "Co_HCP_4_3 - Co_HCP_opt" 0.231916 3
EXPR "Co_HCP_5_3 - Co_HCP_opt" 0.646114 1
EXPR "Co_HCP_6_3 - Co_HCP_opt" 1.151308 1

#Surfaces of cobalt carbide
EXPR "Co2C_001_1 / 52 - Co2C_opt / 6" 0.240838656217949 3
EXPR "Co2C_001_2 / 56 - Co2C_opt / 6" 0.392537420476191 3
EXPR "Co2C_001_3 / 60 - Co2C_opt / 6" 0.240442122166666 3
EXPR "Co2C_001_4 / 52 - Co2C_opt / 6" 0.240822464871794 3
EXPR "Co2C_010_1 / 52 - Co2C_opt / 6" 0.219956649871794 3
EXPR "Co2C_010_2 / 56 - Co2C_opt / 6" 0.387477722261904 3
EXPR "Co2C_011_1 / 80 - Co2C_opt / 6" 0.238539261583333 3
EXPR "Co2C_011_2 / 80 - Co2C_opt / 6" 0.360235023083333 3
EXPR "Co2C_011_3 / 88 - Co2C_opt / 6" 0.136239977765151 3
EXPR "Co2C_100_1 / 84 - Co2C_opt / 6" 0.292508886547618 3
EXPR "Co2C_100_2 / 84 - Co2C_opt / 6" 0.292508886666666 3

```

8.1 Appendix A – RF3 Settings File

```

EXPR "Co2C_101_1 / 80 - Co2C_opt / 6" 0.298580093958333 3
EXPR "Co2C_101_2 / 88 - Co2C_opt / 6" 0.432217886174242 3
EXPR "Co2C_101_3 / 96 - Co2C_opt / 6" 0.241921403854166 3
EXPR "Co2C_110_1 / 80 - Co2C_opt / 6" 0.344022909458333 3
EXPR "Co2C_110_2 / 72 - Co2C_opt / 6" 0.323001230555556 3
EXPR "Co2C_110_3 / 88 - Co2C_opt / 6" 0.432198854469696 3
EXPR "Co2C_111_1 / 76 - Co2C_opt / 6" 0.30701487122807 3
EXPR "Co2C_111_2 / 92 - Co2C_opt / 6" 0.366126335072463 3
EXPR "Co2C_112_1 / 128 - Co2C_opt / 6" 0.283865960598958 3
EXPR "Co2C_112_2 / 136 - Co2C_opt / 6" 0.396240485171568 3
EXPR "Co2C_112_3 / 144 - Co2C_opt / 6" 0.270544115208333 3
EXPR "Co2C_211_1 / 176 - Co2C_opt / 6" 0.265291182424242 3
EXPR "Co2C_211_2 / 160 - Co2C_opt / 6" 0.376484133083333 3
EXPR "Co2C_211_3 / 168 - Co2C_opt / 6" 0.349353734345238 3

#Surfaces of diamond
EXPR "C_surf_100/63 - C_opt/2" 0.955677801428571 3
EXPR "C_surf_110/126 - C_opt/2" 0.416580713730159 3
EXPR "C_surf_111/63 - C_opt/2" 0.849451603174602 3

# Surfaces of Cobalt
EXPR "Co_FCC_100 / 63 - Co_HCP_opt / 2" 0.2925 3
EXPR "Co_FCC_110 / 63 - Co_HCP_opt / 2" 0.3957 3
EXPR "Co_FCC_111 / 63 - Co_HCP_opt / 2" 0.2147 3
EXPR "Co_FCC_211 / 117 - Co_HCP_opt / 2" 0.3696 3
EXPR "Co_BCC_100 / 63 - Co_HCP_opt / 2" 0.4271 3
EXPR "Co_BCC_110 / 126 - Co_HCP_opt / 2" 0.3115 3
EXPR "Co_HCP_001 / 63 - Co_HCP_opt / 2" 0.2021 3
EXPR "Co_HCP_100 / 72 - Co_HCP_opt / 2" 0.3526 3
EXPR "Co_HCP_111 / 63 - Co_HCP_opt / 2" 0.8546 3

#Surface defects cobalt carbide
EXPR "Co2C_SD_001_1/51 - Co2C_001_1/52" 0.023356067997737 1
EXPR "Co2C_SD_001_2/55 - Co2C_001_2/56" -0.005351087961039 1
EXPR "Co2C_SD_001_3/59 - Co2C_001_3/60" -0.000051282138417541 1
EXPR "Co2C_SD_001_4/51 - Co2C_001_4/52" 0.023380993461539 1
EXPR "Co2C_SD_010_1/51 - Co2C_010_1/52" 0.020424724736049 1
EXPR "Co2C_SD_010_2/55 - Co2C_010_2/56" 0.00479595898052 1
EXPR "Co2C_SD_011_1/79 - Co2C_011_1/80" -0.000794470718354 1
EXPR "Co2C_SD_011_2/79 - Co2C_011_2/80" -0.006519400319619 1
EXPR "Co2C_SD_011_3/87 - Co2C_011_3/88" 0.013010698269331 1
EXPR "Co2C_SD_100_1/83 - Co2C_100_1/84" 0.019607728412221 1
EXPR "Co2C_SD_100_2/83 - Co2C_100_2/84" 0.019610570823294 1
EXPR "Co2C_SD_101_1/79 - Co2C_101_1/80" 0.015155159185127 1
EXPR "Co2C_SD_101_2/87 - Co2C_101_2/88" 0.002473252044148 1
EXPR "Co2C_SD_101_3/95 - Co2C_101_3/96" 0.003813147742326 1
EXPR "Co2C_SD_110_1/79 - Co2C_110_1/80" 0.01678486722943 1
EXPR "Co2C_SD_110_2/71 - Co2C_110_2/72" 0.006333398904538 1
EXPR "Co2C_SD_110_3/87 - Co2C_110_3/88" 0.00252633903605 1
EXPR "Co2C_SD_111_1/75 - Co2C_111_1/76" 0.019335237105264 1
EXPR "Co2C_SD_111_2/91 - Co2C_111_2/92" 0.027775812491639 1
EXPR "Co2C_SD_112_1/127 - Co2C_112_1/128" -0.009160742895546 1
EXPR "Co2C_SD_112_2/135 - Co2C_112_2/136" -0.006423887060458 1
EXPR "Co2C_SD_112_3/143 - Co2C_112_3/144" 0.003667834243882 1
EXPR "Co2C_SD_211_1/175 - Co2C_211_1/176" 0.005405741851947 1
EXPR "Co2C_SD_211_2/159 - Co2C_211_2/160" -0.001124711227988 1
EXPR "Co2C_SD_211_3/167 - Co2C_211_3/168" -0.004876098526875 1

#Differences between surface defects
EXPR "C_surfDef_100/62 - C_opt/2" 0.776039540645161 1
EXPR "C_surfDef_110/125 - C_opt/2" 0.435301858399999 1

# Surface defects
EXPR "Co_FCC_100_SD/62 - Co_HCP_opt / 2" 0.3052 1
EXPR "Co_FCC_110_SD/62 - Co_HCP_opt / 2" 0.4101 1
EXPR "Co_FCC_111_SD/62 - Co_HCP_opt / 2" 0.2407 1
EXPR "Co_FCC_211_SD/116 - Co_HCP_opt / 2" 0.3756 1
EXPR "Co_BCC_100_SD/62 - Co_HCP_opt / 2" 0.4185 1

```

```

EXPR "Co_HCP_001_SD/62 - Co_HCP_opt / 2"      0.2280      1
EXPR "Co_HCP_100_SD/71 - Co_HCP_opt / 2"      0.3704 1

#Cobalt carbide stacking faults
EXPR "Co2C_SF_001_1/52 æ" Co2C_001_1/52"    0.027202189807692  1
EXPR "Co2C_SF_001_3/60 æ" Co2C_001_3/60"    0.073528114833334  1
EXPR "Co2C_SF_001_4/52 - Co2C_001_4/52"    0.027674501923078  1
EXPR "Co2C_SF_010_1/52 - Co2C_010_1/52"    0.046832868653847  1
EXPR "Co2C_SF_111_1/76 - Co2C_111_1/76"    0.05775855131579  1

# Diamond stacking faults
EXPR "C_stackF_111/63 - C_opt/2"            0.856251073968254  1

# Cobalt stacking faults
EXPR "-Co_HCP_opt / 2 + Co_FCC_111_SF / 63"  0.2096 1
EXPR "-Co_HCP_opt / 2 + Co_HCP_001_SF / 63"  0.2833 1
EXPR "-Co_HCP_opt / 2 + Co_HCP_100_SF / 72"  0.4013 1

# Cobalt carbide clusters
EXPR "CoC2 / 3 - Co2C_opt / 6"2.056641705      1
EXPR "Co2C2 / 4 - Co2C_opt / 6"2.03039362083333  1
EXPR "Co3C2 / 5 - Co2C_opt / 6"2.12783879233333  1
EXPR "Co4C2 / 6 - Co2C_opt / 6"2.12764004166667  1
EXPR "Co5C2 / 7 - Co2C_opt / 6"2.13684346833333  1

#Differences between clusters
EXPR "C_clus2/2 - C_opt/2"                  4.32437978      1
EXPR "C_clus3_linear/3 - C_opt/2"           2.76781199666667  1
EXPR "C_clus3_cyclic/3 - C_opt/2"           2.93879250666667  1
EXPR "C_clus4_linear/4 - C_opt/2"           3.108208895      1
EXPR "C_clus4_lincyc/4 - C_opt/2"           4.11074663      1
EXPR "C_clus4_cluster/4 - C_opt/2"           4.17034054      1
EXPR "C_clus5_linear/5 - C_opt/2"           1.99300227      1
EXPR "C_clus5_lincyc/5 - C_opt/2"           2.213648142     1
EXPR "C_clus5_linclus/5 - C_opt/2"           2.46761896      1
EXPR "C_clus5_cluster/5 - C_opt/2"           2.488233626     1
EXPR "C_clus6_linear/6 - C_opt/2"           1.924821995     1
EXPR "C_clus6_lincyc/6 - C_opt/2"           2.123448185     1
EXPR "C_clus6_linclus/6 - C_opt/2"           2.12686289166667  1
EXPR "C_clus6_bicyc/6 - C_opt/2"           2.20905344833333  1
EXPR "C_clus6_cluster/6 - C_opt/2"           2.15655088333333  1
EXPR "C_clus6_cyclic/6 - C_opt/2"           1.86919984333333  1
EXPR "C_clus7/7 - C_opt/2"                   1.81006861142857  1
EXPR "C_clus8/8 - C_opt/2"                   1.70034284875    1
EXPR "C_clus9/9 - C_opt/2"                   1.54995145555556  1
EXPR "C_clus10/10 - C_opt/2"                 1.213694295     1
EXPR "C_clus11/11 - C_opt/2"                 1.28822920545455  1
EXPR "C_clus12/12 - C_opt/2"                 1.25807545      1
EXPR "C_clus13/13 - C_opt/2"                 1.19641399692308  1
EXPR "C_clus14/14 - C_opt/2"                 1.41794300571429  1
EXPR "C_clus15/15 - C_opt/2"                 1.31959363666667  1
EXPR "C_clus16/16 - C_opt/2"                 1.219743486875   1
EXPR "C_clus17/17 - C_opt/2"                 1.30823526058823  1
EXPR "C_clus18/18 - C_opt/2"                 1.12169204611111  1
EXPR "C_clus19/19 - C_opt/2"                 1.16435522368421  1

# Cobalt clusters
EXPR "Co3 / 3 - Co_HCP_opt / 2"              3.309988563     1
EXPR "Co4 / 4 - Co_HCP_opt / 2"              2.833302853     1
EXPR "Co5 / 5 - Co_HCP_opt / 2"              2.578957016     1
EXPR "Co6 / 6 - Co_HCP_opt / 2"              2.176101263     1
EXPR "Co7 / 7 - Co_HCP_opt / 2"              2.167479196     1
EXPR "Co13 / 13 - Co_HCP_opt / 2"            1.840712002     1
EXPR "Co19 / 19 - Co_HCP_opt / 2"            1.488768171     1
EXPR "Co55 / 55 - Co_HCP_opt / 2"            0.995403231     1

#Carbon on cobalt surfaces
EXPR "(Co_C100_1 - Co_FCC_100 - 2*C_gas)/65" -0.248058419846154  3

```

8.1 Appendix A – RF3 Settings File

```

EXPR "(Co_C100_2_1 - Co_FCC_100 - 4*C_gas)/67" -0.479081072985074 3
EXPR "(Co_C100_2_2 - Co_FCC_100 - 4*C_gas)/67" -0.483947913880597 3
EXPR "(Co_C110_1 - Co_FCC_110 - 2*C_gas)/65" -0.227613815692307 3
EXPR "(Co_C110_2_1 - Co_FCC_110 - 4*C_gas)/67" -0.446341746865672 3
EXPR "(Co_C110_2_2 - Co_FCC_110 - 4*C_gas)/67" -0.426989963134329 3
EXPR "(Co_C110b_1 - Co_FCC_110 - 2*C_gas)/65" -0.224471786769231 3
EXPR "(Co_C110b_2_1 - Co_FCC_110 - 4*C_gas)/67" -0.429298401044776 3
EXPR "(Co_C110b_2_2 - Co_FCC_110 - 4*C_gas)/67" -0.433841685671642 3
EXPR "(Co_C111_1 - Co_FCC_111 - 2*C_gas)/65" -0.206878103076923 3
EXPR "(Co_C111_2_1 - Co_FCC_111 - 4*C_gas)/67" -0.425893498656716 3
EXPR "(Co_C111_2_2 - Co_FCC_111 - 4*C_gas)/67" -0.394990435522388 3
EXPR "(Co_C111_2_3 - Co_FCC_111 - 4*C_gas)/67" -0.405892189552239 3
EXPR "(Co_C211_1_1 - Co_FCC_211 - 2*C_gas)/119" -0.129411164789917 3
EXPR "(Co_C211_1_2 - Co_FCC_211 - 2*C_gas)/119" -0.129413856386556 3
EXPR "(Co_C211_2_1 - Co_FCC_211 - 4*C_gas)/121" -0.249080213719009 3
EXPR "(Co_C211_2_2 - Co_FCC_211 - 4*C_gas)/121" -0.252789849917356 3
EXPR "(Co_C211_2_3 - Co_FCC_211 - 4*C_gas)/121" -0.252792861983472 3
EXPR "(Co_C211_2_4 - Co_FCC_211 - 4*C_gas)/121" -0.248621905950414 3
EXPR "(Co_C211_2_5 - Co_FCC_211 - 4*C_gas)/121" -0.238471661404959 3
EXPR "(Co_C211_2_6 - Co_FCC_211 - 4*C_gas)/121" -0.243176428264463 3
EXPR "(Co_C211_2_7 - Co_FCC_211 - 4*C_gas)/121" -0.231138349338844 3
EXPR "(Co_C211_2_8 - Co_FCC_211 - 4*C_gas)/121" -0.243023510495869 3
EXPR "(Co_C211_2_9 - Co_FCC_211 - 4*C_gas)/121" -0.235018338842976 3
EXPR "(Co_C211_2_10 - Co_FCC_211 - 4*C_gas)/121" -0.252790774049588 3
EXPR "(Co_C211_2_11 - Co_FCC_211 - 4*C_gas)/121" -0.243178539421488 3
EXPR "(Co_C211_2_12 - Co_FCC_211 - 4*C_gas)/121" -0.252787782231406 3
EXPR "(Co_C211_2_13 - Co_FCC_211 - 4*C_gas)/121" -0.241750414958679 3
EXPR "(Co_C211_2_14 - Co_FCC_211 - 4*C_gas)/121" -0.238265703223142 3
EXPR "(Co_C211_2_15 - Co_FCC_211 - 4*C_gas)/121" -0.235016000247934 3
EXPR "(Co_C211_2_16 - Co_FCC_211 - 4*C_gas)/121" -0.243025591652894 3
EXPR "(Co_C211_2_17 - Co_FCC_211 - 4*C_gas)/121" -0.244232124049588 3
EXPR "C_gas - C_gas" 0.000000000000000 10
EXPR "(Co_C100_top - Co_FCC_100 - 2*C_gas)/65" -0.104080171692308 5
EXPR "(Co_C110_top - Co_FCC_110 - 2*C_gas)/65" -0.103438851230769 5
EXPR "(Co_C111_top - Co_FCC_111 - 2*C_gas)/65" -0.107656849538462 5
EXPR "(Co_C211_top - Co_FCC_211 - 2*C_gas)/119" -0.054712837230771 5
EXPR "(Co_C100_bridge - Co_FCC_100 - 2*C_gas)/65" -0.154190683692308 5
EXPR "(Co_C110_bridge - Co_FCC_110 - 2*C_gas)/65" -0.133614535846154 5
EXPR "(Co_C111_bridge - Co_FCC_111 - 2*C_gas)/65" -0.158409459384615 5
EXPR "(Co_C211_bridge - Co_FCC_211 - 2*C_gas)/119" -0.094987092769232 5
EXPR "(repulsie_top - Co_FCC_111 - 2*C_gas)/65" 0.860168098923078 5
EXPR "(repulsie_bridge - Co_FCC_111 - 2*C_gas)/65" 0.341425817538462 5

# OPTIMIZATION SETTINGS
#
GA_GENERATIONS = 0
GA_STARTING_GENES = 8
GA_MAX_GENE_POOL = 8
GA_MUTATION_ITERATIONS = 10
GA_MCMC_BETA = 1000
GA_MCMC_VARIANCE = 500

LS_ITERATIONS = 10
LS_RESOLUTION = 6

```

8.2 APPENDIX B – EXTENSION OF A FORCE FIELD USING RF₃

During this research, RF₃, the in-house developed tool used for the fitting of the ReaxFF reactive force field, has been employed in a near-continuous fashion. As a result, through extensive use and trial and error, much experience and knowledge have been gathered about the program in the course of this research. Since information on and experience with RF₃ within the IMC group is fairly limited, especially in the case of force field extension, yet the program is expected to see more operation in the near future, a general procedure has been drafted to ease the use of the program for future users. This procedure starts with the general course of events when fitting a force field in RF₃ but has a stronger focus on the extension of a previously constructed force field with a new element. It also provides strategies to reduce disturbance of earlier fit data points, as well as tips to minimize the computational efforts of the program.

In order to commence a fitting operation, as a first step, the required files for RF₃ have to be set up. Besides geometry files that have to be constructed, the settings file that has to be filled with links to the geometry files and the inclusion of expressions to evaluate based on the training set, a parameter file and boundary files have to be constructed. For the parameter file, a set of parameters has to be chosen and it must be confirmed that the chosen parameters are within the values specified in the lower and upper boundary files. If a set of parameters is not available from previous research within the IMC group, it is strongly suggested to conduct a literature search to find a suitable parameter set for the element under investigation that can be used as an initial guess. If this is unavailable, force field parameters of an element with similar behaviour can be used, but it must be made sure that all non-empirical parameters, such as molecular mass, are adjusted accordingly. Oftentimes, the parameter sets found in literature are not accompanied by boundary files. As a completely empirical rule of thumb, a good initial guess is to remain within the same order of magnitude, e.g. a parameter value of 3.5 is limited between 0.0 and 10.0; a parameter value of 59.3 is limited between 0.0 and 100.0. Parameter values, however, should be monitored from time to time during the fitting process so that the boundaries of variable parameters can be adjusted in order to prevent limitation when it is encountered that the boundaries are being pushed. Finally, the modifiable parameters should be selected. A convenient tool in selecting the parameters to vary is the ReaxFF cheat sheet, which can be found at the end of this Appendix. The parameters classified under general parameters are mostly left untouched and, therefore, parameters are predominantly chosen from the other classifications, depending on the parameters in use. Often, a set of variables is chosen based on the energies they correspond with according to the ReaxFF cheat sheet. For example, from the off-diagonal parameters the first three parameters 'D', 'r_vdw' and 'alpha' would be an appropriate set of variables, as they all correspond with the van der Waals energy. The more variables are selected, the more options RF₃ has to explore to obtain a better fit, but it does increase the computational cost. It is, therefore, advised to only increase the number of variables when the fitness appears to stagnate on a certain level.

Now that all the files are set up, the fitting can commence. Usually, the first set of expressions that are evaluated is the bulk energy, the so-called equation of state. This is done for the reason that in most cases this set of expressions contains the reference value of the optimum that most other expressions are based on, and it is, therefore, important to achieve an accurate description of this optimum. Once this has been achieved, the training set can be expanded with more expressions. This should be done in a stepwise

8.2 Appendix B – Extension of a Force Field Using RF3

fashion, adding a couple of expressions per step and fitting this new set until satisfaction is achieved. Usually, a selection of similar expressions such as expressions evaluating surfaces is chosen as a set of additions. It is vital to add expressions in a stepwise fashion of proportional size, as adding too many expressions at once increases the odds of disturbing the already fit expressions. From chapter 2, it can be recalled that RF₃ evaluates the expressions through a cost function and each expression has a weight factor attached to it. Including too many expressions at once results in a sudden increase in the total weight that is evaluated and therefore the weight factor of the already fit expressions drops, relatively speaking. This is what increases the odds of disturbing the already fit expressions, as it becomes relatively more favourable to increase the fitness of the new expressions at the cost of sacrificing fitness of the earlier evaluated expressions. Once a parameter set has been obtained that describes a ReaxFF reactive force field to the desired accuracy, a trivial but paramount moment is reached: it is time to make a back-up. Making back-ups is a good practice in general, and it is highly advisable to do this in more intermediate stages of the fitting process in order to have decent parameters set to be able to fall back on, in case the fit is disturbed in an undesired way. The current stage, however, is paramount due to this being a result of its own. A force field has been created that accurately describes the behaviour of a certain element in the specific situations it was trained for. Therefore, it is a result that brings options: it could be utilized in many combinations with different elements that still describe the same process and it could serve as a good initial guess for the same element in a different context. Thus, it is important to assure that reproduction of the achieved result is possible.

Now that the first element has been successfully described with the ReaxFF reactive force field, it is time to move on to the second element, in other words: to extend the force field. In essence, the beginning of this process is the same as the process described in the last paragraph. Nevertheless, a recommendation on this proceeding is made. It is recommended that there is continued with the same files as used for the previous element and that these are extended, instead of repeating the process from scratch. The reason for this is risk-aversion. By preventing merging the file in a later stage of the process, the chances of confusion and resulting mistakes are diminished. It might be expected that by applying this recommendation computational costs are increased and the results for the previous elements could be altered. However, with some simple adjustments, this can all be prevented or reduced to a negligible amount. By disabling all the variations possible to the parameters of the first element, not only computational costs are diminished by reducing the number of variables, but also the parameter set for the first element essentially gets locked to a static set of parameters. As a consequence, obtained results for the evaluated expressions can no longer be altered since there are no possibilities of altering the parameters that describe the force field and the force field described for this element will thus be set in stone. Note that this can only be done when no additional data is added, that considers only one element. Therefore, as an example, cobalt surfaces used in the expressions of cobalt surfaces with carbon adsorbates should already be included in the original training set for cobalt. Subsequently, the expressions used to fit the first element will no longer have to be evaluated, which reduces computational costs even further. Finally, with many expressions no longer considered, a lot of geometry files are no longer used and disabling the unused geometry files in the settings file reduces computational costs as well. Surprisingly, disabling the reading of the geometry files seems to have the most significant effect on computational costs, as the energy of the system is calculated for each geometry, regardless of whether it is used in the expressions

or not. So, in conclusion, by continuing to work in the same files, potential trouble can be avoided with no downsides involved.

Once the second element has resulted in a satisfactory force field, the step towards fitting molecules consisting of both elements can be made. Before this, similar to the finalisation of the first element, a back-up should be made and the variable parameters, expressions and geometries for the second element should once again be disabled to stop the obtained results from changing any further and to keep computational costs low. Now, with a solid base for both individual elements, it comes down to the multi-body interactions to provide a decent fit for systems consisting of both elements. Variable parameters should, therefore, only be selected from parameters that involve both elements, as these parameters do not have an influence on the outcome of the already evaluated expressions. Once again, it is advised to start with a lower amount of variables and expressions and to add them gradually. It is also suggested to have a look at what parameters have been used in literature for force fields that involve both these elements. This should, eventually, result in a parameter set describing the ReaxFF force field with the desired properties.

With this, the most systematic and computationally efficient approach has been set out. There are, however, still two noteworthy points left to discuss. The first point to discuss will be the weight factors. Weight factors are used to determine the relative importance of evaluated expressions. More importantly, however, it is a way to exercise a subtle control over the program. RF₃ is essentially making trade-offs between different expressions on a continuous basis and since weight factors are included in this trade-off, they can be used to prioritise certain expressions. A higher weight factor means that if a trade-off is unfavourable for the expression with the higher weight factor, it is less likely to accept the trade-off since the reduction of the error of the expression on the other end of the trade-off has to be much larger. At the same time, and for an analogous reason, it is also quicker to accept a trade-off in favour of the expression with the higher weight factor. Experimenting with these weight factors is, therefore, a useful tool to drive the fit in a certain direction. Though it should be used with caution as increasing the weight factor of one expression too much, might result in a disturbance of the other expressions under evaluation. There is, however, one useful exception to this. If an expression has already reached a satisfactory agreement with the target energy, the weight factor can be increased significantly, for example for by a factor of hundred, to prevent the expression from being disturbed again, though this does make the rest of the system more rigid and therefore more difficult to operate.

RF₃ is a useful tool for fitting the force field but it requires one major resource: time. Throughout this section, options to increase computational efficiency have already been presented. Yet, there is still one final point worth discussing left: personal efficiency with regards to operating the program. Since time is a major constraint, it is important to use it as effectively as possible. The suggested strategy here is to divide the way RF₃ is operated in two ways: short runs and long runs. Short runs are runs with a low amount of iterations. They are best run at times of high work activity, i.e. working hours. At these moments they can be effectively monitored and therefore aptly adjusted in between runs. Longer runs are runs with a high amount of iterations that are best run at downtimes, for example overnight or over the weekend. Ideally, a long run continues on a parameter set that delivered promising results in short runs and can, therefore, be explored for a longer time. RF₃ conveniently displays the amount of time that was required for previous iterations and therefore careful estimates can be made about the time that an amount of

8.2 Appendix B – Extension of a Force Field Using RF3

iterations requires. Using this information, the uptime can be optimised and RF₃ can be used to its fullest potential.

ReaxFF Cheat Sheet

General Parameters

p_boc1	---	p_pen3		p_coa4	
p_boc2	norb_low <i>fixed</i>	p_pen4		p_ovun4	
p_coa2	norb_cut <i>fixed</i>	---	p_ovun3		
---	---	p_tor2		p_val8	
---	p_val6	p_tor3		---	
---	p_lpl	p_tor4		---	
p_ovun6	p_val9	---		p_coa3	
---	p_val10	p_cot2		---	
p_ovun7	---	p_vdw1			
p_ovun8	p_pen2	bo_cut <i>fixed</i>			

Atomic Parameters

r_s <i>positive</i>	va1 <i>fixed</i>	mass <i>fixed</i>	r_vdw	epsilon	gamma	r_pi <i>positive</i>	val_e <i>fixed</i>
alpha	gamma_w	val_boc <i>fixed</i>	p_ovun5	---	chi	eta	p_hbond
r_pi_pi <i>positive</i>	p_lp2	---	b_o_13 boc4	b_o_132 boc5	b_o_133 boc5	---	---
p_ovun2	p_val3	---	val_val <i>fixed</i>	p_val5	r_core2	ecore2	acore2

Two Body Parameters

de_s <i>if_bond</i>	de_p <i>if_bond</i>	de_pp <i>if_bond</i>	p_be1	p_bo5	v13cor	p_bo6	p_ovun1
p_be2	p_bo3	p_bo4	---	p_bo1	---	ovc	---

OffDiagonal Parameters

0	r_vdw	alpha	r_s <i>positive</i>	r_pi <i>positive</i>	r_pi_pi <i>positive</i>
---	-------	-------	------------------------	-------------------------	----------------------------

ValenceAngle Parameters

theta_0	p_val1	p_val2	p_coa1	p_val7	p_pen1	p_val14
---------	--------	--------	--------	--------	--------	---------

TorsionAngle Parameters

v1	v2	v3	p_tor1	p_cot1
----	----	----	--------	--------

Hydrogen Bond Parameters

r_o_hb	p_hb1	p_hb2	p_hb3
--------	-------	-------	-------

e_bond	e_pen	e_vdw			
e_ov	e_coa	e_pi			
e_lp	e_hb	e_pi			
e_ang	e_con	e_pi			

DESCRIPTION
 value if fixed
 always larger than 0
 only non-zero if such a bond can exist

LABEL
 fixed
 positive
 if_bond

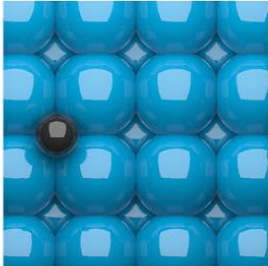
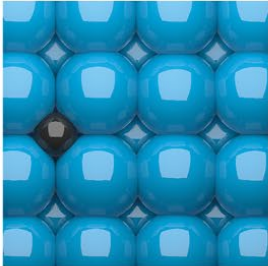
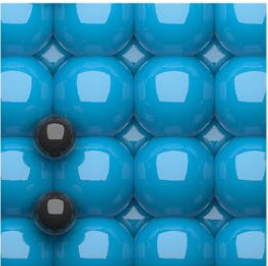
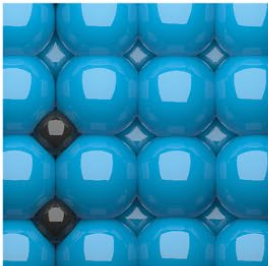
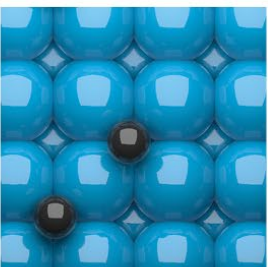
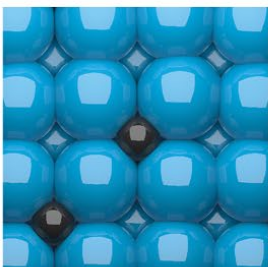
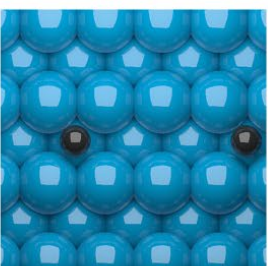
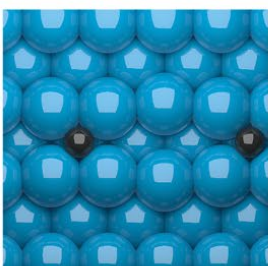
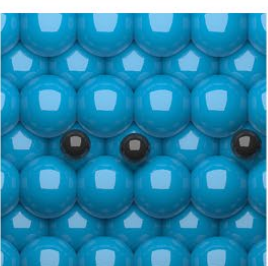
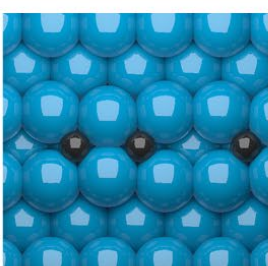
Legend:
 Yellow: implemented
 Green: to be implemented
 Blue: unused
 Red: not used

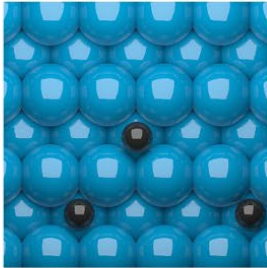
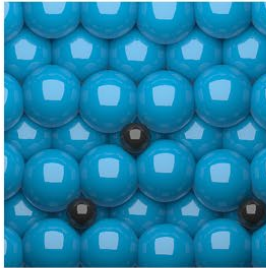
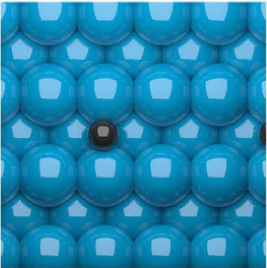
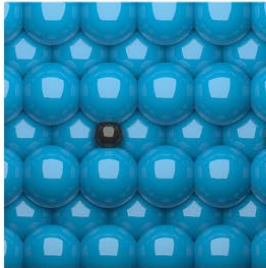
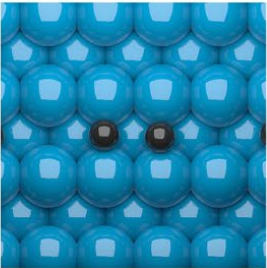
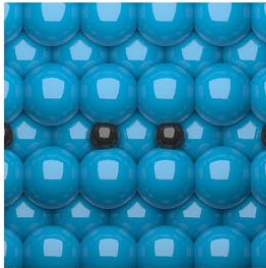
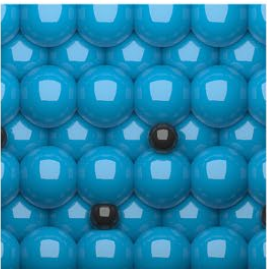
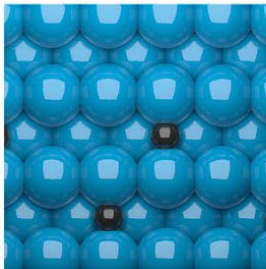
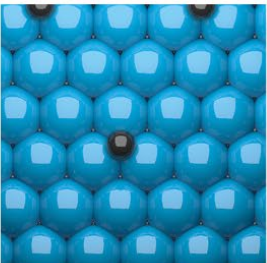
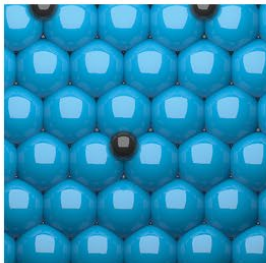
NOTES
 In principle, the valence values for the first two rows of atoms are fixed
 (i.e. C,H,N,O...)



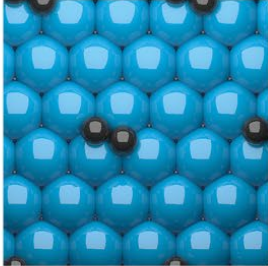
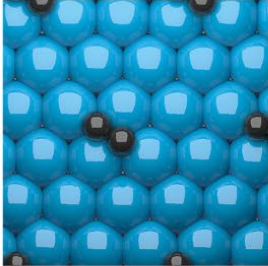
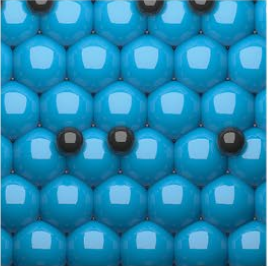
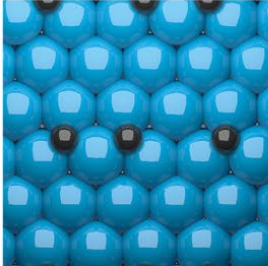
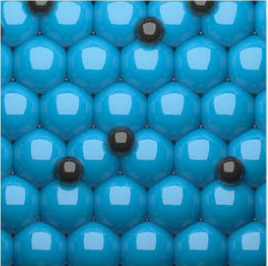
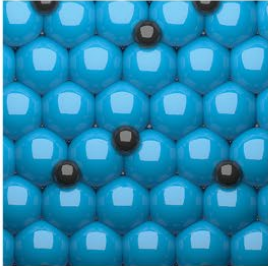
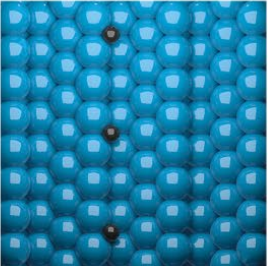
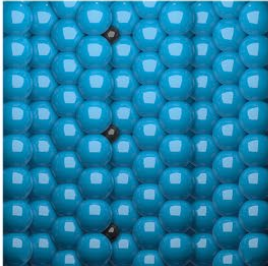
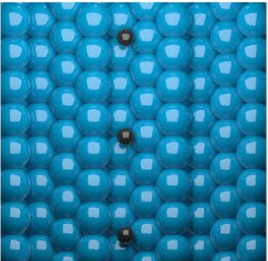
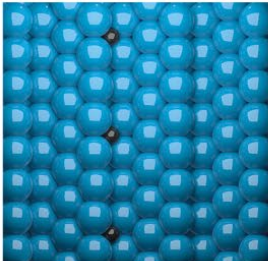
Author: No Filot <i.a.w.filot@tue.nl>

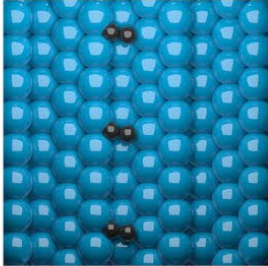
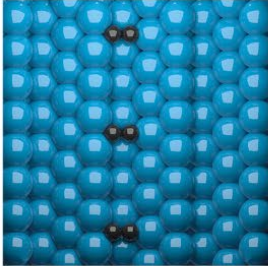
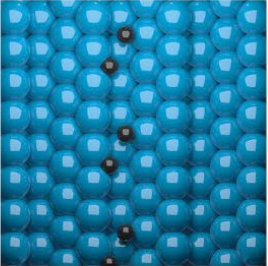
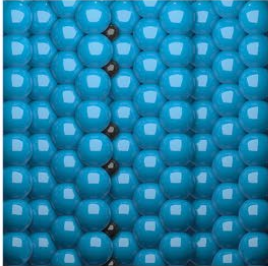
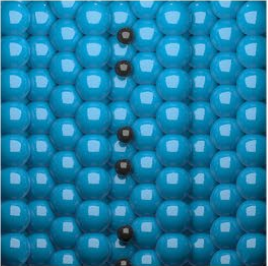
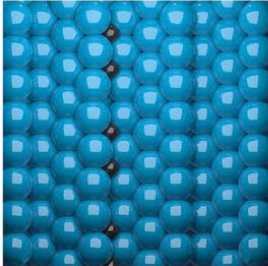
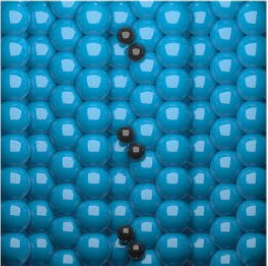

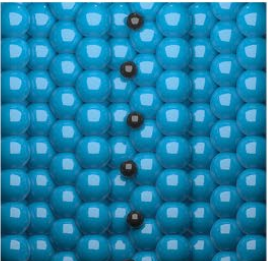
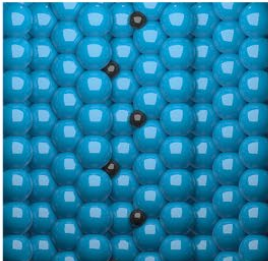
8.3 APPENDIX C – GEOMETRY AND ENERGY RESULTS AFTER DFT

Geometry	Input	Output	System energy (eV)
fcc(100) 1			-448.047
fcc(100) 2.1			-466.660
fcc(100) 2.2			-466.986
fcc(110) 1 set 1			-440.217
fcc(110) 2.1 set 1			-457.965

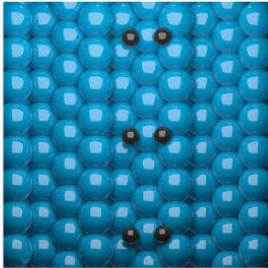
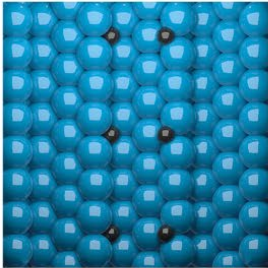
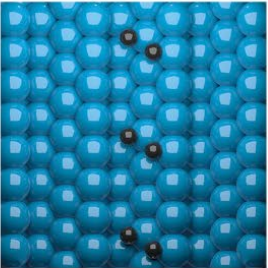
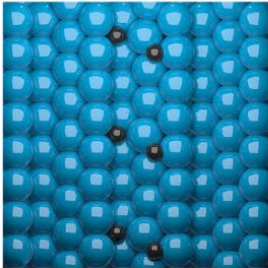
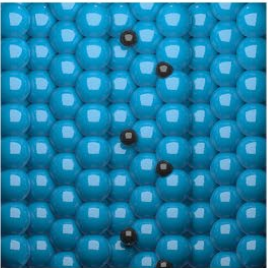
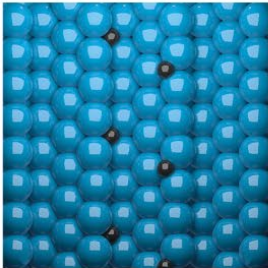
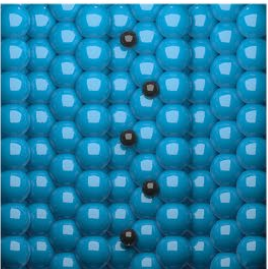
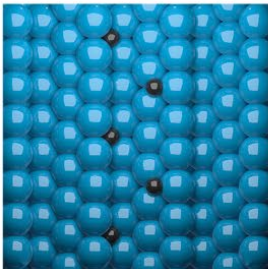
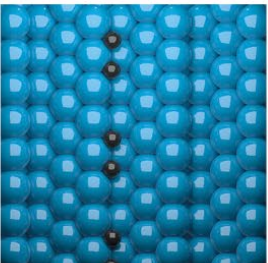
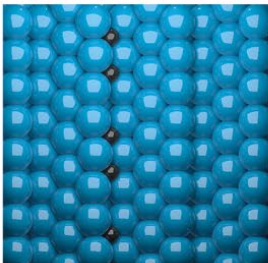
Geometry	Input	Output	System energy (eV)
fcc(110) 2.2 set 1			-456.668
fcc(110) 1 set 2			-440.012
fcc(110) 2.1 set 2			-456.823
fcc(110) 2.2 set 2			-457.127
fcc(111) 1			-450.272

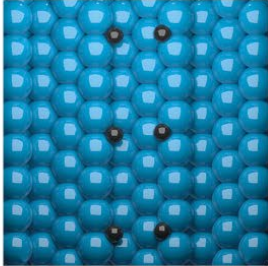
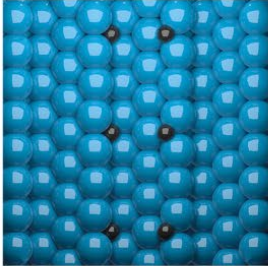
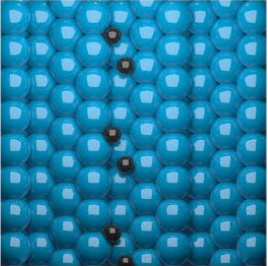
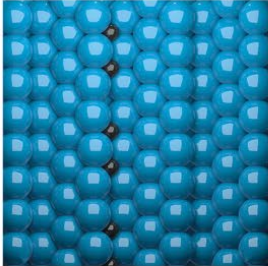
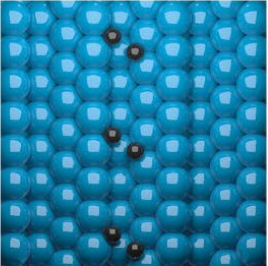
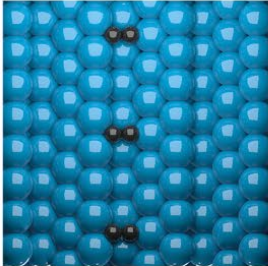
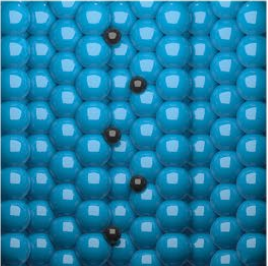
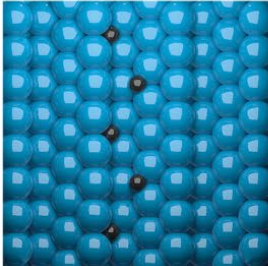
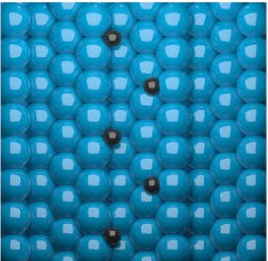
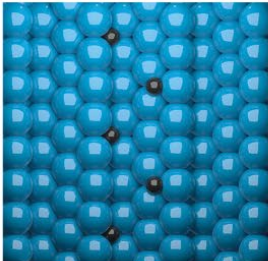
8.3 Appendix C – Geometry and Energy Results After DFT

Geometry	Input	Output	System energy (eV)
fcc(111) 2.1			-467.998
fcc(111) 2.2			-465.927
fcc(111) 2.3			-466.678
fcc(211) 1.1			-806.261
fcc(211) 1.2			-806.261

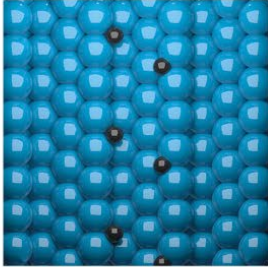
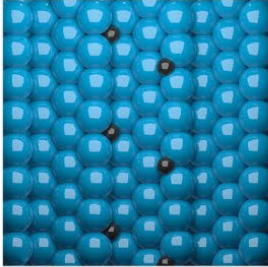
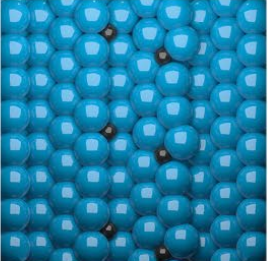
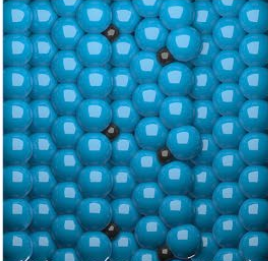
Geometry	Input	Output	System energy (eV)
fcc(211) 2.1			-823.638
fcc(211) 2.2			-824.087
fcc(211) 2.3			-824.087
fcc(211) 2.4			-823.583
fcc(211) 2.5			-822.354

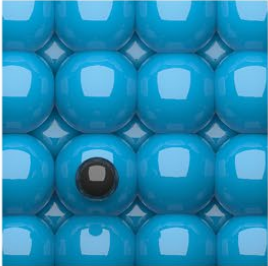
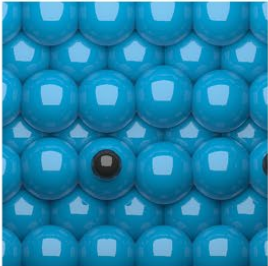
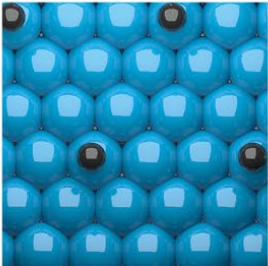
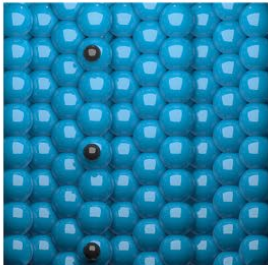
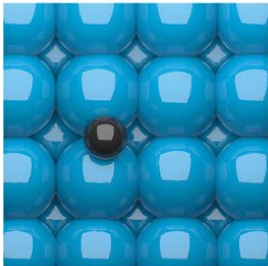
8.3 Appendix C – Geometry and Energy Results After DFT

Geometry	Input	Output	System energy (eV)
fcc(211) 2.6			-822.924
fcc(211) 2.7			-821.467
fcc(211) 2.8			-822.905
fcc(211) 2.9			-821.937
fcc(211) 2.10			-824.087

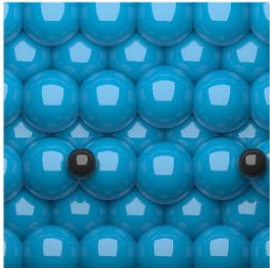
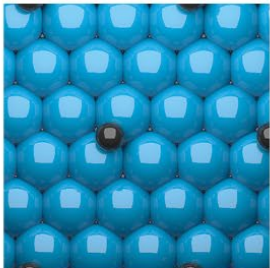
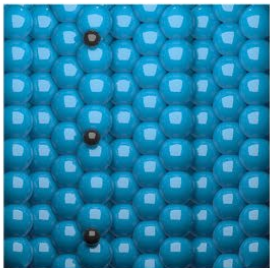
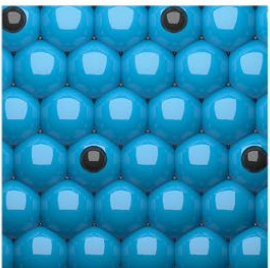
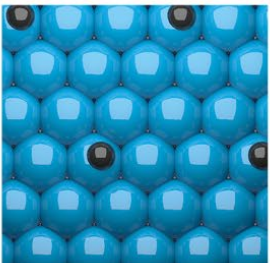
Geometry	Input	Output	System energy (eV)
fcc(211) 2.11			-822.934
fcc(211) 2.12			-824.087
fcc(211) 2.13			-822.751
fcc(211) 2.14			-822.329
fcc(211) 2.15			-821.936

8.3 Appendix C – Geometry and Energy Results After DFT

Geometry	Input	Output	System energy (eV)
fcc(211) 2.16			-822.905
fcc(211) 2.17			-823.051

Geometry	Input = Output (1 iteration)	System energy (eV)
fcc(100) top		-438.688
fcc(110) top		-432.145
fcc(111) top		-443.822
fcc(211) top		-794.417
fcc(100) bridge		-441.946

8.3 Appendix C – Geometry and Energy Results After DFT

Geometry	Input = Output (1 iteration)	System energy (eV)
fcc(110) bridge		-434.107
fcc(111) bridge		-447.121
fcc(211) bridge		-797.035
fcc(111) top repulsive in- teraction		-380.914
fcc(111) bridge repulsive interaction		-414.632

8.4 APPENDIX D – ORIGINAL RESULTS OF THE FITTING PROCEDURE

Appendix D1 – Results for the constructed force field

id	target	reaxff	weight	err2	cumul	formula		
1	0.57404	0.69766	300	4.58438	4.58438	Co2C_5/6	-	Co2C_opt/6
2	0.24	0.38422	500	10.40013	14.98451	Co2C_6/6	-	Co2C_opt/6
3	0.06037	0.16318	800	8.45598	23.44048	Co2C_7/6	-	Co2C_opt/6
4	0.00043	0.00801	1000	0.05745	23.49793	Co2C_8/6	-	Co2C_opt/6
5	0.03308	-0.11465	800	17.45874	40.95667	Co2C_9/6	-	Co2C_opt/6
6	0.1357	0.0805	500	1.5239	42.48057	Co2C_10/6	-	Co2C_opt/6
7	0.2895	0.27453	300	0.06718	42.54775	Co2C_11/6	-	Co2C_opt/6
8	0.47862	0.64034	100	2.6153	45.16304	Co2C_12/6	-	Co2C_opt/6
9	0.69272	0.75523	100	0.3908	45.55384	Co2C_13/6	-	Co2C_opt/6
10	0.92487	0.70783	100	4.71095	50.26479	Co2C_14/6	-	Co2C_opt/6
11	0.91667	1.16776	1	0.06305	50.32784	C_4/2	-	C_opt/2
12	0.48006	0.6536	1	0.03012	50.35796	C_5/2	-	C_opt/2
13	0.19901	0.233	3	0.00347	50.36143	C_6/2	-	C_opt/2
14	0.04641	0.02056	5	0.00334	50.36477	C_7/2	-	C_opt/2
15	0	0	10	0	50.36477	C_opt/2	-	C_opt/2
16	0.04233	0.04141	5	0	50.36477	C_9/2	-	C_opt/2
17	0.15279	0.09322	3	0.01065	50.37542	C_10/2	-	C_opt/2
18	0.31904	0.30341	1	0.00024	50.37566	C_11/2	-	C_opt/2
19	0.52972	0.57556	1	0.0021	50.37777	C_12/2	-	C_opt/2
20	0.77457	0.83903	1	0.00415	50.38192	C_13/2	-	C_opt/2
21	0.90703	0.86702	1	0.0016	50.38352	Ce_4/2	-	Ce_opt/2
22	0.47999	0.4712	1	0.00008	50.3836	Ce_5/2	-	Ce_opt/2
23	0.20207	0.1534	3	0.0071	50.3907	Ce_6/2	-	Ce_opt/2
24	0.04898	-0.00756	5	0.01598	50.40668	Ce_7/2	-	Ce_opt/2
25	0	0	10	0	50.40668	Ce_opt/2	-	Ce_opt/2
26	0.03692	-0.00424	5	0.00847	50.41515	Ce_9/2	-	Ce_opt/2
27	0.14631	0.08132	3	0.01267	50.42783	Ce_10/2	-	Ce_opt/2
28	0.31161	0.24588	1	0.00432	50.43215	Ce_11/2	-	Ce_opt/2
29	0.52274	0.47429	1	0.00235	50.43449	Ce_12/2	-	Ce_opt/2
30	0.77053	0.79306	1	0.00051	50.435	Ce_13/2	-	Ce_opt/2
31	0.89828	0.88065	3	0.00093	50.43593	Ci_4_1/4	-	Ci_8_1/4
32	0.90529	0.87665	3	0.00246	50.4384	Ci_4_3/4	-	Ci_8_3/4
33	0.19785	0.16431	5	0.00562	50.44402	Ci_6_1/4	-	Ci_8_1/4
34	0.20084	0.16137	5	0.00779	50.45181	Ci_6_3/4	-	Ci_8_3/4
35	0	0	10	0	50.45181	Ci_8_1/4	-	Ci_8_1/4
36	0	0	10	0	50.45181	Ci_8_3/4	-	Ci_8_3/4
37	0.14847	0.08098	5	0.02277	50.47458	Ci_10_1/4	-	Ci_8_1/4
38	0.1471	0.0817	5	0.02139	50.49596	Ci_10_3/4	-	Ci_8_3/4
39	0.52509	0.46953	3	0.00926	50.50522	Ci_12_1/4	-	Ci_8_1/4
40	0.52413	0.47134	3	0.00836	50.51358	Ci_12_3/4	-	Ci_8_3/4
41	1.04617	1.18543	1	0.01939	50.53298	Ci_14_1/4	-	Ci_8_1/4

8.4 Appendix D – Original Results of the Fitting Procedure

42	1.04671	1.19763	1	0.02278	50.55575	Ci_14_3/4	-	Ci_8_3/4		
43	0.69851	0.69363	1	0.00002	50.55577	Co_FCC_2	-	Co_FCC_opt		
44	0.33928	0.37775	1	0.00148	50.55725	Co_FCC_3	-	Co_FCC_opt		
45	0.11195	0.11862	3	0.00013	50.55739	Co_FCC_4	-	Co_FCC_opt		
46	0.01292	0.01042	5	0.00003	50.55742	Co_FCC_5	-	Co_FCC_opt		
47	0.00995	0.01267	10	0.00007	50.55749	Co_FCC_6	-	Co_FCC_opt		
48	0.0759	0.09094	5	0.00113	50.55862	Co_FCC_7	-	Co_FCC_opt		
49	0.19532	0.21666	3	0.00137	50.55999	Co_FCC_8	-	Co_FCC_opt		
50	0.35278	0.36803	1	0.00023	50.56022	Co_FCC_9	-	Co_FCC_opt		
51	0.53996	0.52751	1	0.00016	50.56038	Co_FCC_10	-	Co_FCC_opt		
52	0.74482	0.70385	1	0.00168	50.56206	Co_FCC_11	-	Co_FCC_opt		
53	0.96152	0.84432	1	0.01374	50.57579	Co_FCC_12	-	Co_FCC_opt		
54	0.47493	0.3755	3	0.02966	50.60545	Co_BCC_3	-	Co_BCC_opt		
55	0.11342	0.08517	5	0.00399	50.60945	Co_BCC_5	-	Co_BCC_opt		
56	0.00258	0.00044	10	0.00005	50.60949	Co_BCC_7	-	Co_BCC_opt		
57	0.05733	0.05942	5	0.00002	50.60951	Co_BCC_9	-	Co_BCC_opt		
58	0.22398	0.17531	3	0.00711	50.61662	Co_BCC_11	-	Co_BCC_opt		
59	0.46111	0.35784	1	0.01066	50.62729	Co_BCC_13	-	Co_BCC_opt		
60	0.74074	0.57672	1	0.0269	50.65419	Co_BCC_15	-	Co_BCC_opt		
61	0.85948	0.90786	1	0.00234	50.65653	Co_HCP_1_3	-	Co_HCP_opt		
62	0.12884	0.14021	3	0.00039	50.65692	Co_HCP_2_3	-	Co_HCP_opt		
63	0.34355	0.34213	3	0.00001	50.65692	Co_HCP_3_1	-	Co_HCP_opt		
64	0.07627	0.07357	5	0.00004	50.65696	Co_HCP_3_2	-	Co_HCP_opt		
65	0.01267	0.01671	10	0.00016	50.65712	Co_HCP_3_3	-	Co_HCP_opt		
66	0.08878	0.08933	5	0	50.65712	Co_HCP_3_4	-	Co_HCP_opt		
67	0.25442	0.27585	3	0.00138	50.6585	Co_HCP_3_5	-	Co_HCP_opt		
68	0.23192	0.27961	3	0.00682	50.66532	Co_HCP_4_3	-	Co_HCP_opt		
69	0.64611	0.69433	1	0.00232	50.66765	Co_HCP_5_3	-	Co_HCP_opt		
70	1.15131 /	1.12415 6	1	0.00074	50.66839	Co_HCP_6_3	-	Co_HCP_opt	-	Co2C_opt
71	0.24084	1.19741	3	2.7451	53.41349	Co2C_001_1/	52	-	Co2C_opt	/ 6
72	0.39254	-1.46064	3	10.30278	63.71627	Co2C_001_2/	56	-	Co2C_opt	/ 6
73	0.24044	-0.09166	3	0.33088	64.04715	Co2C_001_3/	60	-	Co2C_opt	/ 6
74	0.24082	1.1996	3	2.75779	66.80494	Co2C_001_4/	52	-	Co2C_opt	/ 6
75	0.21996	1.44166	3	4.47765	71.28259	Co2C_010_1/	52	-	Co2C_opt	/ 6
76	0.38748	-1.37682	3	9.33826	80.62085	Co2C_010_2/	56	-	Co2C_opt	/ 6
77	0.23854	0.03618	3	0.12285	80.74369	Co2C_011_1/	80	-	Co2C_opt	/ 6
78	0.36024	-1.06153	3	6.06425	86.80794	Co2C_011_2/	80	-	Co2C_opt	/ 6
79	0.13624	0.8487	3	1.5228	88.33074	Co2C_011_3/	88	-	Co2C_opt	/ 6
80	0.29251	-0.14046	3	0.56238	88.89312	Co2C_100_1/	84	-	Co2C_opt	/ 6
81	0.29251	-0.14064	3	0.56286	89.45597	Co2C_100_2/	84	-	Co2C_opt	/ 6
82	0.29858	1.19363	3	2.40335	91.85932	Co2C_101_1/	80	-	Co2C_opt	/ 6
83	0.43222	-1.55483	3	11.84514	103.70446	Co2C_101_2/	88	-	Co2C_opt	/ 6
84	0.24192	0.01544	3	0.15388	103.85834	Co2C_101_3/	96	-	Co2C_opt	/ 6
85	0.34402	1.19061	3	2.15013	106.00847	Co2C_110_1/	80	-	Co2C_opt	/ 6

Chapter 8: Appendices

86	0.323	0.15762	3	0.08205	106.09053	Co2C_110_2/	72	-	Co2C_opt /	6
87	0.4322	-1.55539	3	11.8515	117.94203	Co2C_110_3/	88	-	Co2C_opt /	6
88	0.30701	0.56232	3	0.19554	118.13756	Co2C_111_1/	76	-	Co2C_opt /	6
89	0.36613	-1.00723	3	5.65833	123.79589	Co2C_111_2/	92	-	Co2C_opt /	6
90	0.28387	0.12255	3	0.07807	123.87396	Co2C_112_1/	128	-	Co2C_opt /	6
91	0.39624	-1.01561	3	5.97999	129.85395	Co2C_112_2/	136	-	Co2C_opt /	6
92	0.27054	-0.1955	3	0.65158	130.50553	Co2C_112_3/	144	-	Co2C_opt /	6
93	0.26529	0.47589	3	0.13305	130.63858	Co2C_211_1/	176	-	Co2C_opt /	6
94	0.37648	-0.84798	3	4.49795	135.13653	Co2C_211_2/	160	-	Co2C_opt /	6
95	0.34935	-0.28735	3	1.21616	136.3527	Co2C_211_3/	168	-	Co2C_opt /	6
96	0.95568	1.01004	3	0.00886	136.36156	C_surf_100/63	-	C_opt/2		
97	0.41658	0.47272	3	0.00945	136.37102	C_surf_110/126	-	C_opt/2		
98	0.84945 /	1.03157 2	3	0.0995	136.47052	C_surf_111/63	-	C_opt/2	-	Co_HCP_opt
99	0.2925 /	0.27989 2	3	0.00048	136.471	Co_FCC_100	/	63	-	Co_HCP_opt
100	0.3957 /	0.45534 2	3	0.01067	136.48167	Co_FCC_110	/	63	-	Co_HCP_opt
101	0.2147 /	0.22746 2	3	0.00049	136.48216	Co_FCC_111	/	63	-	Co_HCP_opt
102	0.3696 /	0.3966 2	3	0.00219	136.48434	Co_FCC_211	/	117	-	Co_HCP_opt
103	0.4271 /	0.4803 2	3	0.00849	136.49284	Co_BCC_100	/	63	-	Co_HCP_opt
104	0.3115 /	0.31308 2	3	0.00001	136.49284	Co_BCC_110	/	126	-	Co_HCP_opt
105	0.2021 /	0.22827 2	3	0.00205	136.4949	Co_HCP_001	/	63	-	Co_HCP_opt
106	0.3526 /	0.40076 2	3	0.00696	136.50186	Co_HCP_100	/	72	-	Co_HCP_opt
107	0.8546 /	0.94646 2	3	0.02531	136.52717	Co_HCP_111	/	63	-	Co_HCP_opt
108	0.02336	-0.4419	1	0.21647	136.74364	Co2C_SD_001_1/51	-	Co2C_001_1/52		
109	-0.00535	0.18133	1	0.03485	136.77849	Co2C_SD_001_2/55	-	Co2C_001_2/56		
110	-0.00005	0.10276	1	0.01057	136.78906	Co2C_SD_001_3/59	-	Co2C_001_3/60		
111	0.02338	-0.44264	1	0.21718	137.00623	Co2C_SD_001_4/51	-	Co2C_001_4/52		
112	0.02042	-0.90231	1	0.85143	137.85767	Co2C_SD_010_1/51	-	Co2C_010_1/52		
113	0.0048	0.14696	1	0.02021	137.87788	Co2C_SD_010_2/55	-	Co2C_010_2/56		
114	-0.00079	0.52082	1	0.27208	138.14996	Co2C_SD_011_1/79	-	Co2C_011_1/80		
115	-0.00652	0.1685	1	0.03063	138.18059	Co2C_SD_011_2/79	-	Co2C_011_2/80		
116	0.01301	0.01298	1	0	138.18059	Co2C_SD_011_3/87	-	Co2C_011_3/88		
117	0.01961	-0.16913	1	0.03562	138.21621	Co2C_SD_100_1/83	-	Co2C_100_1/84		
118	0.01961	-0.16888	1	0.03553	138.25174	Co2C_SD_100_2/83	-	Co2C_100_2/84		
119	0.01516	-0.19255	1	0.04314	138.29488	Co2C_SD_101_1/79	-	Co2C_101_1/80		
120	0.00247	0.11751	1	0.01323	138.30812	Co2C_SD_101_2/87	-	Co2C_101_2/88		
121	0.00381	0.04551	1	0.00174	138.30986	Co2C_SD_101_3/95	-	Co2C_101_3/96		
122	0.01678	-0.12246	1	0.01939	138.32925	Co2C_SD_110_1/79	-	Co2C_110_1/80		
123	0.00633	0.06271	1	0.00318	138.33242	Co2C_SD_110_2/71	-	Co2C_110_2/72		
124	0.00253	0.11754	1	0.01323	138.34565	Co2C_SD_110_3/87	-	Co2C_110_3/88		

8.4 Appendix D – Original Results of the Fitting Procedure

125	0.01934	-0.20867	1	0.05199	138.39764	Co2C_SD_111_1/75	-	Co2C_111_1/76		
126	0.02778	-0.18956	1	0.04723	138.44487	Co2C_SD_111_2/91	-	Co2C_111_2/92		
127	-0.00916	0.18696	1	0.03846	138.48334	Co2C_SD_112_1/127	-	Co2C_112_1/128		
128	-0.00642	0.05399	1	0.00365	138.48699	Co2C_SD_112_2/135	-	Co2C_112_2/136		
129	0.00367	0.0332	1	0.00087	138.48786	Co2C_SD_112_3/143	-	Co2C_112_3/144		
130	0.00541	-0.06958	1	0.00562	138.49348	Co2C_SD_211_1/175	-	Co2C_211_1/176		
131	-0.00112	0.04214	1	0.00187	138.49535	Co2C_SD_211_2/159	-	Co2C_211_2/160		
132	-0.00488	0.06922	1	0.00549	138.50084	Co2C_SD_211_3/167	-	Co2C_211_3/168		
133	0.77604	0.66962	1	0.01133	138.51217	C_surfDef_100/62	-	C_opt/2		
134	0.4353	0.39992	1	0.00125	138.51342	C_surfDef_110/125	-	C_opt/2	/	2
135	0.3052	0.30222	1	0.00001	138.51343	Co_FCC_100_SD/62	-	Co_HCP_opt	/	2
136	0.4101	0.46839	1	0.0034	138.51683	Co_FCC_110_SD/62	-	Co_HCP_opt	/	2
137	0.2407	0.27182	1	0.00097	138.5178	Co_FCC_111_SD/62	-	Co_HCP_opt	/	2
138	0.3756	0.40458	1	0.00084	138.51864	Co_FCC_211_SD/116	-	Co_HCP_opt	/	2
139	0.4185	0.47708	1	0.00343	138.52207	Co_BCC_100_SD/62	-	Co_HCP_opt	/	2
140	0.228	0.2521	1	0.00058	138.52265	Co_HCP_001_SD/62	-	Co_HCP_opt	/	2
141	0.3704	0.41677	1	0.00215	138.5248	Co_HCP_100_SD/71	-	Co_HCP_opt	/	2
142	0.0272	0.41677	1	0.15176	138.67656	Co2C_SF_001_1/52	-	Co2C_001_1/52		
143	0.07353	0.41677	1	0.11781	138.79437	Co2C_SF_001_3/60	-	Co2C_001_3/60		
144	0.02767	0.07882	1	0.00262	138.79699	Co2C_SF_001_4/52	-	Co2C_001_4/52		
145	0.04683	-0.15707	1	0.04158	138.83857	Co2C_SF_010_1/52	-	Co2C_010_1/52		
146	0.05776	-0.83869	1	0.80361	139.64218	Co2C_SF_111_1/76	-	Co2C_111_1/76		
147	0.85625 /	0.69597 63	1	0.02569	139.66787	C_stackF_111/63	-	C_opt/2	+	Co_FCC_111_SF
148	0.2096 /	0.22706 63	1	0.0003	139.66817	-Co_HCP_opt	/	2	+	Co_FCC_111_SF
149	0.2833 /	0.28753 63	1	0.00002	139.66819	-Co_HCP_opt	/	2	+	Co_HCP_001_SF
150	0.4013 /	0.46091 72	1	0.00355	139.67175	-Co_HCP_opt	/	2	+	Co_HCP_100_SF
151	2.05664	1.78256	1	0.07512	139.74687	CoC2	/	3	-	Co2C_opt / 6
152	2.03039	2.61341	1	0.33991	140.08677	Co2C2	/	4	-	Co2C_opt / 6
153	2.12784	1.86254	1	0.07039	140.15716	Co3C2	/	5	-	Co2C_opt / 6
154	2.12764	1.98095	1	0.02152	140.17868	Co4C2	/	6	-	Co2C_opt / 6
155	2.13684	1.37378	1	0.58226	140.76094	Co5C2	/	7	-	Co2C_opt / 6
156	4.32438	4.1153	1	0.04371	140.80465	C_clus2/2	-	C_opt/2		
157	2.76781	3.00609	1	0.05678	140.86143	C_clus3_linear/3	-	C_opt/2		
158	2.93879	2.57025	1	0.13582	140.99725	C_clus3_cyclic/3	-	C_opt/2		
159	3.10821	2.87325	1	0.05521	141.05246	C_clus4_linear/4	-	C_opt/2		
160	4.11075	4.38743	1	0.07655	141.12901	C_clus4_lincyc/4	-	C_opt/2		
161	4.17034	4.26846	1	0.00963	141.13864	C_clus4_cluster/4	-	C_opt/2		
162	1.993	2.22874	1	0.05557	141.19421	C_clus5_linear/5	-	C_opt/2		
163	2.21365	2.46135	1	0.06136	141.25556	C_clus5_lincyc/5	-	C_opt/2		
164	2.46762	2.50299	1	0.00125	141.25681	C_clus5_linclus/5	-	C_opt/2		
165	2.48823	2.225	1	0.06929	141.32611	C_clus5_cluster/5	-	C_opt/2		
166	1.92482	2.05508	1	0.01697	141.34307	C_clus6_linear/6	-	C_opt/2		

Chapter 8: Appendices

167	2.12345	2.27982	1	0.02445	141.36752	C_clus6_lincyc/6	-	C_opt/2		
168	2.12686	2.02051	1	0.01131	141.37884	C_clus6_linclus/6	-	C_opt/2		
169	2.20905	2.43081	1	0.04918	141.42801	C_clus6_bicyc/6	-	C_opt/2		
170	2.15655	2.11313	1	0.00189	141.4299	C_clus6_cluster/6	-	C_opt/2		
171	1.8692	2.4047	1	0.28676	141.71665	C_clus6_cyclic/6	-	C_opt/2		
172	1.81007	1.83003	1	0.0004	141.71705	C_clus7/7	-	C_opt/2		
173	1.70034	1.55905	1	0.01996	141.73702	C_clus8/8	-	C_opt/2		
174	1.54995	1.47397	1	0.00577	141.74279	C_clus9/9	-	C_opt/2		
175	1.21369	1.39259	1	0.032	141.77479	C_clus10/10	-	C_opt/2		
176	1.28823	1.39943	1	0.01236	141.78716	C_clus11/11	-	C_opt/2		
177	1.25808	1.30171	1	0.0019	141.78906	C_clus12/12	-	C_opt/2		
178	1.19641	1.21864	1	0.00049	141.78956	C_clus13/13	-	C_opt/2		
179	1.41794	1.26515	1	0.02335	141.8129	C_clus14/14	-	C_opt/2		
180	1.31959	1.27036	1	0.00242	141.81533	C_clus15/15	-	C_opt/2		
181	1.21974	1.14664	1	0.00534	141.82067	C_clus16/16	-	C_opt/2		
182	1.30824	1.20225	1	0.01123	141.8319	C_clus17/17	-	C_opt/2		
183	1.12169	1.10579	1	0.00025	141.83216	C_clus18/18	-	C_opt/2		
184	1.16436 2	1.10577	1	0.00343	141.83559	C_clus19/19	-	C_opt/2	-	Co_HCP_opt /
185	3.30999 2	3.47157	1	0.02611	141.8617	Co3	/	3	-	Co_HCP_opt /
186	2.8333 2	2.8232	1	0.0001	141.8618	Co4	/	4	-	Co_HCP_opt /
187	2.57896 2	2.39061	1	0.03548	141.89727	Co5	/	5	-	Co_HCP_opt /
188	2.1761 2	2.20009	1	0.00058	141.89785	Co6	/	6	-	Co_HCP_opt /
189	2.16748 2	2.07276	1	0.00897	141.90682	Co7	/	7	-	Co_HCP_opt /
190	1.84071 2	1.55276	1	0.08292	141.98974	Co13	/	13	-	Co_HCP_opt /
191	1.48877 2	1.55276	1	0.00409	141.99383	Co19	/	19	-	Co_HCP_opt /
192	0.9954 2	0.99358	1	0	141.99384	Co55	/	55	-	Co_HCP_opt /
193	-0.24806	-0.28735	300	0.46305	142.45689	(Co_C100_1	-	Co_FCC_100	-	2*C_gas)/65
194	-0.47908 4*C_gas)/67	-0.50187	300	0.15587	142.61275	(Co_C100_2_1	-	Co_FCC_100	-	
195	-0.48395 4*C_gas)/67	-0.46465	300	0.11178	142.72453	(Co_C100_2_2	-	Co_FCC_100	-	
196	-0.22761	-0.27698	300	0.73101	143.45554	(Co_C110_1	-	Co_FCC_110	-	2*C_gas)/65
197	-0.44634 4*C_gas)/67	-0.51371	300	1.3615	144.81704	(Co_C110_2_1	-	Co_FCC_110	-	
198	-0.42699 4*C_gas)/67	-0.44798	300	0.13222	144.94926	(Co_C110_2_2	-	Co_FCC_110	-	
199	-0.22447 2*C_gas)/65	-0.21459	300	0.02929	144.97855	(Co_C110b_1	-	Co_FCC_110	-	
200	-0.4293 4*C_gas)/67	-0.40404	300	0.19145	145.17	(Co_C110b_2_1	-	Co_FCC_110	-	
201	-0.43384 4*C_gas)/67	-0.41322	300	0.12763	145.29763	(Co_C110b_2_2	-	Co_FCC_110	-	
202	-0.20688	-0.15633	300	0.76655	146.06418	(Co_C111_1	-	Co_FCC_111	-	2*C_gas)/65

8.4 Appendix D – Original Results of the Fitting Procedure

203	-0.42589 4*C_gas)/67	-0.27691	300	6.65883	152.72302	(Co_C111_2_1	-	Co_FCC_111	-
204	-0.39499 4*C_gas)/67	-0.14754	300	18.36987	171.09288	(Co_C111_2_2	-	Co_FCC_111	-
205	-0.40589 4*C_gas)/67	-0.16681	300	17.1487	188.24159	(Co_C111_2_3	-	Co_FCC_111	-
206	-0.12941 2*C_gas)/119	-0.14632	300	0.08574	188.32732	(Co_C211_1_1	-	Co_FCC_211	-
207	-0.12941 2*C_gas)/119	-0.14659	300	0.08847	188.41579	(Co_C211_1_2	-	Co_FCC_211	-
208	-0.24908 4*C_gas)/121	-0.35117	300	3.12668	191.54247	(Co_C211_2_1	-	Co_FCC_211	-
209	-0.25279 4*C_gas)/121	-0.24592	300	0.01415	191.55662	(Co_C211_2_2	-	Co_FCC_211	-
210	-0.25279 4*C_gas)/121	-0.24585	300	0.01448	191.5711	(Co_C211_2_3	-	Co_FCC_211	-
211	-0.24862 4*C_gas)/121	-0.32694	300	1.84024	193.41134	(Co_C211_2_4	-	Co_FCC_211	-
212	-0.23847 4*C_gas)/121	-0.13552	300	3.17944	196.59078	(Co_C211_2_5	-	Co_FCC_211	-
213	-0.24318 4*C_gas)/121	-0.23344	300	0.02844	196.61922	(Co_C211_2_6	-	Co_FCC_211	-
214	-0.23114 4*C_gas)/121	-0.14717	300	2.11517	198.73439	(Co_C211_2_7	-	Co_FCC_211	-
215	-0.24302 4*C_gas)/121	-0.22937	300	0.05589	198.79028	(Co_C211_2_8	-	Co_FCC_211	-
216	-0.23502 4*C_gas)/121	-0.21731	300	0.09413	198.88441	(Co_C211_2_9	-	Co_FCC_211	-
217	-0.25279 4*C_gas)/121	-0.24593	300	0.01411	198.89852	(Co_C211_2_10	-	Co_FCC_211	-
218	-0.24318 4*C_gas)/121	-0.23356	300	0.02773	198.92625	(Co_C211_2_11	-	Co_FCC_211	-
219	-0.25279 4*C_gas)/121	-0.24581	300	0.01462	198.94086	(Co_C211_2_12	-	Co_FCC_211	-
220	-0.24175 4*C_gas)/121	-0.23722	300	0.00616	198.94702	(Co_C211_2_13	-	Co_FCC_211	-
221	-0.23827 4*C_gas)/121	-0.24998	300	0.04118	198.98821	(Co_C211_2_14	-	Co_FCC_211	-
222	-0.23502 4*C_gas)/121	-0.21717	300	0.09551	199.08372	(Co_C211_2_15	-	Co_FCC_211	-
223	-0.24303 4*C_gas)/121	-0.22927	300	0.05675	199.14046	(Co_C211_2_16	-	Co_FCC_211	-
224	-0.24423 4*C_gas)/121	-0.23592	300	0.02073	199.1612	(Co_C211_2_17	-	Co_FCC_211	-
225	0	0	1000	0	199.1612	C_gas	-	C_gas	- 2*C_gas)/65
226	-0.10408 2*C_gas)/65	0.10868	5	0.22634	199.38754	(Co_C100_top	-	Co_FCC_100	-
227	-0.10344 2*C_gas)/65	0.11187	5	0.2318	199.61933	(Co_C110_top	-	Co_FCC_110	-
228	-0.10766 2*C_gas)/65	0.1386	5	0.3032	199.92253	(Co_C111_top	-	Co_FCC_111	-
229	-0.05471 2*C_gas)/119	0.05008	5	0.05491	199.97745	(Co_C211_top	-	Co_FCC_211	-
230	-0.15419 2*C_gas)/65	0.11008	5	0.3492	200.32665	(Co_C100_bridge	-	Co_FCC_100	-
231	-0.13361 2*C_gas)/65	0.13303	5	0.35549	200.68214	(Co_C110_bridge	-	Co_FCC_110	-
232	-0.15841 2*C_gas)/65	0.01865	10	0.31349	200.99563	(Co_C111_bridge	-	Co_FCC_111	-

233	-0.09499 2*C_gas)/119	0.10541	5	0.20079	201.19642	(Co_C211_bridge	-	Co_FCC_211	-
234	0.86017 2*C_gas)/65	0.42797	5	0.93399	202.13041	(repulsie_top	-	Co_FCC_111	-
235	0.34143 2*C_gas)/65	0.13761	1200	49.85024	251.98066	(repulsie_bridge	-	Co_FCC_111	-

Appendix D2 – Results for the SCM force field

id	target	reaxff	weight	err2	cumul	formula			
1	0.57404	0.36424	300	13.20552	13.20552	Co2C_5/6	-	Co2C_opt/6	
2	0.24	0.16536	500	2.78573	15.99125	Co2C_6/6	-	Co2C_opt/6	
3	0.06037	0.05657	800	0.01155	16.0028	Co2C_7/6	-	Co2C_opt/6	
4	0.00043	0.00525	1000	0.0233	16.02609	Co2C_8/6	-	Co2C_opt/6	
5	0.03308	-0.01397	800	1.77104	17.79713	Co2C_9/6	-	Co2C_opt/6	
6	0.1357	-0.02334	500	12.64671	30.44384	Co2C_10/6	-	Co2C_opt/6	
7	0.2895	-0.05358	300	35.31092	65.75476	Co2C_11/6	-	Co2C_opt/6	
8	0.47862	-0.0524	100	28.19785	93.95261	Co2C_12/6	-	Co2C_opt/6	
9	0.69272	-0.47417	100	136.16414	230.11675	Co2C_13/6	-	Co2C_opt/6	
10	0.92487	-0.3316	100	157.87147	387.98821	Co2C_14/6	-	Co2C_opt/6	
11	0.91667	3.38855	1	6.11018	394.0984	C_4/2	-	C_opt/2	
12	0.48006	2.38486	1	3.62828	397.72667	C_5/2	-	C_opt/2	
13	0.19901	1.49188	3	5.01451	402.74119	C_6/2	-	C_opt/2	
14	0.04641	0.67425	5	1.97092	404.71211	C_7/2	-	C_opt/2	
15	0	0	10	0	404.71211	C_opt/2	-	C_opt/2	
16	0.04233	-0.30028	5	0.58688	405.29899	C_9/2	-	C_opt/2	
17	0.15279	0.07641	3	0.0175	405.3165	C_10/2	-	C_opt/2	
18	0.31904	0.36456	1	0.00207	405.31857	C_11/2	-	C_opt/2	
19	0.52972	0.90377	1	0.13991	405.45848	C_12/2	-	C_opt/2	
20	0.77457	1.39839	1	0.38915	405.84763	C_13/2	-	C_opt/2	
21	0.90703	3.3039	1	5.74498	411.5926	Ce_4/2	-	Ce_opt/2	
22	0.47999	2.18919	1	2.92136	414.51397	Ce_5/2	-	Ce_opt/2	
23	0.20207	1.30925	3	3.67755	418.19151	Ce_6/2	-	Ce_opt/2	
24	0.04898	0.58442	5	1.43345	419.62497	Ce_7/2	-	Ce_opt/2	
25	0	0	10	0	419.62497	Ce_opt/2	-	Ce_opt/2	
26	0.03692	-0.26365	5	0.4517	420.07667	Ce_9/2	-	Ce_opt/2	
27	0.14631	0.10801	3	0.0044	420.08107	Ce_10/2	-	Ce_opt/2	
28	0.31161	0.37984	1	0.00466	420.08573	Ce_11/2	-	Ce_opt/2	
29	0.52274	0.58171	1	0.00348	420.0892	Ce_12/2	-	Ce_opt/2	
30	0.77053	0.69707	1	0.0054	420.0946	Ce_13/2	-	Ce_opt/2	
31	0.89828	3.30852	3	17.42777	437.52238	Ci_4_1/4	-	Ci_8_1/4	
32	0.90529	3.30369	3	17.25688	454.77926	Ci_4_3/4	-	Ci_8_3/4	
33	0.19785	1.31352	5	6.22361	461.00287	Ci_6_1/4	-	Ci_8_1/4	
34	0.20084	1.31046	5	6.15626	467.15913	Ci_6_3/4	-	Ci_8_3/4	
35	0	0	10	0	467.15913	Ci_8_1/4	-	Ci_8_1/4	
36	0	0	10	0	467.15913	Ci_8_3/4	-	Ci_8_3/4	

8.4 Appendix D – Original Results of the Fitting Procedure

37	0.14847	0.08378	5	0.02092	467.18005	Ci_10_1/4	-	Ci_8_1/4		
38	0.1471	0.08793	5	0.01751	467.19756	Ci_10_3/4	-	Ci_8_3/4		
39	0.52509	0.56889	3	0.00575	467.20331	Ci_12_1/4	-	Ci_8_1/4		
40	0.52413	0.57531	3	0.00786	467.21117	Ci_12_3/4	-	Ci_8_3/4		
41	1.04617	1.10428	1	0.00338	467.21455	Ci_14_1/4	-	Ci_8_1/4		
42	1.04671	1.11187	1	0.00425	467.21879	Ci_14_3/4	-	Ci_8_3/4		
43	0.69851	0.46408	1	0.05496	467.27375	Co_FCC_2	-	Co_FCC_opt		
44	0.33928	0.10543	1	0.05469	467.32844	Co_FCC_3	-	Co_FCC_opt		
45	0.11195	-0.05063	3	0.0793	467.40773	Co_FCC_4	-	Co_FCC_opt		
46	0.01292	-0.04732	5	0.01814	467.42588	Co_FCC_5	-	Co_FCC_opt		
47	0.00995	0.0736	10	0.04051	467.46639	Co_FCC_6	-	Co_FCC_opt		
48	0.0759	0.2723	5	0.19286	467.65925	Co_FCC_7	-	Co_FCC_opt		
49	0.19532	0.51315	3	0.30304	467.96229	Co_FCC_8	-	Co_FCC_opt		
50	0.35278	0.76503	1	0.16995	468.13225	Co_FCC_9	-	Co_FCC_opt		
51	0.53996	0.99929	1	0.21098	468.34323	Co_FCC_10	-	Co_FCC_opt		
52	0.74482	1.19202	1	0.19998	468.54321	Co_FCC_11	-	Co_FCC_opt		
53	0.96152	1.30424	1	0.11746	468.66067	Co_FCC_12	-	Co_FCC_opt		
54	0.47493	0.05692	3	0.5242	469.18487	Co_BCC_3	-	Co_BCC_opt		
55	0.11342	-0.09652	5	0.22039	469.40526	Co_BCC_5	-	Co_BCC_opt		
56	0.00258	-0.01021	10	0.00163	469.40689	Co_BCC_7	-	Co_BCC_opt		
57	0.05733	0.2059	5	0.11038	469.51727	Co_BCC_9	-	Co_BCC_opt		
58	0.22398	0.47505	3	0.1891	469.70637	Co_BCC_11	-	Co_BCC_opt		
59	0.46111	0.74239	1	0.07911	469.78548	Co_BCC_13	-	Co_BCC_opt		
60	0.74074	0.94332	1	0.04104	469.82652	Co_BCC_15	-	Co_BCC_opt		
61	0.85948	0.47294	1	0.14941	469.97593	Co_HCP_1_3	-	Co_HCP_opt		
62	0.12884	-0.08789	3	0.14092	470.11685	Co_HCP_2_3	-	Co_HCP_opt		
63	0.34355	0.2701	3	0.01619	470.13304	Co_HCP_3_1	-	Co_HCP_opt		
64	0.07627	0.05636	5	0.00198	470.13502	Co_HCP_3_2	-	Co_HCP_opt		
65	0.01267	0.11019	10	0.0951	470.23012	Co_HCP_3_3	-	Co_HCP_opt		
66	0.08878	0.34496	5	0.32812	470.55824	Co_HCP_3_4	-	Co_HCP_opt		
67	0.25442	0.67369	3	0.52734	471.08558	Co_HCP_3_5	-	Co_HCP_opt		
68	0.23192	0.68864	3	0.62578	471.71136	Co_HCP_4_3	-	Co_HCP_opt		
69	0.64611	1.33841	1	0.47927	472.19063	Co_HCP_5_3	-	Co_HCP_opt		
70	1.15131 /	1.86901 6	1	0.5151	472.70573	Co_HCP_6_3	-	Co_HCP_opt	-	Co2C_opt
71	0.24084	0.17027	3	0.01494	472.72067	Co2C_001_1/	52	-	Co2C_opt	/ 6
72	0.39254	-0.27457	3	1.33509	474.05576	Co2C_001_2/	56	-	Co2C_opt	/ 6
73	0.24044	-0.06831	3	0.28598	474.34174	Co2C_001_3/	60	-	Co2C_opt	/ 6
74	0.24082	0.17166	3	0.01435	474.35609	Co2C_001_4/	52	-	Co2C_opt	/ 6
75	0.21996	0.12216	3	0.02869	474.38479	Co2C_010_1/	52	-	Co2C_opt	/ 6
76	0.38748	-0.34043	3	1.58956	475.97435	Co2C_010_2/	56	-	Co2C_opt	/ 6
77	0.23854	0.20211	3	0.00398	475.97833	Co2C_011_1/	80	-	Co2C_opt	/ 6
78	0.36024	-0.20169	3	0.94727	476.9256	Co2C_011_2/	80	-	Co2C_opt	/ 6
79	0.13624	0.06298	3	0.0161	476.9417	Co2C_011_3/	88	-	Co2C_opt	/ 6
80	0.29251	-0.10576	3	0.47585	477.41756	Co2C_100_1/	84	-	Co2C_opt	/ 6

Chapter 8: Appendices

81	0.29251	-0.10612	3	0.47672	477.89428	Co2C_100_2/	84	-	Co2C_opt /	6
82	0.29858	0.15448	3	0.06229	477.95657	Co2C_101_1/	80	-	Co2C_opt /	6
83	0.43222	-0.38036	3	1.98083	479.9374	Co2C_101_2/	88	-	Co2C_opt /	6
84	0.24192	-0.13703	3	0.43081	480.36821	Co2C_101_3/	96	-	Co2C_opt /	6
85	0.34402	0.1804	3	0.08032	480.44853	Co2C_110_1/	80	-	Co2C_opt /	6
86	0.323	-0.18039	3	0.76022	481.20875	Co2C_110_2/	72	-	Co2C_opt /	6
87	0.4322	-0.37966	3	1.97735	483.18609	Co2C_110_3/	88	-	Co2C_opt /	6
88	0.30701	0.05176	3	0.19547	483.38156	Co2C_111_1/	76	-	Co2C_opt /	6
89	0.36613	-0.30585	3	1.35465	484.73621	Co2C_111_2/	92	-	Co2C_opt /	6
90	0.28387	0.12434	3	0.07634	484.81255	Co2C_112_1/	128	-	Co2C_opt /	6
91	0.39624	-0.28628	3	1.39751	486.21006	Co2C_112_2/	136	-	Co2C_opt /	6
92	0.27054	-0.08034	3	0.36935	486.57941	Co2C_112_3/	144	-	Co2C_opt /	6
93	0.26529	0.01956	3	0.18115	486.76056	Co2C_211_1/	176	-	Co2C_opt /	6
94	0.37648	-0.28941	3	1.33025	488.09081	Co2C_211_2/	160	-	Co2C_opt /	6
95	0.34935	-0.12395	3	0.67205	488.76286	Co2C_211_3/	168	-	Co2C_opt /	6
96	0.95568	3.01824	3	12.76246	501.52531	C_surf_100/63	-	C_opt/2		
97	0.41658	0.58121	3	0.08131	501.60663	C_surf_110/126	-	C_opt/2		
98	0.84945 /	1.45217 2	3	1.08981	502.69644	C_surf_111/63	-	C_opt/2	-	Co_HCP_opt
99	0.2925 /	0.17546 2	3	0.0411	502.73753	Co_FCC_100	/	63	-	Co_HCP_opt
100	0.3957 /	0.27514 2	3	0.0436	502.78114	Co_FCC_110	/	63	-	Co_HCP_opt
101	0.2147 /	0.14515 2	3	0.01451	502.79565	Co_FCC_111	/	63	-	Co_HCP_opt
102	0.3696 /	0.23607 2	3	0.05349	502.84913	Co_FCC_211	/	117	-	Co_HCP_opt
103	0.4271 /	0.485 2	3	0.01006	502.85919	Co_BCC_100	/	63	-	Co_HCP_opt
104	0.3115 /	0.36048 2	3	0.0072	502.86639	Co_BCC_110	/	126	-	Co_HCP_opt
105	0.2021 /	0.1331 2	3	0.01428	502.88067	Co_HCP_001	/	63	-	Co_HCP_opt
106	0.3526 /	0.22135 2	3	0.05168	502.93235	Co_HCP_100	/	72	-	Co_HCP_opt
107	0.8546 /	0.54964 2	3	0.27901	503.21136	Co_HCP_111	/	63	-	Co_HCP_opt
108	0.02336	-0.06367	1	0.00757	503.21893	Co2C_SD_001_1/51	-	Co2C_001_1/52		
109	-0.00535	-0.00183	1	0.00001	503.21894	Co2C_SD_001_2/55	-	Co2C_001_2/56		
110	-0.00005	0.03011	1	0.00091	503.21985	Co2C_SD_001_3/59	-	Co2C_001_3/60		
111	0.02338	-0.06385	1	0.00761	503.22746	Co2C_SD_001_4/51	-	Co2C_001_4/52		
112	0.02042	-0.04195	1	0.00389	503.23135	Co2C_SD_010_1/51	-	Co2C_010_1/52		
113	0.0048	0.01396	1	0.00008	503.23143	Co2C_SD_010_2/55	-	Co2C_010_2/56		
114	-0.00079	-0.04058	1	0.00158	503.23302	Co2C_SD_011_1/79	-	Co2C_011_1/80		
115	-0.00652	0.02475	1	0.00098	503.234	Co2C_SD_011_2/79	-	Co2C_011_2/80		
116	0.01301	0.01504	1	0	503.234	Co2C_SD_011_3/87	-	Co2C_011_3/88		
117	0.01961	-0.04317	1	0.00394	503.23794	Co2C_SD_100_1/83	-	Co2C_100_1/84		
118	0.01961	-0.04267	1	0.00388	503.24182	Co2C_SD_100_2/83	-	Co2C_100_2/84		
119	0.01516	-0.03213	1	0.00224	503.24406	Co2C_SD_101_1/79	-	Co2C_101_1/80		

8.4 Appendix D – Original Results of the Fitting Procedure

120	0.00247	-0.00055	1	0.00001	503.24407	Co2C_SD_101_2/87	-	Co2C_101_2/88		
121	0.00381	0.02042	1	0.00028	503.24434	Co2C_SD_101_3/95	-	Co2C_101_3/96		
122	0.01678	-0.03507	1	0.00269	503.24703	Co2C_SD_110_1/79	-	Co2C_110_1/80		
123	0.00633	0.02525	1	0.00036	503.24739	Co2C_SD_110_2/71	-	Co2C_110_2/72		
124	0.00253	-0.00098	1	0.00001	503.2474	Co2C_SD_110_3/87	-	Co2C_110_3/88		
125	0.01934	-0.04498	1	0.00414	503.25154	Co2C_SD_111_1/75	-	Co2C_111_1/76		
126	0.02778	-0.04219	1	0.0049	503.25643	Co2C_SD_111_2/91	-	Co2C_111_2/92		
127	-0.00916	0.00819	1	0.0003	503.25673	Co2C_SD_112_1/127	-	Co2C_112_1/128		
128	-0.00642	0.01405	1	0.00042	503.25715	Co2C_SD_112_2/135	-	Co2C_112_2/136		
129	0.00367	0.00868	1	0.00003	503.25718	Co2C_SD_112_3/143	-	Co2C_112_3/144		
130	0.00541	-0.01759	1	0.00053	503.25771	Co2C_SD_211_1/175	-	Co2C_211_1/176		
131	-0.00112	0.00597	1	0.00005	503.25776	Co2C_SD_211_2/159	-	Co2C_211_2/160		
132	-0.00488	0.00729	1	0.00015	503.2579	Co2C_SD_211_3/167	-	Co2C_211_3/168		
133	0.77604	1.09505	1	0.10177	503.35967	C_surfDef_100/62	-	C_opt/2		
134	0.4353	0.4332	1	0	503.35968	C_surfDef_110/125	-	C_opt/2	/	2
135	0.3052	0.18907	1	0.01349	503.37316	Co_FCC_100_SD/62	-	Co_HCP_opt	/	2
136	0.4101	0.28248	1	0.01629	503.38945	Co_FCC_110_SD/62	-	Co_HCP_opt	/	2
137	0.2407	0.17062	1	0.00491	503.39436	Co_FCC_111_SD/62	-	Co_HCP_opt	/	2
138	0.3756	0.24163	1	0.01795	503.41231	Co_FCC_211_SD/116	-	Co_HCP_opt	/	2
139	0.4185	0.42395	1	0.00003	503.41234	Co_BCC_100_SD/62	-	Co_HCP_opt	/	2
140	0.228	0.15037	1	0.00603	503.41837	Co_HCP_001_SD/62	-	Co_HCP_opt	/	2
141	0.3704	0.23303	1	0.01887	503.43724	Co_HCP_100_SD/71	-	Co_HCP_opt	/	2
142	0.0272	0.23303	1	0.04236	503.4796	Co2C_SF_001_1/52	-	Co2C_001_1/52		
143	0.07353	0.23303	1	0.02544	503.50504	Co2C_SF_001_3/60	-	Co2C_001_3/60		
144	0.02767	-0.0741	1	0.01036	503.5154	Co2C_SF_001_4/52	-	Co2C_001_4/52		
145	0.04683	-0.02741	1	0.00551	503.52091	Co2C_SF_010_1/52	-	Co2C_010_1/52		
146	0.05776	-0.03782	1	0.00914	503.53005	Co2C_SF_111_1/76	-	Co2C_111_1/76		
147	0.85625 /	1.06326 63	1	0.04285	503.5729	C_stackF_111/63	-	C_opt/2	+	Co_FCC_111_SF
148	0.2096 /	0.13906 63	1	0.00498	503.57788	-Co_HCP_opt	/	2	+	Co_FCC_111_SF
149	0.2833 /	0.2211 63	1	0.00387	503.58174	-Co_HCP_opt	/	2	+	Co_HCP_001_SF
150	0.4013 /	0.34013 72	1	0.00374	503.58549	-Co_HCP_opt	/	2	+	Co_HCP_100_SF
151	2.05664	-0.70006	1	7.59938	511.18487	CoC2	/	3	-	Co2C_opt / 6
152	2.03039	-0.6794	1	7.34298	518.52785	Co2C2	/	4	-	Co2C_opt / 6
153	2.12784	-0.72251	1	8.12446	526.65232	Co3C2	/	5	-	Co2C_opt / 6
154	2.12764	-1.14616	1	10.71776	537.37008	Co4C2	/	6	-	Co2C_opt / 6
155	2.13684	-1.2935	1	11.76729	549.13737	Co5C2	/	7	-	Co2C_opt / 6
156	4.32438	3.73772	1	0.34417	549.48153	C_clus2/2	-	C_opt/2		
157	2.76781	2.80853	1	0.00166	549.48319	C_clus3_linear/3	-	C_opt/2		
158	2.93879	3.2965	1	0.12795	549.61114	C_clus3_cyclic/3	-	C_opt/2		
159	3.10821	2.4171	1	0.47763	550.08877	C_clus4_linear/4	-	C_opt/2		
160	4.11075	5.32986	1	1.48624	551.57501	C_clus4_lincyc/4	-	C_opt/2		
161	4.17034	5.87826	1	2.917	554.49201	C_clus4_cluster/4	-	C_opt/2		

Chapter 8: Appendices

162	1.993	2.12539	1	0.01753	554.50953	C_clus5_linear/5	-	C_opt/2		
163	2.21365	2.65422	1	0.19411	554.70364	C_clus5_lincyc/5	-	C_opt/2		
164	2.46762	2.95998	1	0.24242	554.94606	C_clus5_linclus/5	-	C_opt/2		
165	2.48823	3.07573	1	0.34515	555.29121	C_clus5_cluster/5	-	C_opt/2		
166	1.92482	1.97898	1	0.00293	555.29415	C_clus6_linear/6	-	C_opt/2		
167	2.12345	2.32878	1	0.04216	555.33631	C_clus6_lincyc/6	-	C_opt/2		
168	2.12686	2.41663	1	0.08397	555.42027	C_clus6_linclus/6	-	C_opt/2		
169	2.20905	2.64972	1	0.19418	555.61446	C_clus6_bicyc/6	-	C_opt/2		
170	2.15655	2.47501	1	0.10142	555.71587	C_clus6_cluster/6	-	C_opt/2		
171	1.8692	3.33799	1	2.15735	557.87322	C_clus6_cyclic/6	-	C_opt/2		
172	1.81007	2.97577	1	1.35886	559.23208	C_clus7/7	-	C_opt/2		
173	1.70034	2.5956	1	0.80148	560.03356	C_clus8/8	-	C_opt/2		
174	1.54995	2.21497	1	0.44225	560.47581	C_clus9/9	-	C_opt/2		
175	1.21369	2.10784	1	0.7995	561.27531	C_clus10/10	-	C_opt/2		
176	1.28823	1.64623	1	0.12816	561.40347	C_clus11/11	-	C_opt/2		
177	1.25808	1.30082	1	0.00183	561.4053	C_clus12/12	-	C_opt/2		
178	1.19641	1.3995	1	0.04125	561.44654	C_clus13/13	-	C_opt/2		
179	1.41794	1.70295	1	0.08123	561.52777	C_clus14/14	-	C_opt/2		
180	1.31959	1.61957	1	0.08999	561.61776	C_clus15/15	-	C_opt/2		
181	1.21974	1.38589	1	0.02761	561.64536	C_clus16/16	-	C_opt/2		
182	1.30824	1.66566	1	0.12775	561.77311	C_clus17/17	-	C_opt/2		
183	1.12169	1.3947	1	0.07453	561.84764	C_clus18/18	-	C_opt/2		
184	1.16436 2	1.27574	1	0.01241	561.86005	C_clus19/19	-	C_opt/2	-	Co_HCP_opt /
185	3.30999 2	2.77561	1	0.28556	562.1456	Co3 /	3	-	Co_HCP_opt	/
186	2.8333 2	2.32442	1	0.25896	562.40457	Co4 /	4	-	Co_HCP_opt	/
187	2.57896 2	1.6034	1	0.9517	563.35627	Co5 /	5	-	Co_HCP_opt	/
188	2.1761 2	1.26768	1	0.82524	564.18151	Co6 /	6	-	Co_HCP_opt	/
189	2.16748 2	1.14919	1	1.03691	565.21842	Co7 /	7	-	Co_HCP_opt	/
190	1.84071 2	0.83212	1	1.01725	566.23567	Co13 /	13	-	Co_HCP_opt	/
191	1.48877 2	0.83212	1	0.43118	566.66685	Co19 /	19	-	Co_HCP_opt	/
192	0.9954 2	0.5352	1	0.21178	566.87863	Co55 /	55	-	Co_HCP_opt	/
193	-0.24806	0.04032	300	24.9489	591.82753	(Co_C100_1 -	Co_FCC_100	-	2*C_gas)/65	
194	-0.47908 4*C_gas)/67	0.13655	300	113.70018	705.5277	(Co_C100_2_1	Co_FCC_100	-		
195	-0.48395 4*C_gas)/67	0.10294	300	103.33121	808.85892	(Co_C100_2_2	Co_FCC_100	-		
196	-0.22761	0.08833	300	29.94698	838.80589	(Co_C110_1 -	Co_FCC_110	-	2*C_gas)/65	
197	-0.44634 4*C_gas)/67	0.17099	300	114.33087	953.13676	(Co_C110_2_1	Co_FCC_110	-		
198	-0.42699 4*C_gas)/67	0.15251	300	100.74583	1053.8826	(Co_C110_2_2	Co_FCC_110	-		
199	-0.22447 2*C_gas)/65	0.04707	300	22.12101	1076.00361	(Co_C110b_1	Co_FCC_110	-		

8.4 Appendix D – Original Results of the Fitting Procedure

200	-0.4293 4*C_gas)/67	0.09239	300	81.64879	1157.6524	(Co_C110b_2_1	-	Co_FCC_110	-
201	-0.43384 4*C_gas)/67	0.09037	300	82.4385	1240.0909	(Co_C110b_2_2	-	Co_FCC_110	-
202	-0.20688	0.02537	300	16.18109	1256.27199	(Co_C111_1	-	Co_FCC_111	2*C_gas)/65
203	-0.42589 4*C_gas)/67	-0.1879	300	16.99204	1273.26403	(Co_C111_2_1	-	Co_FCC_111	-
204	-0.39499 4*C_gas)/67	0.07715	300	66.8747	1340.13873	(Co_C111_2_2	-	Co_FCC_111	-
205	-0.40589 4*C_gas)/67	0.06523	300	66.58735	1406.72608	(Co_C111_2_3	-	Co_FCC_111	-
206	-0.12941 2*C_gas)/119	0.03615	300	8.22317	1414.94925	(Co_C211_1_1	-	Co_FCC_211	-
207	-0.12941 2*C_gas)/119	0.03597	300	8.20563	1423.15487	(Co_C211_1_2	-	Co_FCC_211	-
208	-0.24908 4*C_gas)/121	-0.0838	300	8.19505	1431.34992	(Co_C211_2_1	-	Co_FCC_211	-
209	-0.25279 4*C_gas)/121	0.07076	300	31.40508	1462.75501	(Co_C211_2_2	-	Co_FCC_211	-
210	-0.25279 4*C_gas)/121	0.07081	300	31.41495	1494.16996	(Co_C211_2_3	-	Co_FCC_211	-
211	-0.24862 4*C_gas)/121	-0.08217	300	8.31196	1502.48192	(Co_C211_2_4	-	Co_FCC_211	-
212	-0.23847 4*C_gas)/121	0.30298	300	87.95029	1590.43221	(Co_C211_2_5	-	Co_FCC_211	-
213	-0.24318 4*C_gas)/121	0.0572	300	27.06709	1617.4993	(Co_C211_2_6	-	Co_FCC_211	-
214	-0.23114 4*C_gas)/121	0.06753	300	26.76006	1644.25935	(Co_C211_2_7	-	Co_FCC_211	-
215	-0.24302 4*C_gas)/121	0.05759	300	27.11013	1671.36949	(Co_C211_2_8	-	Co_FCC_211	-
216	-0.23502 4*C_gas)/121	0.0527	300	24.83426	1696.20374	(Co_C211_2_9	-	Co_FCC_211	-
217	-0.25279 4*C_gas)/121	0.07082	300	31.41813	1727.62187	(Co_C211_2_10	-	Co_FCC_211	-
218	-0.24318 4*C_gas)/121	0.05724	300	27.07557	1754.69744	(Co_C211_2_11	-	Co_FCC_211	-
219	-0.25279 4*C_gas)/121	0.07081	300	31.41503	1786.11247	(Co_C211_2_12	-	Co_FCC_211	-
220	-0.24175 4*C_gas)/121	-0.00166	300	17.29251	1803.40498	(Co_C211_2_13	-	Co_FCC_211	-
221	-0.23827 4*C_gas)/121	0.0534	300	25.52039	1828.92537	(Co_C211_2_14	-	Co_FCC_211	-
222	-0.23502 4*C_gas)/121	0.05292	300	24.87171	1853.79708	(Co_C211_2_15	-	Co_FCC_211	-
223	-0.24303 4*C_gas)/121	0.05759	300	27.11083	1880.90791	(Co_C211_2_16	-	Co_FCC_211	-
224	-0.24423 4*C_gas)/121	0.07814	300	31.17786	1912.08577	(Co_C211_2_17	-	Co_FCC_211	-
225	0	0	1000	0	1912.08577	C_gas	-	C_gas	2*C_gas)/65
226	-0.10408 2*C_gas)/65	0.02164	5	0.07903	1912.16479	(Co_C100_top	-	Co_FCC_100	-
227	-0.10344 2*C_gas)/65	0.04197	5	0.10571	1912.27051	(Co_C110_top	-	Co_FCC_110	-
228	-0.10766 2*C_gas)/65	0.01046	5	0.06976	1912.34027	(Co_C111_top	-	Co_FCC_111	-
229	-0.05471 2*C_gas)/119	0.01148	5	0.02191	1912.36218	(Co_C211_top	-	Co_FCC_211	-

Chapter 8: Appendices

230	-0.15419 2*C_gas)/65	0.03496	5	0.17888	1912.54106	(Co_C100_bridge	-	Co_FCC_100	-
231	-0.13361 2*C_gas)/65	0.04558	5	0.16056	1912.70162	(Co_C110_bridge	-	Co_FCC_110	-
232	-0.15841 2*C_gas)/65	0.031	10	0.35877	1913.06039	(Co_C111_bridge	-	Co_FCC_111	-
233	-0.09499 2*C_gas)/119	0.01611	5	0.06172	1913.12211	(Co_C211_bridge	-	Co_FCC_211	-
234	0.86017 2*C_gas)/65	0.42586	5	0.94313	1914.06524	(repulsie_top	-	Co_FCC_111	-
235	0.34143 2*C_gas)/65	0.2755	1200	5.21594	1919.28118	(repulsie_bridge	-	Co_FCC_111	-

8.5 Appendix E – Parameter Sets of Used Force Fields

8.5 APPENDIX E – PARAMETER SETS OF USED FORCE FIELDS

Appendix E1 – Parameter set of the constructed force field

```
ReaxFF - generated by the Myocastor suite of software
39      ! Number of general parameters
      50 ! Bonder order correction 1
      9.5469 ! Bonder order correction 2
      26.5405 ! Valency angle conjugation parameter
      1.7224 ! Triple bond stabilisation parameter
      6.8702 ! Triple bond stabilisation parameter
      60.485 ! C2 correction
      1.0588 ! Undercoordination parameter
      4.6 ! Triple bond stabilisation parameter
      12.1176 ! Undercoordination parameter
      13.3056 ! Undercoordination parameter
      -70.5044 ! Triple bond stabilisation energy
      0 ! Lower Taper-radius
      10 ! Upper Taper-radius
      2.8793 ! Not used
      33.8667 ! Valency Undercoordination
      6.0891 ! Valency angle/lone pair parameter
      1.0563 ! Valency angle
      2.0384 ! Valency angle parameter
      6.1431 ! Not used
      6.929 ! Double bond/angle parameter
      0.3989 ! Double bond/angle parameter: overcoord
      3.9954 ! Double bond/angle parameter: overcoord
      -2.4837 ! Not used
      5.7796 ! Torsion/BO parameter
      10 ! Torsion overcoordination
      1.9487 ! Torsion overcoordination
      -1.2327 ! Conjugation 0 (not used)
      2.1645 ! Conjugation
      1.5591 ! vdWaals shielding
      0.1 ! Cutoff for bond order (*100)
      2.1365 ! Valency angle conjugation parameter
      0.6991 ! Overcoordination parameter
      50 ! Overcoordination parameter
      1.8512 ! Valency/lone pair parameter
      0.5 ! Not used
      20 ! Not used
      5 ! Molecular energy (not used)
      0 ! Molecular energy (not used)
      2.6962 ! Valency angle conjugation parameter
      2 ! Nr of atoms; cov.r; valency;a.m;Rvdw;Evdw;gammaEEM;cov.r2;
      alfa;gammavdW;valency;Eunder;Eover;chiEEM;etaEEM;n.u.
      cov r3;Elp;Heat inc.;n.u.;n.u.;n.u.;n.u.
      ov/un;vall;n.u.;val3,vval4
C      1.3298 4.0000 12.0000 2.0368 0.0528 0.9162 1.1415 4.0000
      9.0225 2.6014 4.0000 30.0000 79.5548 5.4507 6.8520 0.0000
      1.2185 0.0000 170.4002 13.8985 32.8340 14.9010 0.8563 0.0000
      -2.7500 2.1920 1.0564 3.2035 2.9663 0.0000 0.0000 0.0000
Co     2.4960 3.0000 58.9330 1.7231 0.2328 0.8139 0.2089 3.0000
      12.6998 15.0031 3.0000 0.0000 0.0000 4.8038 7.3852 0.0000
      -0.9623 0.0000 96.9473 1.6928 4.3501 0.4034 0.8563 0.0000
      -2.5000 2.9330 1.0338 2.8790 2.5791 0.0000 0.0000 0.0000
      3 ! Nr of bonds; Edisl;LPpen;n.u.;pbe1;pbo5;l3corr;pbo6
      pbe2;pbo3;pbo4;Etrip;pbol;pbo2;ovcorr
      1 1 113.3050 85.7214 179.7547 1.5254 -1.7029 1.0000 8.6724 0.5271
      0.3013 -0.2477 6.6682 1.0000 -0.0611 6.2721 1.0000 0.0000
      1 2 {87.7556} 26.5765 88.1979 1.4555 0.1056 1.0000 7.0258 0.0038
      1.1066 -0.0206 2.2283 1.0000 -0.0760 8.9990 1.0000 0.0000
      2 2 53.5381 0.0000 0.0000 -0.2729 -0.2000 0.0000 16.0000 0.2915
      7.2786 -0.2000 15.0000 1.0000 -0.0976 7.9115 0.0000 0.0000
      0 ! Nr off off-diagonal terms; Ediss;Ro;gamma;rsigma;rpi;rpi2
      5 ! Nr of angles;at1;at2;at3;Thetao,o;ka;kb;pv1;pv2
      1 1 1 93.4024 53.4022 0.7634 0.0000 -0.4776 17.4509 1.2988
```

```

1 2 1 113.7864 130.1851 2.1940 0.0000 4.7295 0.0000 0.5126
1 1 2 42.0303 117.3027 24.7183 0.0000 0.1309 0.0000 4.9947
2 1 2 85.6957 146.7542 0.1383 0.0000 4.9651 0.0000 1.0881
1 2 2 138.7212 23.9950 24.8219 0.0000 -0.6112 0.0000 4.9930
3 ! Nr of torsions;at1;at2;at3;at4;;V1;V2;V3;V2(BO;vconj;n.u;n.u
1 1 1 1 0.1807 119.9657 -0.2524 -5.8796 -1.9524 0.0000 0.0000
1 1 1 2 0.7487 20.4179 -4.0218 6.4815 0.0000 0.0000 0.0000
2 1 1 2 -4.9431 -4.8963 -5.0000 2.4970 0.0000 0.0000 0.0000
0 ! Nr of hydrogen bonds;at1;at2;at3;Rhb;Dehb;vhb1

```

Appendix E2 – Parameter set of the SCM force field ‘CHONSSiPtZrNiCuCo.ff’

Reactive MDforce field: Nielson et al., J. Phys. Chem. A, 109, 493-499 (2005),
<http://dx.doi.org/10.1021/jp046244d>

```

39 ! Number of general parameters
50.0000 !p(boc1)
4.3822 !p(boc2)
21.2839 !p(coa2)
0.0000 !Not used (n.u.)
0.0000 !n.u.
53.9706 !kc2
1.0053 !p(ovun6)
0.0000 !n.u.
7.6280 !p(ovun7)
14.5067 !p(ovun8)
0.0000 !n.u.
0.0000 !Lower Taper-radius (swa)
10.0000 !Upper Taper-radius (swb)
0.0000 !n.u.
33.8667 !p(val7)
25.6125 !p(lp1)
1.1177 !p(val9)
1.9645 !p(val10)
0.0000 !n.u.
6.6623 !p(pen2)
0.1809 !p(pen3)
3.9954 !p(pen4)
0.0000 !n.u.
4.8815 !p(tor2)
10.0000 !p(tor3)
2.3276 !p(tor4)
0.0000 !n.u.
1.7905 !p(cot2)
1.5591 !p(vdW1)
0.1000 !Cutoff for bond order*100 (cutoff)
2.8921 !p(coa4)
1.6356 !p(ovun4)
5.6937 !p(ovun3)
2.5067 !p(val8)
0.0000 !n.u.
0.0000 !n.u.
0.0000 !n.u.
0.0000 !n.u.
1.6052 !p(coa3)
2 ! Nr of atoms. atomID;ro(sigma);Val;atom mass;RvdW;Dij;gamma;ro(pi);Val(e)
    alfa;gamma(w);Val(angle);p(ovun5);n.u.;chiEEM;etaEEM;n.u.
    ro(pipi);p(lp2);Heat increment;p(boc4);p(boc3);p(boc5);n.u.;n.u.
    p(ovun2);p(val3);n.u.;Val(boc);p(val5);n.u.;n.u.;n.u.
C 1.3647 4.0000 12.0000 1.9091 0.1597 0.8712 1.2018 4.0000
  9.5729 2.7769 4.0000 35.6314 79.5548 5.7254 6.9235 0.0000
  1.2661 0.0000 -0.0526 5.0514 29.6014 11.9957 0.8563 0.0000
-17.6107 2.9280 1.0564 4.0000 2.9663 0.0000 0.0000 0.0000
Co 2.0075 3.0000 63.5460 1.8480 0.2056 0.8218 0.1000 3.0000
  12.3582 3.4682 3.0000 0.0000 0.0000 4.8038 7.3852 0.0000
  -1.0000 0.0000 92.5070 6.2293 5.2294 0.1542 0.8563 0.0000
  -3.3353 2.9867 1.0338 3.0000 2.5791 0.0000 0.0000 0.0000

```

8.5 Appendix E – Parameter Sets of Used Force Fields

```
3      ! Nr of bonds. at1;at2;De(sigma);De(pi);De(pipi);p(be1);p(bo5);
      corr;n.u.;p(bo6);p(ovun1);p(be2);p(bo3);p(bo4);n.u.;p(bo1);p(bo2)
1 1 142.9877 117.7932 70.0184 0.2152 -1.0820 1.0092 50.0568 0.1436
      0.1120 -0.1904 8.5003 1.0000 -0.0966 5.9567 1.0000 0.0000
1 2 {83.8766} 7.6132 0.0000 0.1332 -0.2000 1.0000 16.0000 0.2308
      0.7624 -0.2167 7.4106 1.0000 -0.1291 5.2562 1.0000 0.0000
2 2 68.1504 0.0000 0.0000 -0.4743 -0.2000 0.0000 16.0000 0.2865
      1.3468 -0.2000 15.0000 1.0000 -0.0596 8.1864 0.0000 0.0000
1      ! Nr of off-diagonal terms. at1;at2;Dij;RvdW;alfa;ro(sigma);ro(pi);ro(pipi)
1 2 0.0879 1.7302 11.8588 1.4583 1.4235 -1.0000
3      ! Nr of angles.
at1;at2;at3;Thetao,o;p(val1);p(val2);p(coal1);p(val7);p(pen1);p(val4)
1 1 1 77.0860 49.1556 0.7273 0.0000 0.0933 15.5317 1.0400
1 2 1 84.6882 18.1124 1.0794 0.0000 1.7791 0.0000 1.8728
1 1 2 36.1871 8.8505 5.3270 0.0000 1.7712 0.0000 1.7983
1      ! Nr of torsions. at1;at2;at3;at4;;V1;V2;V3;p(tor1);p(cot1);n.u;n.u.
1 1 1 1 0.0000 35.6556 0.2614 -6.3913 -1.7021 0.0000 0.0000
0      ! Nr of hydrogen bonds. at1;at2;at3;r(hb);p(hb1);p(hb2);p(hb3)
```